Plantwide simulation and monitoring of offshore oil and gas production facility

By

Mohammad Shalauddin Khaled

A thesis submitted to the

School of Graduate Studies

in partial fulfillment of the requirements for the degree of

Master of Engineering

Department of Process Engineering (Oil and Gas Program)

Faculty of Engineering and Applied Science

Memorial University of Newfoundland

May 2020

St. John's Newfoundland and Labrador Canada

I dedicate this thesis to my parents (Md. Haris Uddin & Halima Begum),

my wife Sharminur Afroza

And

To my little princes Wareesha Khaled.

Abstract

Monitoring is one of the major concerns in offshore oil and gas production platform since the access to the offshore facilities is difficult. Also, it is quite challenging to extract oil and gas safely in such a harsh environment, and any abnormalities may lead to a catastrophic event. The process data, including all possible faulty scenarios, is required to build an appropriate monitoring system. Since the plant wide process data is not available in the literature, a dynamic model and simulation of an offshore oil and gas production platform is developed by using Aspen HYSYS. Modeling and simulations are handy tools for designing and predicting the accurate behavior of a production plant. The model was built based on the gas processing plant at the North Sea platform reported in Voldsund et al. (2013). Several common faults from different fault categories were simulated in the dynamic system, and their impacts on the overall hydrocarbon production were analyzed. The simulated data are then used to build a monitoring system for each of the faulty states. A new monitoring method has been proposed by combining Principal Component Analysis (PCA) and Dynamic PCA (DPCA) with Artificial Neural Network (ANN). The application of ANN to process systems is quite difficult as it involves a very large number of input neurons to model the system. Training of such large scale network is time-consuming and provides poor accuracy with a high error rate. In PCA-ANN and DPCA-ANN monitoring system, PCA and DPCA are used to reduce the dimension of the training data set and extract the main features of measured variables. Subsequently ANN uses this lower-dimensional score vectors to build a training model and classify the abnormalities. It is found that the proposed approach reduces the time to train ANN and successfully diagnose, detects and classifies the faults with a high accuracy rate.

ACKNOWLEGEMENT

First, I want to convey my earnest gratitude and respect to my supervisors, Dr. Syed Imtiaz, Dr. Salim Ahmed, and Dr. Sohrab Zendehboudi, for their encouragement, guidance and constructive feedback throughout the development of this thesis. Without their continuous help, research ideas, and patience, this work would not have been accomplished. I would also like to gratefully acknowledge my former supervisor, Dr. Enamul Hossain, who introduced me to the area.

I am grateful to my beloved parents and my only elder sister for their mental support and incessant pray. Especially I am thankful to my wife for being the source of my inspiration. Without her help, care, and love, I wouldn't be able to overcome the challenges of life and complete my Master's program.

I would like to thank all of my colleagues especially I must recognize the contribution of Eugenio Turco Neto and Rajeevan Arun, who always helped me smilingly in any programming related issue. I also thank Tina Dwyer and Colleen Mahoney for making a friendly and welcoming atmosphere at the university.

Finally, I would like to thank the School of Graduate Studies (SGS) and Equinor (former Statoil) Canada Ltd. for providing financial support to accomplish this research. I am also thankful to the Memorial University of Newfoundland for all kinds of support for this research.

Table of Contents

Chapter 6: Conclusion

List of Tables

List of Figures

List of Abbreviations

ANFIS	Adaptive Neuro Fuzzy Inference System.
AR	Analytical Redundancy.
AI	Artificial Intelligent.
ANN	Artificial Neural Network.
BBN	Bayesian Belief Network.
BN	Bayesian Network.
BG	Bond Graph.
CVA	Canonical Variate Analysis.
CBR	Case Based Reasoning.
CD	Casual Dependency.
CGBN	Conditional Gaussian Bayesian Network.
CUSUM	Cumulative Sum.
DR	Decorrelated Residual.
DLA	Deep Learning Algorithm.
DWT	Discrete Wavelet Transform.
DBN	Dynamic Bayesian Network.
DPCA	Dynamic Principle Component Analysis.
DTW	Dynamic Time Warping.
ES	Expert System.
EWMA	Exponentially Weighted Moving Average.
EKF	Extended Kalman Filter.

ELS	Extended Least Square.
EUIO	Extended Unknown Input Observer.
FDD	Fault Detection and Diagnosis.
FDCs	Fault Discriminant Components.
FDKPCA	Fault Discriminant-enhanced Kernel PCA.
FT	Fault Tree.
FDA	Fisher discriminant Analysis.
FCCU	Fluid Catalytic Cracking Unit.
GOR	Gas Oil Ratio.
GLO	Generalized Luenberger Observer.
GA	Genetic Algorithm.
GS	Grid Search.
HBN	Hybrid Bayesian Network.
ICA	Independent Component Analysis.
KFDM	Kalman Filter Diagnosis Model.
KF	Kalman Filter.
KLNPDA	Kernel Local-Nonlocal Preserving Discriminant Analysis.
KPLS	Kernel Partial Least Square.
KPCA	Kernel PCA.
kNNs	K-Nearest Neighbors.
KIFS	Knowledge-based Ingredient Formulation System.
KLID	Kullback-Leibner Information Distance.
LS	Least Square.

LCL	Lower Control Limit.
MDA	Mahalanobis Distance Analysis.
MWPCA	Moving Window PCA.
MBPCA	Multiblock PCA.
MLP	Multi-Layer Perception.
MPP	Multiparametric Programming.
MSPCA	Multi-Scale PCA.
MSPM	Multivariate Statistical Process Monitoring.
MPCA	Multiway PCA.
PLS	Partial Least Square.
PSO	Particle Swarm Optimization.
PCEG	Possible Cause and Effect Graph.
PCA	Principle Component Analysis.
PCs	Principle Components.
QTA	Qualitative Trend Analysis.
SOM	Self-Organizing Map.
SP	Signal Processing.
SDG	Signed Directed Graph.
SLP	Single Layer Perception.
SVD	Singular Value Decomposition.
SPE	Square Prediction Error.
SAMMELF	Stage-Wise Additive Modeling Multi-class Exponential Loss Function.
SVM	Support Vector Machine.

TE	Tennessee Eastman.
UIO	Unknown Input Observer.
UKF	Unscented Kalman Filter.
UT	Unscented Transformation.
UCL	Upper Control Limit.

List of symbols

μ	Mean.
σ	Standard deviation.
Cv	Valve coefficient.
G	Specific gravity.
ΔP	Differential pressure in (lb./in2).
Q	Volumetric flow in U.S gal/min.
Y(s)	System output.
G(s)	Transfer function.
X(s)	System input.
ω	Frequency of oscillation.
K	Amplitude.
s	Laplace transform variable.
K	Gain.

Chapter 1

Introduction

1.1 Background

The demand for energy is increasing with the increase in the world's population. To fulfill the energy demand, offshore oil, and gas exploration and production have grown in the last few decades (Yong & Qiang, 2018). It is estimated that almost 30% of global energy comes from offshore oil and gas. Therefore, oil and gas industries have been joining efforts to enhance this energy supply range (Yang et al., 2013). It is very important to maintain all the safety procedures during the extraction of oil and gas in the offshore platform for both economic and lifesaving purposes. Uncontrolled events can lead to severe life-threating accidents, for example, explosion in BP Texas City refinery during the startup time of the raffinate splitter column (Manca & Brambilla, 2012), well control failure of an oil rig in Macondo British Petroleum (BP) LLC (Board, 2012) and an explosion with river pollution at the Jilin chemical plant due to wrong order of operations (Zhang et al., 2010). Accidents also cause substantial economic loss. It is reported that the petroleum and chemical industries of USA are losing 20 billion US dollars in every year due to the failure of proper fault diagnosis in time (Nimmo, 1995) where the UK is paying 27 billion dollars per year for the same reason (Venkatasubramanian, 2005). Operators need to be engaged in such a remote and restricted area for an extended period. The work environment is not only limited in space but also remains full of harsh noise. Process uncertainty with various new difficulties is a common thing associated with offshore oil and gas industries. The combinations of such stressful and challenging environment with intrinsic jeopardy of nature

are the primary and foremost reason behind the maximum number of accidents. The incidents cause not only the loss of life but also increase the downtime of production, which precedes a remarkable financial loss to the industry. For these reasons it is important to monitor the offshore production facilities remotely to ensure safe and event free operation.

Oil and gas production in offshore started since the eighteenth century and developed gradually from then. First offshore oil production began in 1896, the south of Santa Barbara, California, United States (BP Deep Horizon Oil Spill Commission, 2010). Successful milestone has been achieved in 1947, when a company called Kerr-McGee completed the first oil rig and productive well at Louisiana coast, Gulf of Mexico. It is also considered as the beginning of the offshore Oil and gas industry (Chakrabarti et al., 2005). Schematic of an offshore oil and gas platform is shown in Fig. 1.1 and 1.2.

Fig. 1.1: North Sea oil and gas platform obtained from Fiona Macleod CEng FIChemE and Stephen Richardson (The chemical engineer).

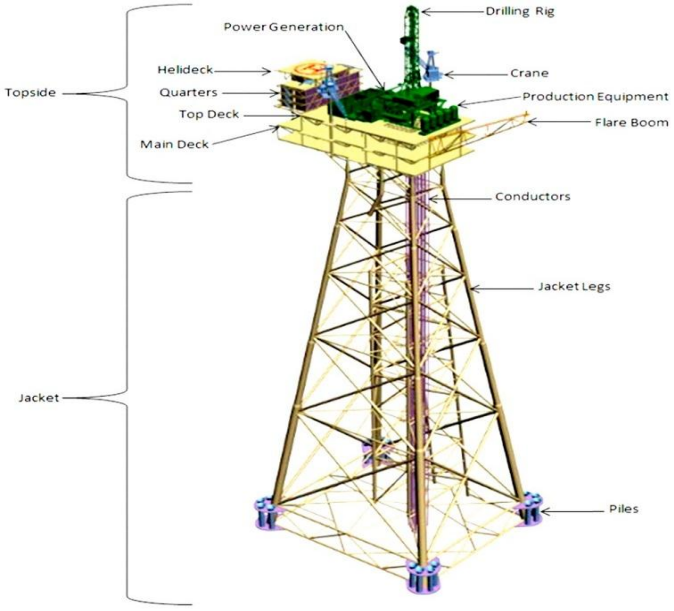

Fig. 1.2: Schematic of a generalized offshore oil and gas platform. Adapted from (Bull & Love, 2019).

Natural gas exploration in the North Sea started in the year 1960 (Schempf, 2004). In 1970, the first oil and gas field successfully discovered, which is now known as Ekofisk and Forties (Pratt et al., 1997). After the exploration of these oil and gas fields, it became very challenging to keep the platform safe because of severe adverse weather such as a tremendous cold, a massive storm, and sea waves. For that reason, oil and gas companies started developing new ways and ideas to keep the system safe. From then, the industry operating personnel started planning to detect any system abnormality at the beginning of fault occurrence, so that they can take preventive actions before happening of any severe accidents. But working in such remote and harsh areas with facility limitations, sometimes it is not possible to detect the failure within the shortest possible time. For that reason, in such a situation, a continuous monitoring tool is needed, which can continuously supervise and can control any system abnormalities and failure of safety-related issues. So, the process industries started following some strategies to obtain such a safety process system. Initially, industries started to follow the proactive strategy, such as to build the plant with optimal design and layout, proper equipment installation and operation, and field configuration. Although this strategy increased the system safety and identified most of the hazards, it was not economically and technically feasible to eliminate them. So, the reactive approach came forward to meet and overcome those challenges and improving the process control by utilizing monitoring and supervision techniques (jörgner & rilby, 2016). These techniques can detect faults due to any system failure, even when the platform is still functional in a controllable situation. Therefore, it can improve not only the system performance but also reduce productivity loss.

Modeling and simulation are vital for risk management and hazardous event analysis such as loss or disposal of the process fluid. It represents the combination of reality and mathematics that

transforms any practical problems into some equivalent mathematical equations (Cameron & Hangos, 2001). By using this mathematical model, it is possible to predict and subsequently reduce the risk and cost for reconstruction of the process equipment. The main objective of process modeling is to investigate the actual behavior of the process in any given situation in order to decrease the experimental cost, and any severe catastrophic event (Hyvärinen, 2012).

Advances in sensors and distributed control system (DCS) have made it easy to log a large number of variables. This has created an opportunity to monitor process systems and prevent any catastrophic event. Hence, fault detection and diagnosis (FDD) has become an integral part of any process system to determine the system's operating state at every single moment. Among the various types of FDD approaches, multivariate statistical methods are very useful for the analysis of complex process behavior and cope with highly correlated process variables in a large number of data (Tidriri et al., 2016). The machine learning approach is one of the most popular and efficient FDD methods to obtain knowledge from a large amount of process data by utilizing intensive computation power (Md Nor et al., 2019). Therefore, by implementing advanced data-driven techniques, it is possible to build a highly accurate FDD model to predict and prevent an accident by monitoring such a large number of variables.

In this work, A dynamic model for an offshore production facility in the North Sea is simulated using Aspen HYSYS simulator to predict the dynamic behaviors during normal and various faulty operating conditions. A hybrid approach integrating principle component analysis (PCA) / Dynamic PCA (DPCA) and artificial neural network (ANN) is proposed. PCA/DPCA reduces the dimension and ANN uses the lower dimensional data for pattern recognition. The proposed PCA-ANN and DPCA-ANN approaches are implemented and compared with conventional ANN.

1.2 Objective

The goal of this research is to (1) develop a plantwide offshore dynamic model and (2) develop an improved fault detection and diagnosis tools to detect and classify the faults quickly and promptly so that the operating personnel can take preventive steps to avoid accidents. The main objectives of this thesis are:

1. Build a plantwide dynamic model for offshore oil and gas platforms.
2. Record the behavior in normal and transient conditions.
3. Create several faulty conditions associated with the real production plant.
4. Detect the faults and classify the specific fault type.
5. Improve the limited diagnostic capacity of ANN by integrating the benefits of PCA and DPCA to detect the faults accurately within short processing time.

1.3 Thesis Structure

The outline of this dissertation is as follows:

In Chapter 1, the definition of fault detection and diagnosis, as well as the consequences of faults followed by the motivation of the research topic, is introduced, and the objectives of the research are identified.

Chapter 2 provides an extensive literature review on HYSYS simulation and different Fault detection and diagnostic methods. Emphasis has been given on the techniques relevant to this thesis.

In Chapter 3, A steady-state model of an offshore process plant has been built. The model is designed based on a real North see oil and gas platform. The model output is validated with the actual production output of the plant reported by Voldsund et al. (2013).

In Chapter 4, The steady state model presented in chapter 3, is transformed into dynamic state. The basic faults associated in the plants are considered, and the data for each scenario are recorded for monitoring purposes.

In Chapter 5, first ANN-based FDD method is used to detect and classify the process faults. The processing time, accuracy level, and error rete were calculated from the result. After that, a hybrid framework combining PCA and DPCA with ANN is formulated. Finally, all the outcomes from each methods were compared, and a decision has been made.

The outcomes of this thesis are summarized, and some future directions to improve this research are presented in Chapter 6.

1.4 Software Used

Aspen HYSYS version V9 is used for modeling and simulation of an offshore oil and gas plant. This is commercial software and very useful to simulate the steady-state model as well as dynamic model. Since the applications of the proposed algorithms have been demonstrated in the simulated data, a well-known and available software, student version of MATLAB has been used in this thesis. It can be downloaded from https://my.mun.ca/student. All the necessary codes are written in MATLAB and approached Neural Network Tools (NN tools) for modeling and classification of both ANN and DPCA-ANN based methods.

References

Bai, Y., & Bai, Q. (2018). Subsea engineering handbook. Gulf Professional Publishing.

Board, M. (2012). Macondo Well Deepwater Horizon Blowout: Lessons for Improving Offshore Drilling Safety. National Academies Press.

BP Deep Horizon Oil Spill Commission. (2010). A brief history of offshore oil drilling. National Commission on the BP Deepwater Horizon Oil Spill and Offshore Drilling.

Cameron, I. T., & Hangos, K. (2001). Process modelling and model analysis (Vol. 4). Elsevier.

Chakrabarti, S., Halkyard, J., & Capanoglu, C. (2005). Historical development of offshore structures. In Handbook of Offshore Engineering (pp. 1-38). Elsevier.

Hyvärinen, L. P. (2012). Mathematical modeling for industrial processes (Vol. 19). Springer Science & Business Media.

JÖRGNER, L., & RILBY, E. Dynamic simulations of an oil and gas well stream.

Manca, D., & Brambilla, S. (2012). Dynamic simulation of the BP Texas City refinery accident. Journal of Loss Prevention in the Process Industries, 25(6), 950–957. https://doi.org/10.1016/j.jlp.2012.05.008

Md Nor, N., Che Hassan, C. R., & Hussain, M. A. (2019). A review of data-driven fault detection and diagnosis methods: Applications in chemical process systems. Reviews in Chemical Engineering, 0(0). https://doi.org/10.1515/revce-2017-0069

Nimmo, I. (1995). Adequately address abnormal operations. Chemical Engineering Progress, 91(9), 36-45.

Pratt, J. A., Priest, T., & Castaneda, C. J. (1997). Offshore pioneers: Brown & Root and the history of offshore oil and gas. Gulf Professional Publishing.

Schempf, F. J. (2004). The history of offshore: developing the E and P infrastructure. Offshore, 64(1), 20-22.

Tidriri, K., Chatti, N., Verron, S., & Tiplica, T. (2016). Bridging data-driven and model-based approaches for process fault diagnosis and health monitoring: A review of researches and future challenges. Annual Reviews in Control, 42, 63–81. https://doi.org/10.1016/j.arcontrol.2016.09.008

Venkatasubramanian, V. (2005). Prognostic and diagnostic monitoring of complex systems for product lifecycle management: Challenges and opportunities. Computers & Chemical Engineering, 29(6), 1253–1263. https://doi.org/10.1016/j.compchemeng.2005.02.026

Yang, Z., Stigkæ, J. P., & Løhndorf, B. (2013). Plant-wide Control for Better De-oiling of Produced Water in Offshore Oil & Gas Production. IFAC Proceedings Volumes, 46(20), 45–50. https://doi.org/10.3182/20130902-3-CN-3020.00143

Zhang, W., Lin, X., & Su, X. (2010). Transport and fate modeling of nitrobenzene in groundwater after the Songhua River pollution accident. Journal of Environmental Management, 91(11), 2378–2384. https://doi.org/10.1016/j.jenvman.2010.06.025

Chapter 2
Literature Review

2.1 Modeling and simulation

Modeling and simulation are essential for design, prediction and optimization of process plants. Though extensive modelling and simulation studies have been done for land based oil and gas industries only very few studies have been conducted on the plant-wide modeling and simulation of offshore process facilities for economic performances in the past few decades.

Plant-wide modeling and simulation using Aspen HYSYS are routinely used for a wide-ranging process oil & gas industries, refineries, and engineering companies to optimize process design and operation (Rasmussen, 2015). A dynamic model of the downstream processing system using HYSYS plant simulator on Cranfield University's control and three-phase rig units was proposed by Hyprotech, (1999). Natarajan & Srinivasan (2010) developed a dynamic model in HYSYS for simulating offshore gas production platform considering three common faults such as the leak in the master valve, test separator controller failure, and biased temperature sensor on the flowline of the wellhead. Normal, faulty, and maintenance scenarios have been taken into consideration for simulation. A valve is used to represent the pipe resistance as the version of HYSYS was used didn't have scope for dynamic unit operation for the pipe segment. The simulation result is an approximation because it cannot represent the real pressure drop of the pipeline and fluid production characteristics.

Oliveira & Hombeeck (1997) examined a Brazilian oil platform, focusing on separation, compression, and pumping units in their study. It is reported that the heating unit and compression system are responsible for higher energy consumption. Exergetic efficiency is inferior in the separation unit due to the heat difference compared with the combustion unit, and it can be improved by using centrifugal separation. Voldsund et al. (2013) conducted analysis on the Norwegian offshore oil platform considering several topside facilities such as separation unit, recompression unit, reinjection unit, etc. It is found that the most significant exergy destruction occurs in the production manifold and gas reinjection process due to considerable pressure change (increase and decrease). Nguyen et al. (2013) conducted an analysis of the Norwegian oil and gas process platform and reported that the most exergy destruction occurs in (i) production manifold due to well fluid depressurization (ii) gas compression system due to the poor performance of the compressors and, (iii) recycles followed by recompression and separation process. Nguyen et al. (2014a) designed a simulation model in HYSYS for the offshore platform by considering three different representative stages of production schemes. In this research, energy consumption has been assessed by conducting exergy analysis, an unavoidable performance loss of about 55 to 60% occurred at the gas turbines. Nguyen et al. (2014b) analyzed and compared the energy and exergy efficiency using HYSYS simulator for several matured offshore oil and gas processing platform based on two different production days. Energy is mainly destroyed in the high-pressure zone, where the pressure of the produced gas is increased. On the other hand, exergy is destroyed in subsystems where the pressure is significantly decreased and increased. This research suggested anti-surge recycling around the compressor unit to increase the hydrocarbons flow entering the plant to prevent exergy destruction. Voldsund et al. (2014) also got similar findings after analyzing two other oil and gas

platforms where the system configurations are entirely different than the previous study. HYSYS is used for modeling in both pieces of research.

Abdel-Aal et al. (2003) analyzed oil production facilities based on the performance of oil separation. This study was involved with few perspectives, such as preserving the heavy compounds, intermediate compounds, and light mixtures in the oil. However, the light compounds contained in liquid oil flash cause economic loss due to its easy vaporization during transportation. In order to maximize the oil recovery, the most crucial factor of offshore oil production facilities involves the separation of light and intermediate compounds into oil and gas products. Besides this, Boyer & O'Connell (2005) developed an estimation of flash gas loss using Aspen HYSYS as well as the sampling data of crude oil. Bahadori et al. (2008) investigated the impact of a separator pressure on production optimization and to improve operating conditions using HYSYS. Oil production was investigated by setting up different pressure in each stage of separation and determined optimum pressure for maximum production based on GOR (gas-oil ratio). Extensive analysis is carried out on cost/day and has shown an overall profit after implementing the desired pressure. However, the oil damage due to the gaseous stream in the mid-stage process is not considered in this research. A graphical technique is developed by Mourad et al. (2009), to estimate the intermediate stage pressure to minimize the compressor cost. Voldsund et al. (2012) analyzed an offshore platform to reduce power consumption by optimizing the system performance. It is reported that reducing anti-surge recycling not only improves the efficiency of the compressor but also reduces the losses in the manifolds. Hence, significant power can be saved. Rasheed (2013) focused on increasing the yearly benefit by optimizing the process condition. HYSYS simulation was used in this research and considered temperature and pressure as the key factor for the optimization process. A flash

column was investigated without changing any system configuration of the original process, such as separation stages, number of separators, and pressure specification of the separators. Kim et al. (2014) presented a stochastic strategy using HYSYS for simulation and optimization of appropriate offshore process platform for maximizing profit. It is estimated from the difference between oil and gas product sales and several factors such as operation cost of the steam, cooling water, and electricity consumption. By implementing an integrated differential equation of state, these simulators can easily calculate the vapor-liquid phase equilibrium and thermodynamic behavior of any states. Nguyen et al. (2016) conducted modeling, analyzing, and improvement investigation of an offshore platform focusing on four individual platforms with different processing, operating conditions, and strategy. It is reported that overall power and fuel gas consumption can be saved around 20% by installing gas turbines and waste heat recovery unit within the processing system. Cho et al. (2018) analyzed the improvement of environmental standards, reducing utility consumption and maximizing the profit of the offshore oil and gas platform considering four separate process compositions. It is reported that for pick oil production, the recycle stream enables more oil production that leads to higher economic profit. For peak gas production, lower heat duty is required for preheating heat exchangers, and for peak water production, the financial benefit is significantly lower.

2.2 Fault Detection and Diagnosis

Fault Detection and Diagnosis (FDD) methods are developed to detect abnormal changes in the process variables within the system. It is essential to detect as early as possible to prevent process failure. Fault detection identifies the presence of faults within the system where fault diagnosis provides specific information about the faults to isolate the affected part from the

healthy system. Many techniques have been developed and can be broadly categorized into four approaches, such as model-based approach, knowledge-based approach, data-based approach, and hybrid approach (Venkatasubramanian et al. 2003a, 2003b).

2.2.1 Data base methods

Because of expanding process complexity, data-based methods are getting popular nowadays. This method is also known as a process history-based method because it trains the monitoring scheme using the historical process data. The data-driven method basically follows two strategies, such as fault detection and classification. Fault detection correlates the cases with expected faults, and classification determines the class or types of fault. The classification can be supervised or unsupervised learning types. In supervised classification, the history of data is used to construct a base model that is used to compare with new measured data to classify the faults. ANN and BN are the most popular supervised learning approach. On the other hand, the unsupervised learning method does not need any prior knowledge of data. The PCA, PLS, Control chart, etc. are the example of some unsupervised learning (Tidriri et al., 2016). Statistical process control includes both univariate and multivariate methods. The univariate techniques are classified as Shewhart control chart or $\overline{X}$ chart, Exponentially Weighted Moving Average (EWMA) control chart, and Cumulative Sum (CUSUM) control chart. Shewhart chart (Shewhart, 1930) is a well-established and widely used univariate control chart. This chart consists of plotting the observations sequentially with Upper Control Limit (UCL) and Lower Control Limit (LCL). If any of the observations exceed these control limits, a statistically significant deviation from normal operation is deemed to have occurred. Usually, the limits are calculated using mean (μ) and standard deviation (σ) which can be represented in equation form

as $\mu + 3\sigma$ and $\mu - 3\sigma$. CUSUM is another statistical procedure for monitoring stable univariate processes (Woodward & Goldsmith, 1964). In CUSUM techniques, the variables are compared with a predetermined reference value, and the cumulative sum of the deviations from this value is recorded. If the cumulation reaches or exceeds the predetermined decision interval, it indicates that a change has occurred in the mean level of variables. The EWMA chart was introduced by Roberts (1959) and it is used to detect persistent shifts in a process. It can detect the small and moderate shifts quickly. The main benefit of the univariate monitoring approach is that it is very easy to implement rather than a multivariate approach. But they are more expensive, and the functionality is mostly dependent on the selection of the tuning parameter (Montgomery & Runger, 2010). Also, a separate control chart is needed for monitoring a single variable, which makes the system more complicated. Hence it is not practical to monitor all the process variables in the system (Kourti & MacGregor, 1995). Multivariate Statistical Process Monitoring (MSPM) technique eliminates the drawbacks of univariate methods. It introduced several statistics, such as Hotelling's T^2, I^2 statistics, squared prediction error, etc. These techniques make the process data to use in a lower-dimensional space and establish the correlation between the process variables. The PCA is a multivariate statistical approach that can reduce data dimensionality (Montgomery, 2007). Also, it is not only able to capture the variances of the data but also establish the correlation between the process variables. Its range of applications has increased with the development of computers. It has been used in a wide variety of areas for the last 50 years (Jolliffe, 1986). It has a wide range of application in process monitoring (Kourti & MacGregor, 1996; Zhou, et al., 2014), anomaly detection (Zadakbar et al., 2013), dynamic risk assessment (Adedigba et al., 2017), etc. PCA reduces the dimensionality by performing the linear transformation of the original data set of one characteristic to another smaller set of data

with different characteristics. Mainly this approach rotates the data such that each consecutive axis represents a decreasing among variance, which is known as principal components (PCs) (Dunia et al., 1996). Pcs are uncorrelated and orthogonal to each other so that the first few PCs hold most of the variation present in all the original attributes. The first PC has the greatest possible variance in the data set. The second PC project the data in such a way that it is uncorrelated with the first PC and can be considered the next highest containing variance of the data. PCs are calculated using eigenvalue decomposition or singular value decomposition (SVD). Meanwhile, the data set contains the characteristics of different units and scales. So, it is necessary to standardize the data matrix, which will turn each of the dimensions to have a unity (1.0) variance. The scaling makes all the axis to have the same length corresponding to their various dimensions. These scaled values are used to calculate the covariance matrix, and then SVD decomposes this covariance matrix into a set of vectors. Q statistic, also known as Squared Prediction Error (SPE) statistic and the Hotelling's T^2 statistic are the two important tools that are commonly used in the PCA approach. SPE analyzes the residual data matrix to signify the inconsistencies of the projection data in a residual subspace. The T^2 statistic is basically used to estimate the distance between sample space and the center of the feature space. In other words, it analyzes the score matrix to check the variations of the projected data in the new space of the PCs. There are several methods to determine how many PCs need to be considered and ignored. It is normally done by taking only the PCs that are contributing to the highest variability to the data. Thus, focusing on a few PCs within many variables, the dimensionality of the data is significantly reduced. Also, the scree plot and loading plot are the very attractive and informative features of PCA. The scree plot gives valuable information about the groupings of the samples and outliers, where the loading plot provides the scope to identify the attributes equivalent to the

outliers. By utilizing these two plots at the same time, the simultaneous display of both objects and attributes can be achieved. However, one of the limitations of the PCA approach is that it is a linear technique, whereas most of the real processes are nonlinear. To solve this problem, many extended methods have been developed. PCA and projection to latent structures are extended to build a multiblock projection method to improve fault interpretation (MacGregor et al., 1994). It allows contribution or monitoring charts for each process subsections and exposes within which any fault or abnormal event has occurred. DPCA method using 'time lag shift' has been proposed to detect the presence of the disturbances and to isolate their sources from the system (Ku et al., 1995). Multiblock PCA (MBPCA) methods have been proposed and compared with hierarchical PCA models to improve the interpretability of multivariate techniques (Westerhuis et al., 1998). Qin (2001) proposed a MBPCA approach for decentralized monitoring and diagnosis in terms of regular PCA scores and residuals. The method helps to block the appropriate process variables and limit the root cause of the faults in a decentralized system. A new enhanced fault isolation MBPCA technique has been developed for better analyzation of each sub-block in the batch processing unit (Hong et al., 2014). Multiway principal component analysis (MPCA) has been applied to reduce the dimensionality by using PCs. The proposed technique was capable of tracking batch runs and the occurrences by establishing simple monitoring charts (Nomikos & MacGregor, 1994). A multi-scale PCA (MSPCA) approach has been proposed for batch process monitoring by combining the application of wavelet filtering (Misra et al., 2002; Nielsen & Jensen, 2009). Li et al. (2000) designed a recursive PCA algorithm to reduce the false alarm by recursively updating the number of PCs and the confidence limits for process monitoring. Moving Window PCA (MWPCA) method has been introduced to improve the performance of process monitoring by continuously updating the PCA

model and the control limits with the change of time (Jeng, 2010). Another technique known as Kernel PCA (KPCA) has been developed to improve the dimensionality reduction performance of the nonlinear process (Choi et al., 2005; Lee et al., 2004). By using kernel tricks, KPCA can select the number of PCs very efficiently in high dimensional spaces that are correlated to the input space through a few nonlinear mapping.

In recent years, ANN has been used extensively in various applications, commonly in pattern recognition, fault prediction, and classification (Zhang, 2000). ANN is inspired by biological neural networks and acquired learning intellectual properties like human brains (Jain et al., 1996). A NN is a set of connected cells in which each cell receives a response from input or other neurons depending on the types of the model. It produces a transformation between the neurons transmitting information to the other neurons or the output cells (Jha, 2007). This method is also very efficient for optimization (Haykin, 2001), disturbance detection (Yu et al., 2009; Wentao et al., 2012), and the excellent identifier of trends in data and patterns (Ogwueleka et al., 2012). This approach has been successfully used in many areas such as in power system (Vankayala & Rao, 1993), manufacturing (Wang et al., 1993), control system (Demiroren et al., 2001), signal processing (Bogdan et al., 2003), visual arts (Barni et al., 2005), quality management (Kaminski et al., 2008), medical diagnosis (Mazurowski et al., 2008), bankruptcy prediction and credit scoring (Tsai & Wu, 2008) and group search optimization (Shan & Xiaoli, 2008), robotic data classification (Gopalapillai et al., 2013), public transportation (Garrido et al., 2014), image classification (Barat & Ducottet, 2016), sentiment analysis (Vinodhini & Chandrasekaran, 2016), business analysis (Le et al., 2016) etc. Linear classifiers (Bywater & Middleton, 2016), Single-layer perceptron (SLP) (Hertz, 2018) and multilayer perceptron (MLP) (Anarghya et al., 2018) are the most common and widely used supervised ANN. The k-nearest

neighbors (kNNs) (Keller et al., 1985) and support vector machines (SVMs) (Zhang et al., 2018; Cao et al., 2017) are also two popular supervised ANN method used in applications. On the other hand, autoencoders (Baldi, 2012), k-means (Koonsanit et al., 2012), and expectation-maximization (Verma et al., 2015) are some commonly used unsupervised ANN method.

2.2.2 Hybrid Methods

It has been reported that the application of any particular method is not capable of fulfilling all the prerequisite conditions for accurate fault diagnosis. A single method that performs well under one circumstance may not be good in another phase of the process because each method has its strengths and limitations (Ding et al., 2009; 2011). A hybrid model is a unique approach where several individual methods combinedly share their strengths. The techniques in the hybrid model are a complement to each other and can overcome the limitations of individual methods when they used separately. Venkatasubramanian et al. (2003c) compared several individual methods (Observer, Digraph method, Abstraction Hierarchy, ES, Qualitative Trend Analysis (QTA), Principle Component Analysis (PCA) and Neural Network (NN)) and have shown that none of the single methods is adequate to perform all the requirements for a perfect diagnostic system. Seng Ng & Srinivasan (2010) Focused the advantages and limitations of different FDD method (QTA, ES, PCA, Partial Least Square (PLS), KF, Dynamic Time Warping (DTW), Deep Learning Algorithm (DLA) and NN) and suggested only hybrid model can achieve higher diagnostic resolution compared to the other individual application. Tidriri et al. (2016) described many hybrid approaches and have shown that it can significantly improve the performance and the resolution of the overall system diagnostic capability. The method called ‘two-tier’ approach proposed (Venkatasubramanian & Rich, 1988b) which is one of the earliest Hybrid methods in

fault diagnostic history. The model integrates compiled knowledge on top tier and deep level knowledge in the bottom tier. It can quickly identify and generate the root cause of any potential abnormalities. Frank (1990) suggested using the knowledge-based method with an existing analytical and algorithmic approach to mitigate the fundamental problem for anomaly detection. This hybrid model provides the opportunity to utilize several knowledges in a single framework and has the highest achievable robustness by decoupling the effects of faults. Dinkar (1996) also presented a blackboard based hybrid model (Dkit) as an alternative to the individual method where different methods of the hybrid system investigate the same issue independently. A scheduler is used to coordinate with these diagnostic methods to make an authentic decision. Both hybrid frameworks were validated using a diagnosis study on Amoco model IV fluid catalytic cracking unit. Researchers of Purdue university (Mylaraswamy & Venkatasubramanian, 1997) have proposed the hybrid method for large scale blackboard based process fault diagnosis known as Dkit. The proposed model was verified successfully in different scenarios through a Fluid Catalytic Cracking Unit (FCCU). Vedam et al. (1999) developed an intelligent operator decision support system called Op-Aide based on the distributed blackboard based knowledge. This model was developed to assist the operator in quantitative diagnosis and assessment of any unexpected situation. Gertler et al. (1999) proposed an isolation-enhanced PCA approach using a bank of PCA models for fault identification. By using the close equivalence between PCA and parity relations, this model can generate structured residuals (which is a robust property of Analytical Redundancy (AR) that has well-developed fault isolation capability) into the PCA framework. The strong isolating structure has been made by following structured residuals that leads to the disturbance decoupling. A Subspace Identification (SMI) approach is developed (Wang & Qin, 2002), where the model combines the concept of PCA, Dynamic PCA (DPCA),

and observer scheme. Parity space model and PCA can combinedly able to correlate input excitation. Also, the SMI-PCA algorithm with an instrumental variable can predict the possible abnormalities much better than DPCA. Ghosh et al. (2011) developed a model combining EKF as a model-based where PCA, ANN, Self-Organizing Maps (SOM) as a data-driven approach. Each method takes to process data as input and gives the normal or faulty class as an output. The output from each method are combined for consolidating outcome, and evidence-based fusion strategies are followed for decision making. Benkouider et al., (2012) developed a model based on EKF and ANN to detect faults in batch and semi-batch reactors. EKF is used to calculate the overall desired heat transfer coefficient of the reactors, and ANN is used for the diagnosis part considering the estimated parameters. A three-layer generic intelligent approach based on Diagnostic Bayesian Network (DBN) has been proposed (Zhao et al., 2013) to coordinate more valuable data and expert knowledge to improve the reliability of the model outcome. The model was tested in the chiller expert system and found that it has more powerful tools for fault diagnosis even if the data set or information remains incomplete or conflicting.

A model combining Bond Graph (BG) and BN was proposed (Zaidi et al., 2010), where BG is used for residual generation and BN for integrating data based on the reliability of the component. It has been shown the proposed Hybrid Bayesian Network (HBN) can significantly improve the classical binary method of decision making. Zhang & Hoo, (2011) developed a unique hierarchical hybrid approach using BG (system decomposition), PCA (reduce dimension), Discrete Wavelet Transform (DWT) (provide multi-scale decomposition of PCA scores), Mahalanobis Distance Analysis (MDA) (calculate confidence level from chi-squared distribution) and BG-BN (identify the root cause of the faults). A hybrid fault diagnosis method using PCA and SymCure reasoning was developed (Wang et al., 2012). SymCure represents an

expert system which can diagnose the faults. The proposed technique was tested using a lab-scale distillation column. A hybrid method comprised of PCA and Bayesian Belief Network (BBN) for FDD was described (Mallick & Imtiaz, 2013), where PCA identifies the possible faults (using residual plot and Q statistics) and BBN analyzes the root cause. A hybrid model, including a data-driven method and a model-based method under the Bayesian network, was presented (Atoui et al., 2016). The proposed T^2 statistics (using a data-driven approach combined with the residuals generated from model-based approach under Conditional Gaussian Bayesian Network (CGBN)) provides better decision rather than two of these individual methods. The NN classification, based on Kalman Filter (KF) was proposed by Siswantoro et al. (2016), where KF is used to estimate the parameter in order to make the predicted output more convenient to NN. The proposed method can minimize the prediction error by improving its classifier accuracy. Amin et al. (2018) developed a Hybrid hard evidence approach combining PCA with T^2 statistics and Bayesian network called PCA-T^2-BN. Multiple likelihood evidence is used to improve the diagnosis capacity and verified on twelve fault scenarios in CSTH and TE chemical processes. Jung & Sundstrom (2019) developed a unique hybrid approach for residual selection, combining data-driven and model-based methods in an uncertain system. The model section was used to generate the residuals, while the data-driven method was used to detect and isolate different faults. The proposed method successfully introduced the t-SNE algorithm to analyze and verify the accuracy of decoupled faults.

2.2.2.1 Data-driven hybrid methods

Recently the use of data-driven hybridization FDD methods becomes prevalent. Because multiple data-driven methods performing the collective problem-solving in one single FDD

framework is more efficient than using one approach. Chiang & Braatz (2003) developed the modified distance (DI) and modified causal dependency (CD) to incorporate the causal map with the data-driven method. The DI depends on Kullback–Leibner Information Distance (KLID), the mean of measured variables, and the range of the measured variables. The DI was used to quantify the similarity of the measured variable, where CD is used to measure the causal dependency between two of them. Zhang & Zhang (2009) developed a combined ICA-PLS method and kernel trick called (Independent Component Analysis – Kernel PLS) ICA-KPLS to build a nonlinear dynamic approach. Independent Component Analysis (ICA) was utilized to handle the statistically independent non-Gaussian hidden factors and KPLS to perform only the set of observations that follow Gaussian distribution. Maurya et al. (2010) presented a framework using an SGD as a filter to reduce possible faults and QTA to diagnose the faults. Ge et al. (2010) proposed a monitoring method based on the combination of multiple linear subspaces and Bayesian inference for nonlinear processes system. Each linear subspace generates the monitoring results and passes all individual results into fault probabilities by using the Bayesian inference. Salahshoor et al., (2010) proposed a model combining multiple classifiers such as SVM with an Adaptive Neuro-Fuzzy Inference System (ANFIS) to improve FDD tasks. In this approach, one binary support vector classifier is used to separate the members of a specific class, and ANFIS networks perform the diagnosis of the process faults. Rato & Reis (2013) developed a combination of multivariate statistics based on DPCA and on the generation of Decorrelated Residuals (DR) known as DPCA-DR approach to creating a better position for implementing SPC more consistently and stably. An improved boosting method called the Stage-wise Additive Modeling using a Multi-class Exponential Loss Function (SAMMELF) was proposed to improve the classification performance of learning algorithms (Karimi & Jazayeri-

Rad, 2014). Zhang & Ge (2015) designed a model combining results of various methods based on Dempster–Shafer evidence theory for the development of decision fusion systems for fault detection and identification. The boosting method imposes the basic classifier to work on the hard examples in a subsequent round and combine the obtained single classifiers in an ensemble system. Jiang et al. (2015) integrated canonical variate analysis (CVA) and Fisher discriminant analysis (FDA) scheme called CVA–FDA system for fault diagnosis. CVA was used: (i) to reduce the dimensionality of the pretreated datasets compared with the original datasets and (ii) to decrease the degree of overlap. The FDA method was used to classify the associated faults. A three-step framework integrating DI and CD has been proposed (Chiang et al., 2015). It integrates the data-driven and causal connectivity-based techniques with the propagation path-based feature to diagnose known, unknown, and multiple faults. Jiang et al. (2015) designed a canonical variate analysis (CVA) approach based on the feature representation of causal dependency (CD) for monitoring the faults. This method employs CD for pretreating the data and subsequently applied CVA for quantifying dissimilarity. Jiang & Huang (2016) proposed a distributed monitoring system integrating multivariate statistical analysis and BN for large-scale plant-wide processes. A stochastic optimization algorithm based performance-driven process decomposition method based on PCA has been built where Bayesian diagnosis was used for the decision-making system. A multi-class SVM based process supervision and fault diagnosis scheme called GS-PCA has been proposed (Gao & Hou, 2016). In this approach, PCA first used to reduce the feature dimension, optimization of SVM parameters is accomplished with the Grid Search (GS) method to increase prediction accuracy with reducing computational load, Genetic Algorithm (GA) and Particle Swarm Optimization (PSO) used for classification accuracy. Gharahbagheri et al., (2017) developed a new method through the integration of diagnostic

information from various diagnostic tools such as KPCA and sensor validation module and combines them with process knowledge using BN. The sensor check model was used to separate the sensor faults from the process faults where BN was used to diagnose internal state faults and disturbance faults. Deng et al., (2017) proposed an enhanced KPCA model called Fault Discriminant enhanced KPCA (FDKPCA). KPCA was used to generate nonlinear kernel principal components (KPCs) where Kernel Local-nonlocal Preserving Discriminant Analysis (KLNPDA) was used to produce Fault Discriminant Components (FDCs). Monitoring statistics for both KPCA and KLNPDA sub-models were created, and finally, a Bayesian interface was applied to convert it into overall fault probabilities.

2.3. Conclusions

From the above discussion, we can conclude that modeling and simulation are a must for designing and predicting process behavior. Most of the researchers have used Aspen HYSYS for modeling and simulation of offshore oil and gas production facilities. Those models have been built based on steady-state conditions and were primarily developed for design and optimization purposes. To establish a real-time monitoring system, dynamic models are required, which are scarce in the literature for modeling/simulation of offshore production and processing plants. This causes real challenges in developing and testing monitoring systems for offshore facilities.

There are many FDD approach present to detect and diagnose the process faults. The data-driven FDD method is prevalent because of its simplicity. Among the data-driven FDD approach, multivariate statistical methods and machine learning approaches are widely used in process industries due to their accuracy of the process information, practical interpretation of complex process behavior and capability of controlling highly correlated process variables in big

datasets. In the case of a large data set, mostly PCA is used for dimension reduction, where ANN used pattern recognition applications in process industries. Also, DPCA represents the dynamic nature of process variables and more efficient compared to static PCA. Although most of the approaches discussed in the literature mainly focused on solving problems of data characteristics, it is still hard for any single FDD method to perform efficiently for the possible faults. As a result, a hybridization-based framework is required for developing a complete and robust FDD tool. This hybrid approach can accurately detect and diagnose faults by implementing particular methods on specific best suit faulty scenarios.

Considering the above facts, a hybrid method comprising PCA/DPCA and ANN-based approach is proposed. This method utilizes reduced dimensional variables obtained from PCA/DPCA and feeds to the ANN for fault detection and classification. The result shows the proposed method reduces FAR and MAR, less time consuming, and more convenient to use compared to the single ANN.

References

Abdel-Aal, H. K., Aggour, M. A., & Fahim, M. A. (2003). Petroleum and gas field processing. CRC press.

Adedigba, S. A., Khan, F., & Yang, M. (2017). Dynamic Failure Analysis of Process Systems Using Principal Component Analysis and Bayesian Network. Industrial & Engineering Chemistry Research, 56(8), 2094–2106. https://doi.org/10.1021/acs.iecr.6b03356

Amin, Md. T., Imtiaz, S., & Khan, F. (2018). Process system fault detection and diagnosis using a hybrid technique. Chemical Engineering Science, 189, 191–211. https://doi.org/10.1016/j.ces.2018.05.045

Anarghya, A., Harshith, D. N., Rao, N., Nayak, N. S., Gurumurthy, B. M., Abhishek, V. N., & Patil, I. G. S. (2018). Thrust and torque force analysis in the drilling of aramid fibre-reinforced composite laminates using RSM and MLPNN-GA. Heliyon, 4(7), e00703. https://doi.org/10.1016/j.heliyon.2018.e00703

Atoui, M. A., Verron, S., & Kobi, A. (2016). A Bayesian network dealing with measurements and residuals for system monitoring. Transactions of the Institute of Measurement and Control, 38(4), 373–384. https://doi.org/10.1177/0142331215581446

Bahadori, A., Vuthaluru, H. B., & Mokhatab, S. (2008). Optimizing separator pressures in the multistage crude oil production unit. Asia-Pacific Journal of Chemical Engineering, 3(4), 380–386. https://doi.org/10.1002/apj.159

Baldi, P. (2012, June). Autoencoders, unsupervised learning, and deep architectures. In Proceedings of ICML workshop on unsupervised and transfer learning (pp. 37-49).

Barat, C., & Ducottet, C. (2016). String representations and distances in deep Convolutional Neural Networks for image classification. Pattern Recognition, 54, 104–115. https://doi.org/10.1016/j.patcog.2016.01.007

Barni, M., Pelagotti, A., & Piva, A. (2005). Image processing for the analysis and conservation of paintings: Opportunities and challenges. IEEE Signal Processing Magazine, 22(5), 141–144. https://doi.org/10.1109/MSP.2005.1511835

Benkouider, A. M., Kessas, R., Yahiaoui, A., Buvat, J. C., & Guella, S. (2012). A hybrid approach to faults detection and diagnosis in batch and semi-batch reactors by using EKF and neural network classifier. Journal of Loss Prevention in the Process Industries, 25(4), 694–702. https://doi.org/10.1016/j.jlp.2012.03.005

Bogdan, M., Schroder, M., & Rosenstiel, W. (2003). Artificial neural net based signal processing for interaction with peripheral nervous system. First International IEEE EMBS Conference on Neural Engineering, 2003. Conference Proceedings., 134–137. https://doi.org/10.1109/CNE.2003.1196775

Boyer, B. E., & O'Connell, S. (2005). Optimize Separator Operating Pressures to Reduce Flash Losses. SPE/EPA/DOE Exploration and Production Environmental Conference. Presented at the SPE/EPA/DOE Exploration and Production Environmental Conference, Galveston, Texas. https://doi.org/10.2118/94373-MS

Bywater, R. P., & Middleton, J. N. (2016). Melody discrimination and protein fold classification. Heliyon, 2(10), e00175. https://doi.org/10.1016/j.heliyon.2016.e00175

Cao, J., Fang, Z., Qu, G., Sun, H., & Zhang, D. (2017). An accurate traffic classification model based on support vector machines. International Journal of Network Management, 27(1), e1962. https://doi.org/10.1002/nem.1962

Chiang, L. H., & Braatz, R. D. (2003). Process monitoring using causal map and multivariate statistics: Fault detection and identification. Chemometrics and Intelligent Laboratory Systems, 65(2), 159–178. https://doi.org/10.1016/S0169-7439(02)00140-5

Chiang, L. H., Jiang, B., Zhu, X., Huang, D., & Braatz, R. D. (2015). Diagnosis of multiple and unknown faults using the causal map and multivariate statistics. Journal of Process Control, 28, 27–39. https://doi.org/10.1016/j.jprocont.2015.02.004

Cho, Y., Kwon, S., & Hwang, S. (2018). A new approach to developing a conceptual topside process design for an offshore platform. Korean Journal of Chemical Engineering, 35(1), 20–33. https://doi.org/10.1007/s11814-017-0258-z

Choi, S. W., Lee, C., Lee, J.-M., Park, J. H., & Lee, I.-B. (2005). Fault detection and identification of nonlinear processes based on kernel PCA. Chemometrics and Intelligent Laboratory Systems, 75(1), 55–67. https://doi.org/10.1016/j.chemolab.2004.05.001

De Oliveira, S., & Van Hombeeck, M. (1997). Exergy analysis of petroleum separation processes in offshore platforms. Energy Conversion and Management, 38(15–17), 1577–1584. https://doi.org/10.1016/S0196-8904(96)00219-1

Demiroren, A., Zeynelgil, H. L., & Sengor, N. S. (2001). The application of ANN technique to load-frequency control for three-area power system. 2001 IEEE Porto Power Tech Proceedings (Cat. No.01EX502), vol.2, 5. https://doi.org/10.1109/PTC.2001.964793

Deng, X., Tian, X., Chen, S., & Harris, C. J. (2017). Fault discriminant enhanced kernel principal component analysis incorporating prior fault information for monitoring nonlinear processes. Chemometrics and Intelligent Laboratory Systems, 162, 21–34. https://doi.org/10.1016/j.chemolab.2017.01.001

Ding, S. X., Zhang, P., Naik, A., Ding, E. L., & Huang, B. (2009). Subspace method aided data-driven design of fault detection and isolation systems. Journal of Process Control, 19(9), 1496–1510. https://doi.org/10.1016/j.jprocont.2009.07.005

Ding, S. X., Zhang, P., Jeinsch, T., Ding, E. L., Engel, P., & Gui, W. (2011). A survey of the application of basic data-driven and model-based methods in process monitoring and fault diagnosis. IFAC Proceedings Volumes, 44(1), 12380–12388. https://doi.org/10.3182/20110828-6-IT-1002.02842

Dinkar, M. (1996). DKIT: A Blackboard-based, distributed, multi-expert environment for Abnormal Situation Management.

Dunia, R., Qin, S. J., Edgar, T. F., & McAvoy, T. J. (1996). Identification of faulty sensors using principal component analysis. AIChE Journal, 42(10), 2797–2812. https://doi.org/10.1002/aic.690421011

Frank, P. M. (1990). Fault diagnosis in dynamic systems using analytical and knowledge-based redundancy: A survey and some new results. automatica, 26(3), 459-474.

Garrido, C., de Oña, R., & de Oña, J. (2014). Neural networks for analyzing service quality in public transportation. Expert Systems with Applications, 41(15), 6830–6838. https://doi.org/10.1016/j.eswa.2014.04.045

Gao, X., & Hou, J. (2016). An improved SVM integrated GS-PCA fault diagnosis approach of Tennessee Eastman process. Neurocomputing, 174, 906–911. https://doi.org/10.1016/j.neucom.2015.10.018

Ge, Z., Zhang, M., & Song, Z. (2010). Nonlinear process monitoring based on linear subspace and Bayesian inference. Journal of Process Control, 20(5), 676–688. https://doi.org/10.1016/j.jprocont.2010.03.003

Gertler, Janos, Li, W., Huang, Y., & McAvoy, T. (1999). Isolation enhanced principal component analysis. AIChE Journal, 45(2), 323–334. https://doi.org/10.1002/aic.690450213

Gharahbagheri, H., Imtiaz, S. A., & Khan, F. (2017). Root Cause Diagnosis of Process Fault Using KPCA and Bayesian Network. Industrial & Engineering Chemistry Research, 56(8), 2054–2070. https://doi.org/10.1021/acs.iecr.6b01916

Ghosh, K., Ng, Y. S., & Srinivasan, R. (2011). Evaluation of decision fusion strategies for effective collaboration among heterogeneous fault diagnostic methods. Computers & Chemical Engineering, 35(2), 342–355. https://doi.org/10.1016/j.compchemeng.2010.05.004

Gopalapillai, R., Vidhya, J., Gupta, D., & Sudarshan, T. S. B. (2013). Classification of robotic data using artificial neural network. 2013 IEEE Recent Advances in Intelligent Computational Systems (RAICS), 333–337. https://doi.org/10.1109/RAICS.2013.6745497

Haykin, S. (2001). Kalman Filtering and Neural Networks, Wiley series on adaptive and learning systems for signal processing, communications, and control,[sn],[S. l.].

Hertz, J. A. (2018). Introduction to the theory of neural computation. CRC Press.

Hong, J. J., Zhang, J., & Morris, J. (2014). Progressive multi-block modelling for enhanced fault isolation in batch processes. Journal of Process Control, 24(1), 13–26. https://doi.org/10.1016/j.jprocont.2013.10.013

Hyprotech, Dynamic Modeling, Hysys. Plant Manual, pp. 1–5 (1999).

Jain, A. K., Jianchang Mao, & Mohiuddin, K. M. (1996). Artificial neural networks: A tutorial. Computer, 29(3), 31–44. https://doi.org/10.1109/2.485891

Jeng, J.-C. (2010). Adaptive process monitoring using efficient recursive PCA and moving window PCA algorithms. Journal of the Taiwan Institute of Chemical Engineers, 41(4), 475–481. https://doi.org/10.1016/j.jtice.2010.03.015

Jha, G. K. (2007). Artificial neural networks and its applications. IARI, New Delhi, girish_iasri@ rediffmail. com.

Jiang, B., Zhu, X., Huang, D., & Braatz, R. D. (2015). Canonical variate analysis-based monitoring of process correlation structure using causal feature representation. Journal of Process Control, 32, 109–116. https://doi.org/10.1016/j.jprocont.2015.05.004

Jiang, B., Zhu, X., Huang, D., Paulson, J. A., & Braatz, R. D. (2015). A combined canonical variate analysis and Fisher discriminant analysis (CVA–FDA) approach for fault diagnosis. Computers & Chemical Engineering, 77, 1–9. https://doi.org/10.1016/j.compchemeng.2015.03.001

Jiang, Q., & Huang, B. (2016). Distributed monitoring for large-scale processes based on multivariate statistical analysis and Bayesian method. Journal of Process Control, 46, 75–83. https://doi.org/10.1016/j.jprocont.2016.08.006

Jolliffe, I. T. (1986). Principal Component Analysis. Springer, New York.

Jung, D., & Sundstrom, C. (2019). A Combined Data-Driven and Model-Based Residual Selection Algorithm for Fault Detection and Isolation. IEEE Transactions on Control Systems Technology, 27(2), 616–630. https://doi.org/10.1109/TCST.2017.2773514

Kaminski, W., Skrzypski, J., & Jach-Szakiel, E. (2008). Application of Artificial Neural Networks (ANNs) to Predict Air Quality Classes in Big Cities. 2008 19th International Conference on Systems Engineering, 135–140. https://doi.org/10.1109/ICSEng.2008.14

Karimi, P., & Jazayeri-Rad, H. (2014). Comparing the fault diagnosis performances of single neural networks and two ensemble neural networks based on the boosting methods. Journal of Automation and Control, 2(1), 21-32.

Keller, J. M., Gray, M. R., & Givens, J. A. (1985). A fuzzy K-nearest neighbor algorithm. IEEE Transactions on Systems, Man, and Cybernetics, SMC-15(4), 580–585. https://doi.org/10.1109/TSMC.1985.6313426

Kim, I. H., Dan, S., Kim, H., Rim, H. R., Lee, J. M., & Yoon, E. S. (2014). Simulation-Based Optimization of Multistage Separation Process in Offshore Oil and Gas Production Facilities. Industrial & Engineering Chemistry Research, 53(21), 8810–8820. https://doi.org/10.1021/ie500403a

Koonsanit, K., Jaruskulchai, C., & Eiumnoh, A. (2012). Parameter-Free K-Means Clustering Algorithm for Satellite Imagery Application. 2012 International Conference on Information Science and Applications, 1–6. https://doi.org/10.1109/ICISA.2012.6220961

Kourti, T., & MacGregor, J. F. (1995). Process analysis, monitoring and diagnosis, using multivariate projection methods. Chemometrics and Intelligent Laboratory Systems, 28(1), 3–21. https://doi.org/10.1016/0169-7439(95)80036-9

Kourti, T., & MacGregor, J. F. (1996). Multivariate SPC Methods for Process and Product Monitoring. Journal of Quality Technology, 28(4), 409–428. https://doi.org/10.1080/00224065.1996.11979699

Ku, W., Storer, R. H., & Georgakis, C. (1995). Disturbance detection and isolation by dynamic principal component analysis. Chemometrics and Intelligent Laboratory Systems, 30(1), 179–196. https://doi.org/10.1016/0169-7439(95)00076-3

Lee, J.-M., Yoo, C., Choi, S. W., Vanrolleghem, P. A., & Lee, I.-B. (2004). Nonlinear process monitoring using kernel principal component analysis. Chemical Engineering Science, 59(1), 223–234. https://doi.org/10.1016/j.ces.2003.09.012

Le, T., Pardo, P., & Claster, W. (2016). Application of artificial neural network in social media data analysis: a case of lodging business in Philadelphia. In Artificial Neural Network Modelling (pp. 369-376). Springer, Cham.

Li, W., Yue, H. H., Valle-Cervantes, S., & Qin, S. J. (2000). Recursive PCA for adaptive process monitoring. Journal of Process Control, 10(5), 471–486. https://doi.org/10.1016/S0959-1524(00)00022-6

MacGregor, J. F., Jaeckle, C., Kiparissides, C., & Koutoudi, M. (1994). Process monitoring and diagnosis by multiblock PLS methods. AIChE Journal, 40(5), 826–838. https://doi.org/10.1002/aic.690400509

Mallick, M. R., & Imtiaz, S. A. (2013). A Hybrid Method for Process Fault Detection and Diagnosis. IFAC Proceedings Volumes, 46(32), 827–832. https://doi.org/10.3182/20131218-3-IN-2045.00099

Maurya, M. R., Paritosh, P. K., Rengaswamy, R., & Venkatasubramanian, V. (2010). A framework for on-line trend extraction and fault diagnosis. Engineering Applications of Artificial Intelligence, 23(6), 950–960. https://doi.org/10.1016/j.engappai.2010.01.027

Mazurowski, M. A., Habas, P. A., Zurada, J. M., Lo, J. Y., Baker, J. A., & Tourassi, G. D. (2008). Training neural network classifiers for medical decision making: The effects of imbalanced datasets on classification performance. Neural Networks, 21(2–3), 427–436. https://doi.org/10.1016/j.neunet.2007.12.031

Misra, M., Yue, H. H., Qin, S. J., & Ling, C. (2002). Multivariate process monitoring and fault diagnosis by multi-scale PCA. Computers & Chemical Engineering, 26(9), 1281–1293. https://doi.org/10.1016/S0098-1354(02)00093-5

Montgomery, D. C. (2007). Introduction to statistical quality control. John Wiley & Sons.

Montgomery, D. C., & Runger, G. C. (2010). Applied statistics and probability for engineers. John Wiley & Sons.

Mourad, D., Ghazi, O., & Noureddine, B. (2009). Recovery of flared gas through crude oil stabilization by a multi-staged separation with intermediate feeds: A case study. Korean Journal of Chemical Engineering, 26(6), 1706–1716. https://doi.org/10.1007/s11814-009-0236-1

Mylaraswamy, D., & Venkatasubramanian, V. (1997). A hybrid framework for large scale process fault diagnosis. Computers & Chemical Engineering, 21, S935–S940. https://doi.org/10.1016/S0098-1354(97)87622-3

Natarajan, S., & Srinivasan, R. (2010). Multi-model based process condition monitoring of offshore oil and gas production process. Chemical Engineering Research and Design, 88(5–6), 572–591. https://doi.org/10.1016/j.cherd.2009.10.013

Nguyen, T.-V., Pierobon, L., Elmegaard, B., Haglind, F., Breuhaus, P., & Voldsund, M. (2013). Exergetic assessment of energy systems on North Sea oil and gas platforms. Energy, 62, 23–36. https://doi.org/10.1016/j.energy.2013.03.011

Nguyen, T.-V., Fülöp, T. G., Breuhaus, P., & Elmegaard, B. (2014a). Life performance of oil and gas platforms: Site integration and thermodynamic evaluation. Energy, 73, 282–301. https://doi.org/10.1016/j.energy.2014.06.021

Nguyen, T.-V., Jacyno, T., Breuhaus, P., Voldsund, M., & Elmegaard, B. (2014b). Thermodynamic analysis of an upstream petroleum plant operated on a mature field. Energy, 68, 454–469. https://doi.org/10.1016/j.energy.2014.02.040

Nguyen, T.-V., Voldsund, M., Breuhaus, P., & Elmegaard, B. (2016). Energy efficiency measures for offshore oil and gas platforms. Energy, 117, 325–340. https://doi.org/10.1016/j.energy.2016.03.061

Nielsen, T. D., & Jensen, F. V. (2009). Bayesian networks and decision graphs. Springer Science & Business Media.

Nomikos, P., & MacGregor, J. F. (1994). Monitoring batch processes using multiway principal component analysis. AIChE Journal, 40(8), 1361–1375. https://doi.org/10.1002/aic.690400809

Ogwueleka, F. N., Misra, S., Colomo-Palacios, R., & Fernandez, L. (2012). Neural network and classification approach in identifying customer behavior in the banking sector: A case study of an international bank. Human Factors and Ergonomics in Manufacturing & Service Industries, n/a-n/a. https://doi.org/10.1002/hfm.20398

Qin, S. J., Valle, S., & Piovoso, M. J. (2001). On unifying multiblock analysis with application to decentralized process monitoring. Journal of Chemometrics, 15(9), 715–742. https://doi.org/10.1002/cem.667

R. S. Al-Ameeri, Middle East Tech. Conf. Exhib. (2013).

Rasmussen, K. R. (2015). Optimisation of Central Offshore Process Equipment and Weight Estimations (Doctoral dissertation, B. Sc. thesis, Aalborg University, Aalborg, Denmark).

Rato, T. J., & Reis, M. S. (2013). Fault detection in the Tennessee Eastman benchmark process using dynamic principal components analysis based on decorrelated residuals (DPCA-DR). Chemometrics and Intelligent Laboratory Systems, 125, 101–108. https://doi.org/10.1016/j.chemolab.2013.04.002

Roberts, S. W. (1959). Control chart tests based on geometric moving averages. Technometrics, 1(3), 239-250.

Salahshoor, K., Kordestani, M., & Khoshro, M. S. (2010). Fault detection and diagnosis of an industrial steam turbine using fusion of SVM (support vector machine) and ANFIS (adaptive neuro-fuzzy inference system) classifiers. Energy, 35(12), 5472–5482. https://doi.org/10.1016/j.energy.2010.06.001

Seng Ng, Y., & Srinivasan, R. (2010). Multi-agent based collaborative fault detection and identification in chemical processes. Engineering Applications of Artificial Intelligence, 23(6), 934–949. https://doi.org/10.1016/j.engappai.2010.01.026

Shan He, & Xiaoli Li. (2008). Application of a group search optimization based Artificial Neural Network to machine condition monitoring. 2008 IEEE International Conference on Emerging Technologies and Factory Automation, 1260–1266. https://doi.org/10.1109/ETFA.2008.4638562

Shewhart, W. A. (1930). Economic Quality Control of Manufactured Product [1]. Bell System Technical Journal, 9(2), 364–389. https://doi.org/10.1002/j.1538-7305.1930.tb00373.x

Siswantoro, J., Prabuwono, A. S., Abdullah, A., & Idrus, B. (2016). A linear model based on Kalman filter for improving neural network classification performance. Expert Systems with Applications, 49, 112–122. https://doi.org/10.1016/j.eswa.2015.12.012

Tidriri, K., Chatti, N., Verron, S., & Tiplica, T. (2016). Bridging data-driven and model-based approaches for process fault diagnosis and health monitoring: A review of researches and future challenges. Annual Reviews in Control, 42, 63–81. https://doi.org/10.1016/j.arcontrol.2016.09.008

Tsai, C., & Wu, J. (2008). Using neural network ensembles for bankruptcy prediction and credit scoring. Expert Systems with Applications, 34(4), 2639–2649. https://doi.org/10.1016/j.eswa.2007.05.019

Vankayala, V. S. S., & Rao, N. D. (1993). Artificial neural networks and their applications to power systems—A bibliographical survey. Electric Power Systems Research, 28(1), 67–79. https://doi.org/10.1016/0378-7796(93)90081-O

Vedam, H., Dash, S., & Venkatasubramanian, V. (1999). An intelligent operator decision support system for abnormal situation management. Computers & Chemical Engineering, 23, S577–S580. https://doi.org/10.1016/S0098-1354(99)80142-2

Venkatasubramanian, V., & Rich, S. H. (1988b). An object-oriented two-tier architecture for integrating compiled and deep-level knowledge for process diagnosis. Computers & Chemical Engineering, 12(9–10), 903–921. https://doi.org/10.1016/0098-1354(88)87017-0

Venkatasubramanian, V., Rengaswamy, R., Yin, K., & Kavuri, S. N. (2003a). A review of process fault detection and diagnosis: Part I: Quantitative model-based methods. Computers & chemical engineering, 27(3), 293-311.

Venkatasubramanian, V., Rengaswamy, R., & Kavuri, S. N. (2003b). A review of process fault detection and diagnosis: Part II: Qualitative models and search strategies. Computers & chemical engineering, 27(3), 313-326.

Venkatasubramanian, V., Rengaswamy, R., Kavuri, S. N., & Yin, K. (2003c). A review of process fault detection and diagnosis: Part III: Process history based methods. Computers & chemical engineering, 27(3), 327-346.

Verma, N. K., Dwivedi, S., & Sevakula, R. K. (2015). Expectation maximization algorithm made fast for large scale data. 2015 IEEE Workshop on Computational Intelligence: Theories, Applications and Future Directions (WCI), 1–7. https://doi.org/10.1109/WCI.2015.7495515

Vinodhini, G., & Chandrasekaran, R. M. (2016). A comparative performance evaluation of neural network based approach for sentiment classification of online reviews. Journal of

King Saud University - Computer and Information Sciences, 28(1), 2–12. https://doi.org/10.1016/j.jksuci.2014.03.024

Voldsund, M., He, W., Røsjorde, A., Ertesvåg, I. S., & Kjelstrup, S. (2012). Evaluation of the oil and gas processing at a real production day on a North Sea oil platform using exergy analysis. Proceedings of ECOS, 153-166.

Voldsund, M., Ertesvåg, I. S., He, W., & Kjelstrup, S. (2013). Exergy analysis of the oil and gas processing on a North Sea oil platform a real production day. Energy, 55, 716–727. https://doi.org/10.1016/j.energy.2013.02.038

Voldsund, M., Nguyen, T.-V., Elmegaard, B., Ertesvåg, I. S., Røsjorde, A., Jøssang, K., & Kjelstrup, S. (2014). Exergy destruction and losses on four North Sea offshore platforms: A comparative study of the oil and gas processing plants. Energy, 74, 45–58. https://doi.org/10.1016/j.energy.2014.02.080

Wang, S. C., Dong, J. X., & Shen, G. (1993). ANN based Process Control in Manufacturing. 1993 American Control Conference, 2531–2532. https://doi.org/10.23919/ACC.1993.4793349

Wang, J., & Qin, S. J. (2002). A new subspace identification approach based on principal component analysis. Journal of Process Control, 12(8), 841–855. https://doi.org/10.1016/S0959-1524(02)00016-1

Wang, Z., Zhao, J., & Shang, H. (2012). A hybrid fault diagnosis strategy for chemical process startups. Journal of Process Control, 22(7), 1287–1297. https://doi.org/10.1016/j.jprocont.2012.05.015

Wentao Fan, Bouguila, N., & Ziou, D. (2012). Variational Learning for Finite Dirichlet Mixture Models and Applications. IEEE Transactions on Neural Networks and Learning Systems, 23(5), 762–774. https://doi.org/10.1109/TNNLS.2012.2190298

Westerhuis, J. A., Kourti, T., & MacGregor, J. F. (1998). Analysis of multiblock and hierarchical PCA and PLS models. Journal of Chemometrics: A Journal of the Chemometrics Society, 12(5), 301-321.

Woodward, R. H., & Goldsmith, P. L. (1964). Cumulative sum techniques. Imperial Chemical Industries Limited.

Yu, W., He, H., & Zhang, N. (Eds.). (2009). Advances in Neural Networks-ISNN 2009: 6th International Symposium on Neural Networks, ISNN 2009 Wuhan, China, May 26-29, 2009 Proceedings (Vol. 5552). Springer.

Zadakbar, O., Imtiaz, S., & Khan, F. (2013). Dynamic Risk Assessment and Fault Detection Using Principal Component Analysis. Industrial & Engineering Chemistry Research, 52(2), 809–816. https://doi.org/10.1021/ie202880w

Zaidi, A., Tagina, M., & Bouamama, B. O. (2010). Reliability data for improvement of decision-making in Analytical Redundancy Relations Bond Graph based diagnosis. 2010 IEEE/ASME International Conference on Advanced Intelligent Mechatronics, 790–795. https://doi.org/10.1109/AIM.2010.5695771

Zhang, G. P. (2000). Neural networks for classification: A survey. IEEE Transactions on Systems, Man and Cybernetics, Part C (Applications and Reviews), 30(4), 451–462. https://doi.org/10.1109/5326.897072

Zhang, Y., & Zhang, Y. (2009). Complex process monitoring using modified partial least squares method of independent component regression. Chemometrics and Intelligent Laboratory Systems, 98(2), 143–148. https://doi.org/10.1016/j.chemolab.2009.06.001

Zhang, X., & Hoo, K. A. (2011). Effective fault detection and isolation using bond graph-based domain decomposition. Computers & Chemical Engineering, 35(1), 132–148. https://doi.org/10.1016/j.compchemeng.2010.07.033

Zhang, F., & Ge, Z. (2015). Decision fusion systems for fault detection and identification in industrial processes. Journal of Process Control, 31, 45–54. https://doi.org/10.1016/j.jprocont.2015.04.004

Zhang, Y., Deng, Q., Liang, W., & Zou, X. (2018). An Efficient Feature Selection Strategy Based on Multiple Support Vector Machine Technology with Gene Expression Data. BioMed Research International, 2018, 1–11. https://doi.org/10.1155/2018/7538204

Zhao, Y., Xiao, F., & Wang, S. (2013). An intelligent chiller fault detection and diagnosis methodology using Bayesian belief network. Energy and Buildings, 57, 278–288. https://doi.org/10.1016/j.enbuild.2012.11.007

Zhou, J., Guo, A., Celler, B., & Su, S. (2014). Fault detection and identification spanning multiple processes by integrating PCA with neural network. Applied Soft Computing, 14, 4–11. https://doi.org/10.1016/j.asoc.2013.09.024

Chapter 3

Steady State Modeling and Simulation of an Offshore Gas Processing Platform

3.1 Introduction

Modeling and simulation are essential parts of process system engineering. The aim of using modeling and simulation is to predict the real scenarios of a system. The mathematical approach is very efficient for modeling and developing various engineering applications, where it uses several equations and variables to represent the system (Hyvärinen, 1970). A mechanistic model is built based on mass conservation, transportation matrix, energy, and momentum balance (Stephanopoulos, 2009). At first, the mechanisms associated with the process need to be transformed into mathematical equations, and then the predicted outcomes can be utilized to take necessary steps (Hangos & Cameron, 2001). Proper equations and assumptions are required to understand and predict the process behavior accurately (Hyvärinen, 1970). Modeling and simulation can save time and reduces the risk of financial loss. Designing a process plant without using a proper model can lead to the reconstruction of the process equipment's. Besides, a good model helps to earn more profit through improved process optimization, design, and control strategies (Hangos & Cameron, 2001).

To represent the scenario of an offshore oil and gas processing plant, the basic topside design and equipment of a Norwegian platform in the North Sea, is examined. Our ultimate goal is to develop a dynamic model for the Norwegian platform in the North Sea region and develop a

monitoring scheme for the system. The steady-state model needs to be built before implementing and simulating the plantwide dynamic behavior, which will provide the initial conditions for the dynamic model. It is also essential to gather equipment information and flowsheet specifications before starting a dynamic simulation such that a set of differential equations can be solved with respect to time. A steady-state model has been built and validated by using Aspen HYSYS. The simulation results are validated through extensive performance evaluation and comparison with real production data available in the literature (Voldsund et al., 2013). Later this steady-state model is transformed into a dynamic model by modifying necessary design characteristics.

3.2 Process Overview

The overall process is divided into well section, production manifold, separator unit, export pump unit, recompression, drainage system, fuel gas treatment, and reinjection unit. Five separate production wells with different fluid properties such as flow rate, pressure, temperature, etc. are connected in the production manifold. The operating pressure of the well stream varies from 80 to 170 bar. The overall pressure is reduced to 70 bar before entering the separation process. The process flow diagram of the plant is shown in Fig. 3.3.

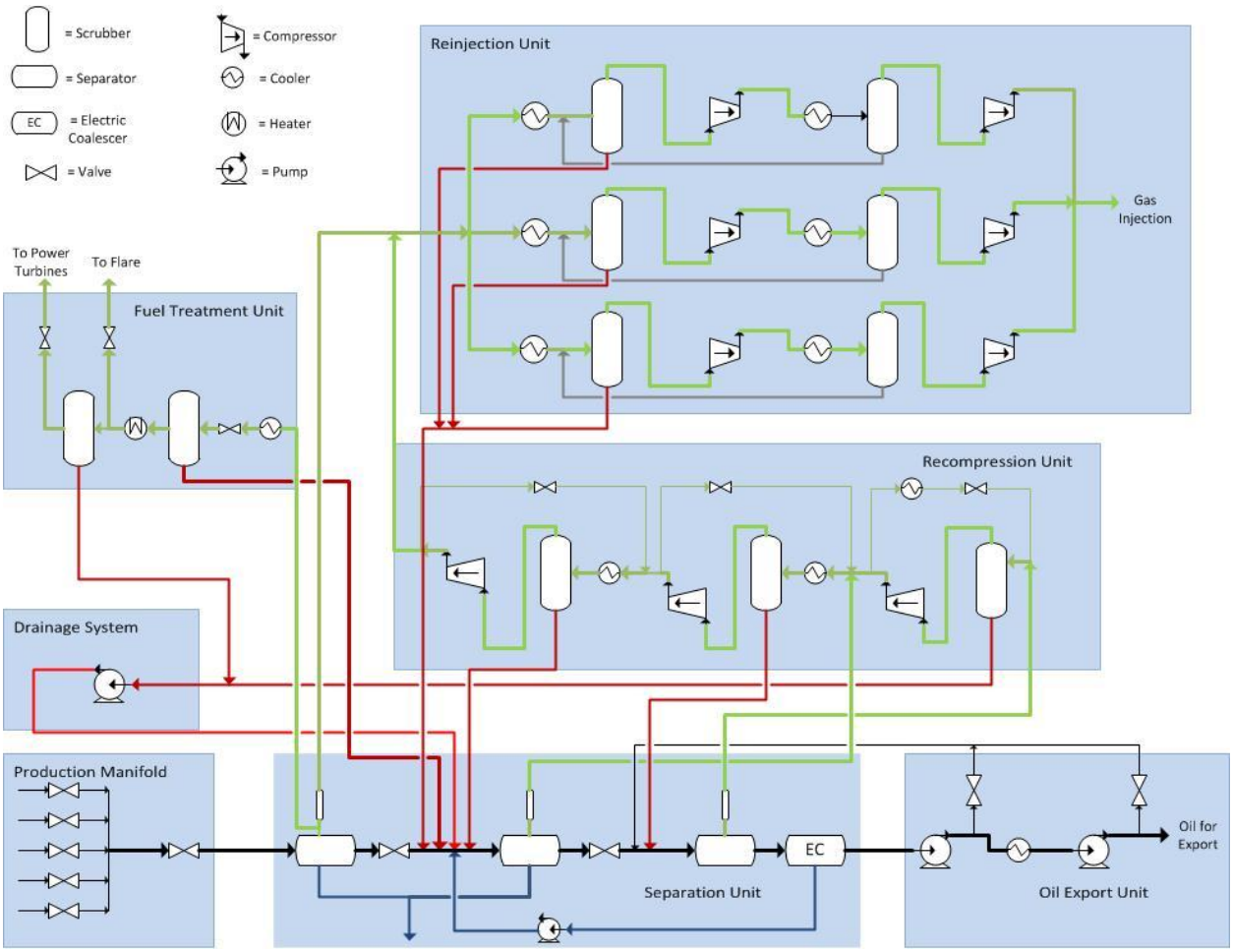

Fig. 3.3: Process flow diagram of the Norwegian Sea oil and gas platform with modifications.

The separation unit shown in Fig. 3.3, consists of two three-phase separators (V-100, V-101), one two-phase separator (V-114) and one electrostatic coalescer (V-102). Gas, oil, and water are separated by using gravitational separation. Before entering into a new separator, the pressure is reduced to optimize the final production. Separated oily water from the first and second stage, three-phase separators enters the water treatment processing unit. A certain proportion of separated fluid (oil and water) is pumped and recycled back to the entry of the second stage, three-phase separator. Oil pressure of the coalescer output is reduced to 2.8 bar and entered into the export pump unit.

The export pump unit consists of one cooler and two pumping sections where the produced oil is cooled and pressurized up to 32 bar. To make a consistent oil flow through the compressors, a certain amount of oil is recycled back to the entry of the third stage, two-phase separator.

The recompression process unit consists of three sub-units, where each of them has one cooler, one scrubber, and one compressor. Scrubbers are used to remove the remaining water from gas, save the compressor from pressure hunting, and increase its efficiency. Gas from the third stage, two-phase separator, with 2.8 bar, enters to the first stage recompression scrubber and is fed into the compressor to increase the pressure. A portion of the gas is recirculated and cooled to the same subsystem, known as the anti-surge recycling system, to keep a minimum constant flow through the compressor and prevent surging. 92%, 69% and 72% of the total gas are recycled to the first, second, and third recompression subsystems, accordingly. The condensed water from the scrubber is sent to the drain system. After leaving the first stage compressor, it enters the second stage recompression where the gas stream from the second stage, three-phase separator mixes with it. Then the condensed water is sent back to the third stage, two-phase separator. Similarly, it enters the third stage and finally leaves the recompression unit with 70 bar. The remaining condensation is sent back to the entry of the second stage, three-phase separator. The gas from the first stage, three-phase separator mixes with it and enters into the reinjection unit.

The reinjection unit consists of three parallel reinjection trains. Each train consists of two scrubbers, two coolers, and two compressors. The main objective of this unit is to increase the gas pressure to match the injection pressure of the well, so the gas can be injected into the

reservoir. The condensation from each unit is then sent back to the entry of the second stage, three-phase separator.

A small portion (3%) of gas from the first stage three-phase separator enters the fuel gas treatment unit. This unit consists of two scrubbers, one cooler, and one heater. After cooling and reducing the gas pressure, it is fed into the first scrubber. Condensation output is sent back to the entry of the second stage three-phase separator. The gas is then heated to remove moisture and is separated into two flows. One flow is fed to the second scrubber, and the other flow is taken for the flare system. After leaving the second scrubber, the remaining gas is supplied to the power turbines, and the condensation is sent to the drain system. The drain system pumps the condensation and recycles it back to the entry of the second stage, three-phase separator.

A steady state simulation study is carried out in this section based on the system described earlier. The feed stream temperature (80ºC to 87ºC) and GOR (2800) is significantly higher in this plant. Besides this, it has a pressure range of 88 to165 bar. The measurement data is chosen in a way that it can represent the average value of a consistent and stable typical production day. The average oil and injected gas flow rates are 132.5 Sm^3/h and 369 × 103 Sm^3/h, where the maximum deviation is 10 Sm^3/h and 103 Sm^3/h, respectively.

3.3 Simulated Model Description

In this study, the Peng-Robinson (Peng & Robinson, 1976) equation of state is used for the prediction of thermodynamic properties. Few assumptions had to be made with respect to the actual physical system to facilitate the modeling in HYSYS. Below we state these assumptions:

1. HYSYS does not have a coalescer in the equipment library. In this study, one two-phase separator has been used instead of the electrostatic coalescer.

2. In the real case, condensation from the coalescer is sent back to the second stage of the three-phase separator. In this simulation it was directed to the third stage of the two-phase separator without using any pump due to the following reasons:
    a. The pump detects vapor fraction in the condensation.
    b. It's not practical to add the recycle (2.8 bar) in the second stage separator without pumping because it significantly reduces the required inlet pressure of the separator.
3. In real conditions, the recycle flow is connected to the system directly, but in this simulation, the mixer is used to take multiple inputs and provide a single output feed to the system.

Based on the above assumptions, a steady-state model for the system is developed for the entire gas processing plant. Since the steady-state model is mostly a reproduction of the model described in (Voldsund et al., 2013), it is not described in this paper. However, a converged and validated steady-state model is a necessary step to build a dynamic model.

3.3.1 Well Trajectory

The material streams for oil, gas, and water are defined to represent five producing well (well 7, 16, 23, 24, 26). Material streams are used to simulate the flow that are entering and leaving the simulation boundaries. The properties of the heavier components or hypothetical components (components with seven carbon atoms or more are lumped together called hypothetical components) are shown in Table 3.1, and the composition (percent value) for all components is shown in Table 3.2.

Table 3.1: Properties of the hypothetical components taken from Voldsund et al. (2013).

Name of Components	**Molecular weight (g/mole)**	**Boiling Temperature (˚C)**	**Liquid Density (kg/m^3)**
Hypothetical C-1	81	73	721.2
Hypothetical C-2	108	99	740.1
Hypothetical C-3	125	152	774.6
Hypothetical C-4	171	230	817.1
Hypothetical C-5	247	316	859.3
Hypothetical C-6	388	437	906.2
Hypothetical C-7	640	618	988.5

Table 3.2: Reservoir fluid compositions of liquid, gas and water phases taken from Voldsund et al. (2013).

Name of Components	**Liquid Percent**	**Gas percent**	**Water percent**
Methane	0.78	0.83	0
Ethane	6.41 e-2	6.81 e-02	0
Propene	3.55 e-2	3.74 e-2	0
i-Butane	5.52 e-3	5.71 e-3	0
n-Butane	1.30 e-2	1.34 e-2	0
i-Pentane	4.39 e-3	4.28 e-3	0
n-Pantane	5.80 e-3	5.51 e-3	0
H_2O	0	0	1
CO_2	8.61 e-03	9.18 e-03	0
N_2	8.61 e-3	9.18 e-03	0
Hypothetical C-1	1.34 e-2	9.07 e-3	0
Hypothetical C-2	1.17 e-2	3.47 e-03	0
Hypothetical C-3	1.49 e-2	7.14 e-04	0
Hypothetical C-4	1.24 e-2	0	0
Hypothetical C-5	9.01 e-3	0	0
Hypothetical C-6	5.22 e-3	0	0
Hypothetical C-7	3.44 e-03	0	0

The measured flowrate data of gas, liquid and water of all corresponding wells are shown in Table 3.3.

Table 3.3: Gas, oil and water flowrate of all corresponding wells.

Well	Gas Flow Rate (Sm^3/h)	Liquid Flow rate (Sm^3/h)	Water Flow Rate (Sm^3/h)
7	5.76E+04	20.6	13.8
16	8.75E+04	27.2	1.5
23	8.05E+04	21.1	13.9
24	8.19E+04	40.1	1.9
26	7.13E+04	23.5	5.4

Each three streams, representing a well, are combined in a mixer. 'Set outlet to lowest inlet' property is selected in design parameters for the mixers and five mixtures (Mix-7,16, 23, 24, 26) are defined for the producing wells. The output of mixer 7, 16, 23, 24, and 26 enters the valve-106, 107, 108, 109, and 110, respectively, which is shown in Fig. 3.4.

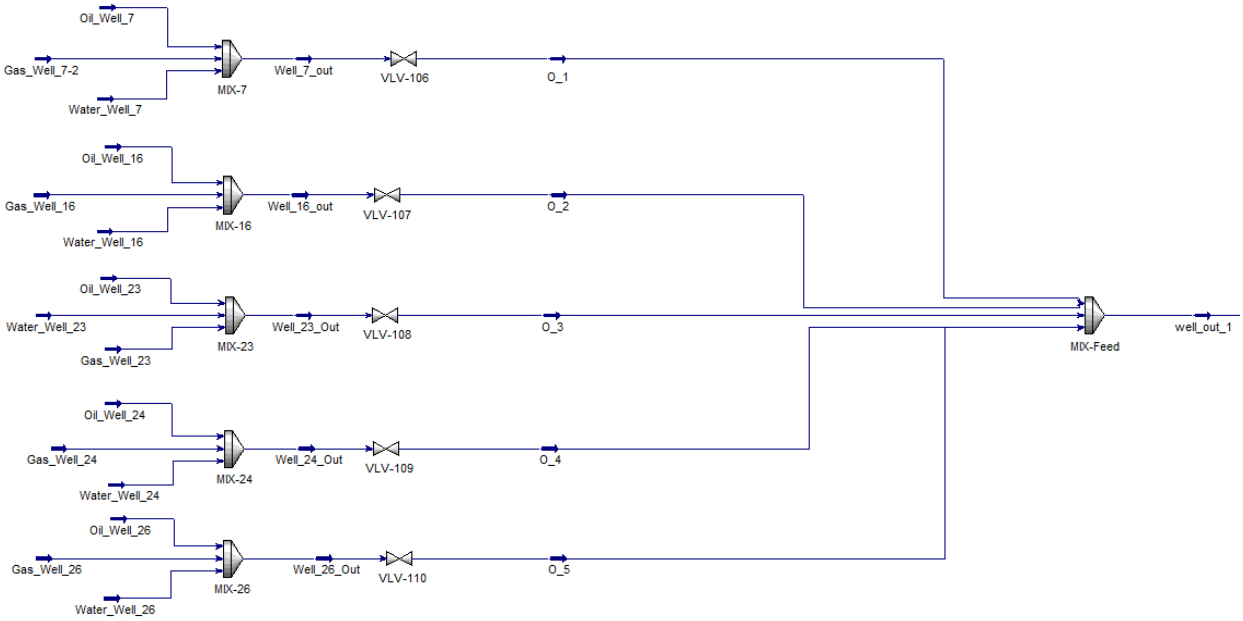

Fig. 3.4: Process flowsheet of the well trajectory.

Operating characteristics for all the valves are considered as linear, and usually they remain open for 50%. Cg, ANSI/ISA, and rigorous Cp/Cv method is selected for sizing the valves. The values for all valve sizing are shown in Table 3.4.

Table 3.4: The sizing values for all the valves used in well trajectory.

Valves	Delta P (kPa)	FI	Cv	Cg	Fp	Xt
VLV-106	5800	0.9000	131.2	4389.5	1.0000	0.70000
VLV-107	4100	0.9000	214.6	7183.1	1.0000	0.70000
VLV-108	9250	0.9000	142.4	4766.6	1.0000	0.70000
VLV-109	1500	0.9000	193.7	6484.0	1.0000	0.70000
VLV-110	1650	0.9000	193.6	6478.8	1.0000	0.70000

The output streams from the valves are defined by 0_1, 0_2, 0_3, 0_4, 0_5. The pressure, temperature, and flow rate of each input/output stream are observed which is shown in Table 3.5.

Table 3.5: The streams and their corresponding properties in well section.

Stream	Pressure (kPa)	Temperature (˚C)	Flowrate (Sm^3/h)
well_7_out	13100	88.98	75870
O_1	7300	80.22	75870
well_16_out	11400	89.67	89520
O_2	7300	81.04	89520
well_23_out	16600	90.17	103200
O_3	7350	77.79	103200
well_24_out	8800	81.58	84460
O_4	7300	76.89	84460
well_26_out	8900	80.21	78480
O_5	7250	75.26	78480

All the output streams from the valves are combined in a mixer (Mix-Feed) and finally leaves (wel_out_1) from mixer with 78.27˚C temperature, 7250 kPa pressure, and 431600 Sm^3/h flow rate.

3.3.2 Separator Unit

The HYSYS design diagram for separator unit is shown in Fig. 3.5. The stream (well_out_1) from production manifold is fed to the first stage of the three phase separator.

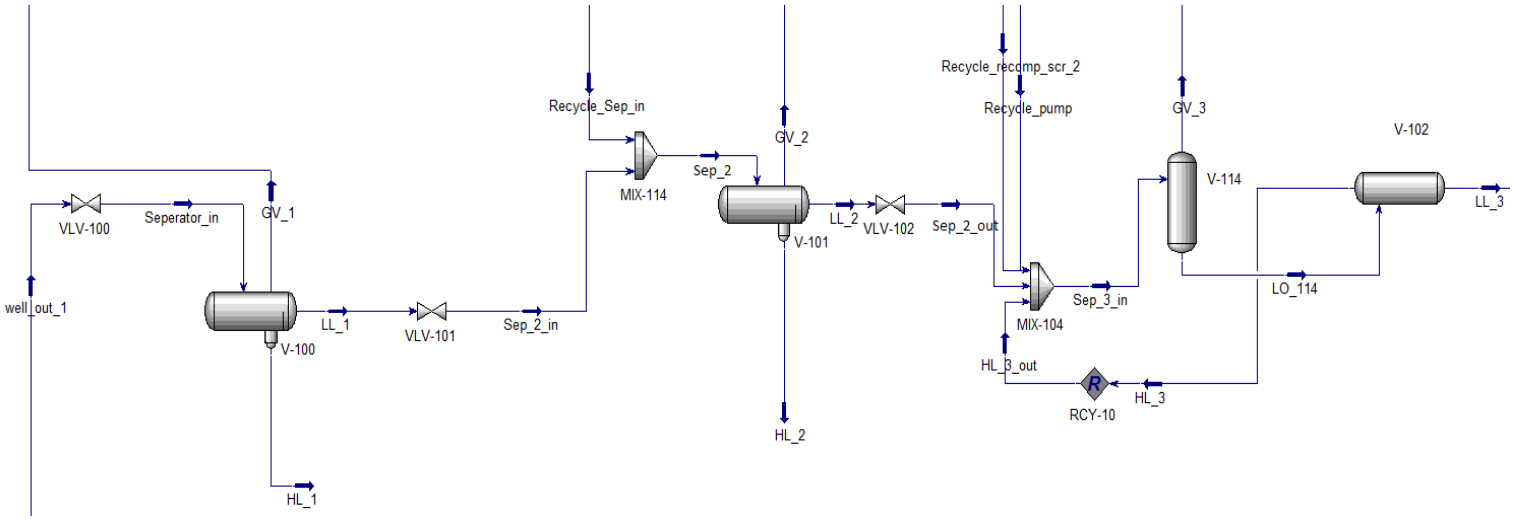

Fig. 3.5: Process flowsheet of the separation unit.

'Basic-1' is selected for a fluid vessel package for all the separators. The Pressure drop (Delta P) inside the vessel is 200 kPa. The feed stream is separated into vapor, 'GV_1', light liquid, 'LL_1', and heavy liquid, 'HL_1' fractions, where 'GV_1' goes to the reinjection section, 'HL_1' (oily water) goes for further processing (not shown), and 'LL_1' is mixed with combined recycles coming from reinjection unit, first and third stage, recompression unit and fuel treatment unit and fed to second stage three phase separator (V-101). The properties of these streams are shown in Table 3.6.

Table 3.6: Properties of the separated oil, gas and water in first stage three phase separator.

Stream	Pressure (kPa)	Temperature (˚C)	Flowrate (Sm^3/h)
Seperator_in	7000	77.66	431600
GV_1	6800	76.99	368200
LL_1	7000	77.66	102.9
HL_1	7000	77.66	34.31

The outputs of the separator, vapor fraction (GV_2) goes to the recompression second stage scrubber, 'HL_2' (oily water) goes for further processing before released into the sea. The light liquid 'LL_2' is mixed with the recycles coming from the second stage recompression scrubber, pump unit, and electrostatic coalescer (two-phase separator) in mixer, MIX-104 and fed to the third stage two-phase separator and divided into vapor, GV_3 and light liquid, LO_114. The, GV_3 goes to the first stage scrubber of the recompression unit, and LO_114 is entered to the electrostatic coalescer (two-phase separator). Finally, the output (LL_3) from the coalescer goes to the pump unit. The operating conditions of the streams are given in Table 3.7 and 3.8.

Table 3.7: Properties of the incoming and outgoing streams in second stage, three phase separator.

Stream	Pressure (kPa)	Temperature (˚C)	Flowrate (Sm^3/h)
Sep_2_in	850	70.86	102.9
Recycle_Sep_in	852	12.51	32.87
Sep_2_in_F	850	54.56	135.3
GV_2	850	54.56	8366
LL_2	850	54.56	112.8
HL_2	850	54.56	1.936

Table 3.8: Properties of the incoming and outgoing streams in third stage, 2-phase separator.

Stream	Pressure (kPa)	Temperature (˚C)	Flowrate (Sm^3/h)
Sep_2_out	280	51.09	112.8
Sep_3_in	280	50.21	153.4
GV_3	280	50.21	4.415
LO_114	280	50.21	149.6

Sizing values for all the valves used in separation unit are shown in Table 3.9.

Table 3.9: The sizing values for valves used in separation section.

Valves	Delta P (kPa)	FI	Cv	Cg	Fp	Xt
VLV-100	250	0.9000	3660	1.2249e+005	1.000	0.70000
VLV-101	6150	0.9000	27.34	914.98	1.000	0.70000
VLV-102	570	0.9000	97.64	3267.8	1.000	0.70000

3.3.3 Export Pump Unit

The light liquid output, 'LL_3' from the separator unit is entered to the pump, P-100 of the export pumping unit. The adiabatic efficiency of the pump is 75%, pressure drop (Delta P) is 1050 kPa, and the pressure ratio is 4.750. The duty of the pump is calculated for 60.5739 kW. The pump output, 'cooler_1_in' then goes to the splitter, 'TEE-106'. It splits into 'Tee_out_1' and 'Tee_out_2', where the flow ratio is 0.1317 and 0.8683 respectively. The HYSYS design diagram for the Pump unit is shown in Fig. 3.6.

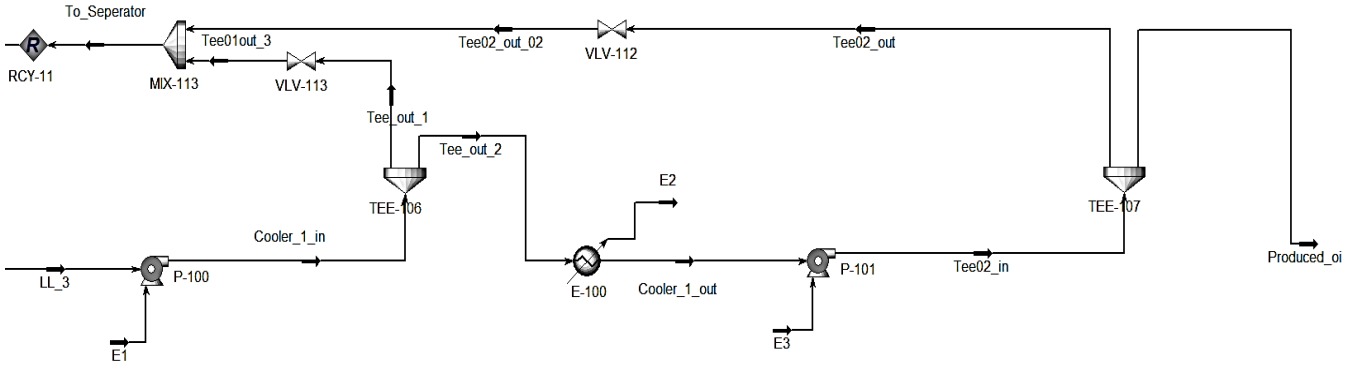

Fig. 3.6: Process flowsheet of the export pump unit.

The stream, 'Tee_out_2' goes to the cooler, E-100 where the Delta P, Delta T and the Duty of the cooler is 49.00 kPa, -2.606˚C, and 5.485e5 kJ/h, respectively. The output stream from the cooler, 'cooler_1_out' is entered to the second pump, P-101. The properties of the pump such as adiabatic efficiency, Delta p, pressure ratio, and the calculated duty is found 75%, 1939 kPa, 2.514 and 96.7338 kW respectively. The output stream, 'tee02_in' from the pump is fed to the second splitter (TEE-107) and divided into 'tee02_out' with 15% flow and 'Produced_oil' with 85% flow ratio respectively. The 'tee02_out' stream is combined with 'Tee_out_1' and recycled to the separation unit where 'Produced_oil' is exported to the transportation pipeline. The pressure, temperature, and flow rate for each stream in the pump unit is shown in Table 3.10.

Table 3.10: Properties of the stream in third stage, 2-phase separator.

Stream	**Pressure (kPa)**	**Temperature (˚C)**	**Flowrate (Sm^3/h)**
Cooler_1_in	1330	50.61	149.6
Tee_out_1	1330	50.61	19.71
To_Seperator	280	50.62	39.42
Tee02_in	3220	48.71	129.9

Tee01out_3	280	51.08	19.71
Tee02_out_02	280	50.16	19.71
Tee_out_2	1330	50.61	129.9
Cooler_1_out	1281	48	129.9
Tee02_out	3220	48.71	19.71

The sizing values of the valves used in this unit is given in Table 3.11.

Table 3.11: The sizing values for valves used in export pump section.

Valves	**Delta P (kPa)**	**FI**	**Cv**	**Cg**	**Fp**	**Xt**
VLV-112	2940	0.9000	7.497	250.90	1.000	0.70000
VLV-113	1050	0.9000	12.58	420.88	1.000	0.70000

3.3.4 Recompression Unit

The separated vapor phase, ‘GV-3’ from the third stage separation unit, is combined with the recycle, ‘Test_Recy_out’ and entered to the first stage recompression scrubber, V-103. Inlet delta P of the scrubber is calculated for 39 kPa. The vapor output, ‘GV_4’ from the scrubber is entered to the compressor, K-100. The operational mode of the compressor is centrifugal, adiabatic efficiency is 47, polytropic efficiency is 49.427, Delta P is 331 kPa, pressure ratio is 2.373, and calculated duty is 99.5221 kW. The HYSYS design diagram for the Recompression unit is shown in Fig. 3.7.

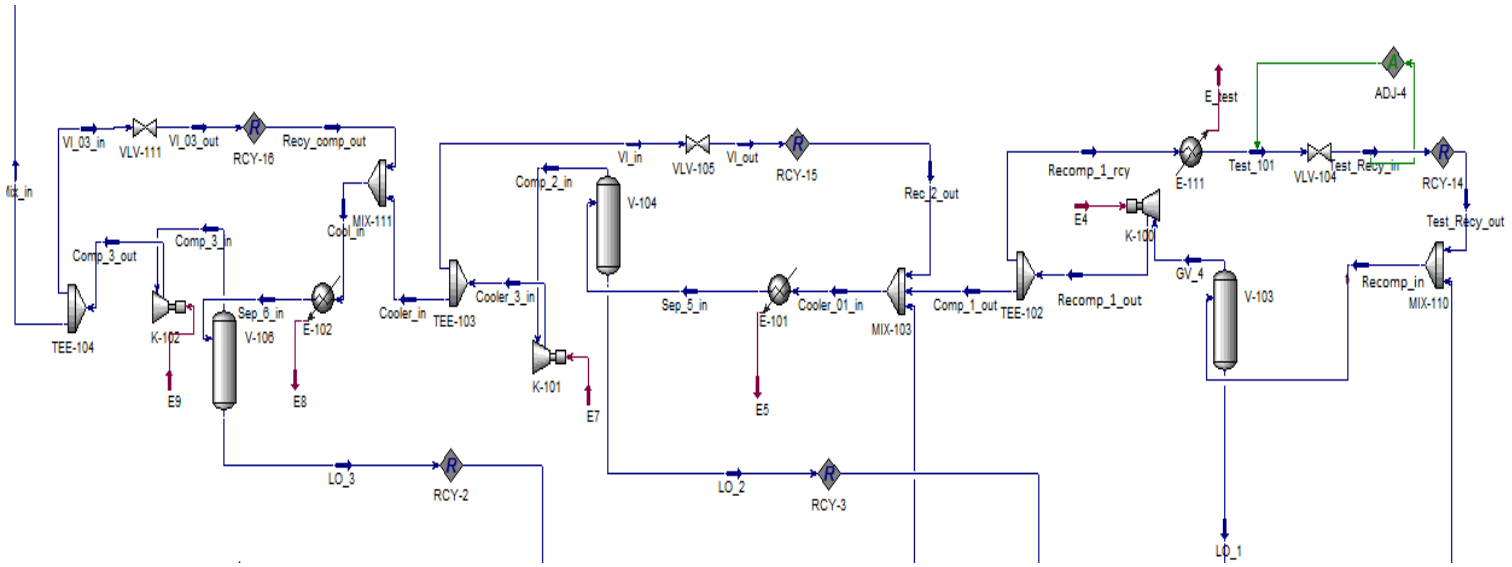

Fig. 3.7: Process flowsheet of the gas recompression unit.

The compressor output, ‘Recomp_1_out’ is divided into ‘comp_1_out’ and ‘Recomp_1_rcy’ in the splitter, Tee-102. The output stream, ‘comp_1_out’ goes to the second stage recompression input and ‘Recomp_1_rcy’ is recycled to the system via a cooler, E-111. The flow ratio of these streams is 0.7471 and 0.2529 respectively. Delta T of the cooler is -60.54˚C and the Duty is 1.123e5 kJ/h. An adjust block, ADJ-4 is used to keep the temperature consistent (specified target value is 40˚C), where ‘Test_101’ is set as an adjusted variable, and ‘Test_Recy_In’ is set as a target variable. The condensation, ‘LO_1’ from the scrubber (V-103) is recycled to the second stage, three phase separator by using a drainage pump, P-102. The compressor output, ‘Comp_1_out’ is entered to a cooler, E-101 after mixing with vapor, ‘GV_2’ and the recycle, ‘Rec_2_out’ streams. Delta T of the cooler is -54.42 C and the Duty is 2.452e6 kJ/h.

The cooler output goes to the second stage recompression scrubber, V-104 where the inlet delta P of the scrubber is found 55 kPa. The vapor output, ‘comp_2_in’ from the scrubber is entered to the compressor, K-101. The operation mode of the compressor is centrifugal and the

properties such as adiabatic efficiency, polytropic efficiency, Delta P, pressure ratio, and calculated duty is 69, 71.853, 1383 kPa, 3.675, and 777.656 kW respectively. The compressor output, 'cooler_3_in' is divided into two streams in the splitter, Tee-103, where 'cooler_in' stream (68% flow) goes to the third stage recompression and 'VI_in' stream (32% flow) recycled to the system. The condensation, 'LO_2' from the scrubber is combined with other recycle streams from different units and goes to the third stage, two-phase separator.

Similarly, the third stage recompression follows the same procedures as the second stage. The output stream, 'cooler_in' is entered to the third stage recompression unit and mixed with the recycle system. Then it goes to the scrubber, V-106 through a cooler, E-102. Inlet delta P of the scrubber is 60 kPa, Delta T of the cooler is -92.64˚C and the Duty is 3.651e6 kJ/h. The scrubber output, 'Comp_3_in' goes to the compressor, K-102 where the adiabatic efficiency, polytropic efficiency, Delta P, pressure ratio, and the duty of the compressor is calculated 56, 60.606, 5160 kPa, 3.804, and 811.988 kW respectively. The condensation, 'LO_3' from the scrubber is recycled to the second stage, three-phase separator after combining with other recycles from different units. The compressor output, 'Comp_3_out' is divided into two streams where stream, 'Mix_in' (71% flow) goes to the third stage recompression and 'VI_03_in' (0.2895% flow) recycled to the system. The values of all streams in the recompression unit are shown in Table 3.12.

Table 3.12: Properties of the stream in gas recompression unit.

Stream	**Pressure (kPa)**	**Temperature (˚C)**	**Flowrate (Sm^3/h)**
Sep_5_in	572	22	13900
Sep_6_in	1900	24	12640
Recomp_in	280	47.87	5.909
Rcomp_1_rcy	572	112.1	1.495

comp_1_out	572	112.1	4.415
Recy_comp_out	1900	127.8	3417
comp_2_in	517	20.52	13500
comp_3_in	1840	23.35	11800
Gv_4	241	46.02	5.91
Cooler_in	1900	112.9	9222
VI_in	1900	112.9	4276
Rec_2_out	578	106	4277
cooler_3_in	1900	112.9	13500
comp_3_out	7000	146.3	11800
Recomp_1_out	572	112.1	5.91
Mix_in	7000	146.3	8383
VI_03_in	7000	146.3	3416
Test_Recy_out	280	40.07	1.495

And the sizing values for all the valves are shown in Table 3.13.

Table 3.13: Sizing values of the valves in recompression section.

Valves	**Delta P (kPa)**	**FI**	**Cv**	**Cg**	**Fp**	**Xt**
VLV-104	292	0.9000	14.62	489.33	1.0000	0.70000
VLV-105	1322	0.9000	39.91	1335.6	1.0000	0.70000
VLV-111	5100	0.9000	8.080	270.42	1.0000	0.70000

3.3.5 Reinjection Unit

The vapor output, ‘Inject’ from the first stage, three-phase separator is combined with recompression unit output, ‘Mix_in’ and entered to a splitter, ‘TEE-101’. The output is divided into three parallel flow streams which is shown in Figure 3.8.

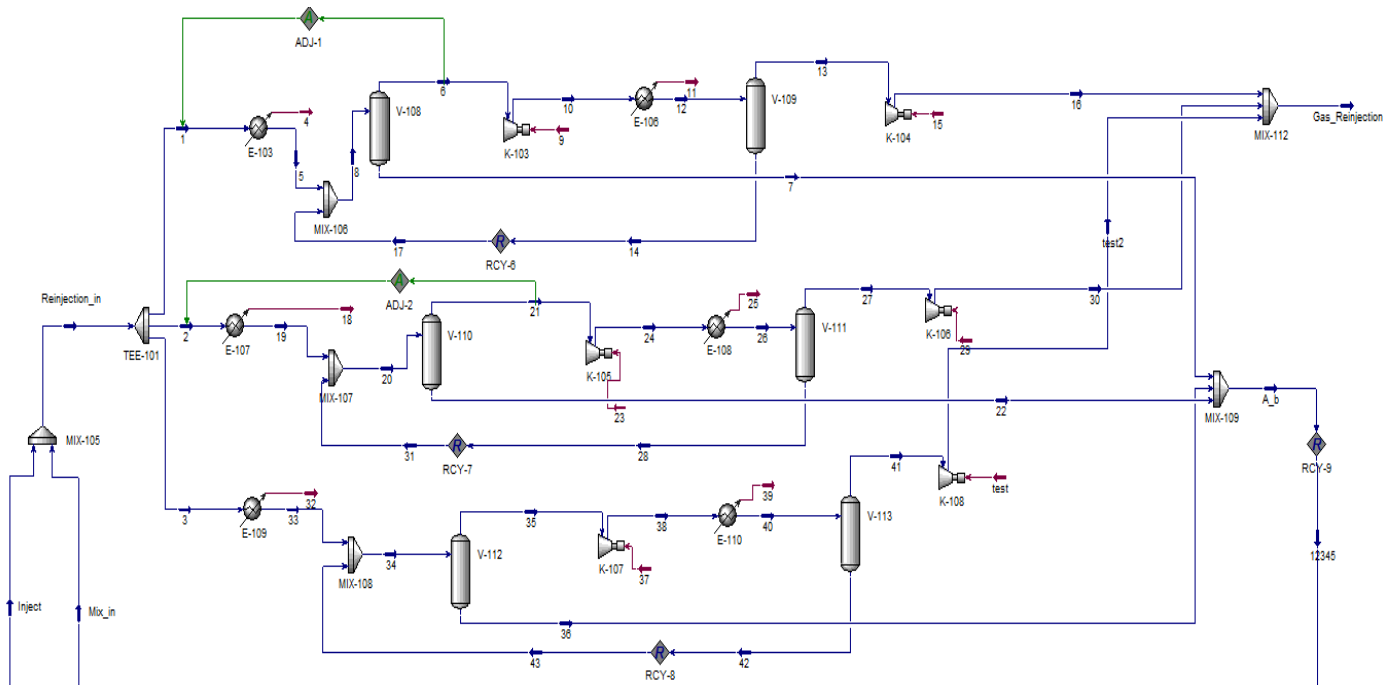

Figure 3.8: Process flowsheet of the gas reinjection unit.

Flow ratio of the stream '1', '2' and '3' is found 26%, 28% and 46% respectively. All the three parallel reinjection units is followed the same process. Stream, '1' enters to the cooler E-103, where the Delta T and the duty is calculated -50.87˚C and 1.257e7 kJ/h. The output stream, '5' of the cooler is combined with the condensation recycle from the second stage scrubber and entered to the first stage scrubber, V-108. The scrubber output, '6' is entered to the first stage compressor, K-103 and the condensation, '7' is combined with all the other condensations from the reinjection unit. The operation mode of the compressor is centrifugal and the properties such as adiabatic efficiency, polytropic efficiency, Delta P, pressure ratio, and calculated duty is 64, 66.526, 7050 kPa, 2.054, and 2698.74 kW respectively. An adjust block, ADJ-1 is used in between vapor output, '6' and cooler inlet, '1'. Liquid volume flow (std condition) is chosen as an adjusted variable of object stream '1' and actual volume flow is selected as a target variable of object stream '6'. The specified target value is set at 1150 m^3/h. The compressor output, '10'

goes to the cooler, E-106 where the Delta T and calculated duty of the cooler is found -68.87˚C, and 1.586e7 kJ/h. The output stream, '12' from the cooler is entered to the second stage scrubber, V-109. Scrubber vapor output, '13' is entered to the second stage compressor, K-104 and the condensation stream, '14' is recycled to the system. Mode of operation of the compressor is centrifugal and the adiabatic efficiency, polytropic efficiency, Delta P, pressure ratio, and the duty of the compressor is calculated 54, 56.183, 9860 kPa, 1.718, and 2195.11 kW respectively. Then output stream, '16' from the compressor is combined with other outputs from different reinjection stages. The values of all the parameters are shown in Table 3.14.

Table 3.14: Stream properties in first stage gas reinjection unit.

Stream	**Pressure (kPa)**	**Temperature (˚C)**	**Flowrate (Sm^3/h)**
1	6800	78.87	92700
5	6800	28	92700
8	6800	28	92720
6	6690	27.59	90320
10	13740	96.87	90320
12	13740	28	90320
13	13740	28	90300
16	23600	78.25	90300

Similarly, the second and third reinjection unit follows the same process. The stream, '2' enters to the cooler E-107 where the Delta T and the duty of the cooler is calculated -50.87˚C, and 1.382e7 kJ/h. An adjust block 'ADJ-2' is used between vapor output, '21' and cooler inlet, '2'. The liquid volume flow (std condition) is chosen as an adjusted variable of object stream, '2' and actual volume flow is selected as a target variable of object stream, '21'. The specified target value is set at 1300 m3/h. The properties of the compressor, K-105 such as adiabatic efficiency,

polytropic efficiency, Delta P, pressure ratio, and calculated duty is 64, 66.538, 7110 kPa, 2.063, and 2686.44 kW respectively. The compressor output, '24' is entered to the cooler, E-108 where the Delta T and the duty of the cooler is found -69.30˚C and 1.756e7 kJ/h. The output of the scrubber (V111), '27' goes to the compressor, K-106, where the adiabatic efficiency, polytropic efficiency, Delta P, pressure ratio, and the duty of the compressor is calculated 57, 59.026, 9800 kPa, 1.710, and 2265.26 kW respectively. The values of the parameters in second unit are shown in Table 3.15.

Table 3.15: Stream properties in second stage gas reinjection unit.

Stream	**Pressure (kPa)**	**Temperature (˚C)**	**Flowrate (Sm^3/h)**
2	6800	78.87	101900
19	6800	28	101900
20	6800	28	101900
21	6690	27.59	99280
24	13800	97.3	99280
26	13800	28	99280
27	13800	28	99260
30	23600	76.03	99260

The stream, '3' is entered to the cooler, E-109 where the Delta T and the duty is found -50.87˚C, and 2.333e7 kJ/h. The properties of the compressor, K-107 such as adiabatic efficiency, polytropic efficiency, Delta P, pressure ratio, and calculated duty is 69, 71.202, 6775 kPa, 2.056, and 4649.98 kW respectively. The compressor output stream, '38' enters to the cooler, E-110 where the Delta T and assessed duty is found -64.80˚C and 2.747e7 kJ/h. The output of the scrubber (V113), '41' goes to the compressor, K-108, where the adiabatic efficiency, polytropic

efficiency, Delta P, pressure ratio, and the duty of the compressor is calculated 64, 65.898, 1066 kPa, 1.824, and 3854.11 kW respectively. Finally, the combined output stream 'Gas_ Reinjection' injected to the reservoir. The values of the parameters for the third unit are shown in Table 3.16.

Table 3.16: Stream properties in third stage gas reinjection unit.

Stream	Pressure (kPa)	Temperature (˚C)	Flowrate (Sm^3/h)
3	6800	78.87	172000
33	6800	28	172000
34	6800	28	172100
35	6415	26.54	167500
38	13190	92.8	167500
40	13190	28	167500
41	12940	27.28	167400
test2	23600	78.24	167400

3.3.6 Fuel Treatment Unit

The vapor output, 'GV_1' splits (in TEE-100) into two streams, 'Treatment' and 'Inject', where the flow ratio is found 2.716e-2 and 0.9728, respectively. Then stream 'Treatment' is entered to the cooler, E-104, where Delta T and the duty is found -28.99˚C and 7.609e5 kJ/h. The diagram for the fuel treatment unit is shown in Fig. 3.9.

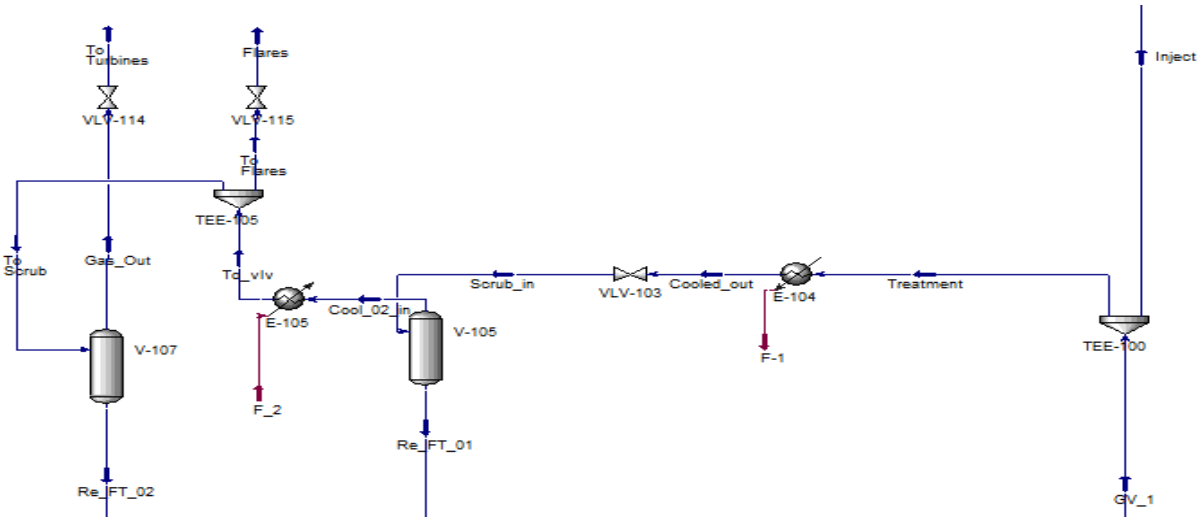

Fig. 3.9: Process flowsheet of the fuel treatment unit.

The output stream, 'cooled_out' goes to the first scrubber, V-105 where the vapor output, 'Cool_02_in' is entered to the heater, E-105. The condensate stream, 'Re_FT_01' recycled to the second stage, three-phase separator. The parameters of the heater such as Delta P, Delta T, and the duty is calculated 40.00 kPa, 26.93 ˚C and 533958 kJ/h respectively. Output stream, 'To_vlv' from heater, splits (in TEE-105) into 'To Flares' and 'To scrub' streams where the flow ratio is 3.243e-2 and 0.9676 respectively. The 'To Flare' stream leaves as flare gas from the system where the 'To scrub' stream enters to the second scrubber, V-107. The vapor output, 'To Turbines' from the scrubber goes to the turbine unit to generate the necessary power of the platform. The condensation stream, 'Re_FT_02' is recycled to the second stage, three-phase separator after combining with other recycles of the system.

3.4 Results

Results from the model validation and the simulation scenarios are presented in this section. Steady-state simulation is compared with production data from the existing system.

3.4.1 Model validation

The model is validated with operational data from an existing well provided by (Voldsund et al., 2013). The comparison was made for different parameters such as pressure, temperature, and flow rate. The results from the validation of oil volume flow rate and pressure are shown in Tables 3.17 and 3.18.

Table 3.17: Validation result of fluid flow rate against measured data from Voldsund et al., 2013.

Produced Fluid	**Unit**	**Measured data**	**Predicted Value**	**Percentage Error**
Export Oil	Sm^3/h	132.5 ± 0.4	110.2	16.5%
Reinjection Gas	10^3 Sm^3/h	369 ± 17	357	1.4%
Produced Water	Sm^3/h	67 ± 5	37	40%
To Flares	Sm^3/h	335 ± 14	320	0.31%
To Power Turbines	Sm^3/h	9630 ± 170	9546	0.9%

Table 3.18: Validation result of Pressure value against measured data from Voldsund et al., 2013.

Produced Fluid	**Unit**	**Measure data**	**Predicted Value**	**Percentage Error**
Export Oil	bar	32.1 ± 0.3	32.2	1.25%
Reinjection Gas	bar	236 ± 2	236	0.85%
Produced Water	bar	8.77 ± 0.09	70.0	706%
To Flares	bar	9.30 ± 0.09	9.30	0.97%
To Power Turbines	bar	18.25 ± 0.18	18.25	0.99%

The predicted values match well with the measured values for most cases except for produced water. In the real system, one or more mechanical valve has been used for water pressure drop which is not described in the reference (Voldsund et al., 2013) as such the conditioned assumed in the present work is significantly different and may have led to the discrepancy.

3.5 Conclusions

This work was focused on the steady-state simulation of an offshore oil and gas processing plant. The North Sea offshore platform has been modeled using the HYSYS plant simulator. The models have been formulated considering the producing wells and surface units such as separation, export pumping, recompression, reinjection units, etc. The data generated from each unit of the model are recorded, and the results presented in this work are compared and validated with a performance assessment of a real-case oil and gas platform located in the Norwegian part of the North Sea. The result and discussion conclude that this steady-state model successfully met all the requirements similar to the real processing platform. The model outcome approximately matched with the actual production data except for the produced water form first and the second stage three-phase separator. This is because of maintaining the pressure requirement of the separator output (oil and gas, reported in table 3.6), the water pressure is also significantly increased, which is not identical with the water pressure in real case scenario.

References

Aspen Technology. Aspen Energy Analyzer. Burlington, USA, 2008.

Aspen Technology. Aspen Flare System Analyzer – Getting Started Guide. Burlington, USA, 2011.

Belsim. Belsim VALI User's Guide. Belsim, 2011.

Bai, Q., & Bai, Y. (2014). Subsea pipeline design, analysis, and installation. Gulf Professional Publishing.

Bull, A. S., & Love, M. S. (2019). Worldwide oil and gas platform decommissioning: A review of practices and reefing options. Ocean & Coastal Management, 168, 274–306. https://doi.org/10.1016/j.ocecoaman.2018.10.024

Devold, H. (2013). Oil and gas production handbook: an introduction to oil and gas production. Lulu. com.

Feliu, J., Grau, I., Alos, M., & Macias-Hernandez, J. (2003). Match Your Process Constraints Using Dynamic Simulation. Chemical Engineering Progress, 99(12), 42-48.

Hangos, K., & Cameron, I. (2001). Process modelling and model analysis (Process systems engineering ; v. 4). San Diego: Academic Press

Hyvärinen, L. (1970). Mathematical Modeling for Industrial Processes. https://doi.org/10.1007/978-3-642-87427-7

Mokhatab, S., & Towler, B. (2007). Dynamic Simulation of Offshore Production Plants. Petroleum Science and Technology, 25(6), 741-757.

Nguyen, T. V., Elmegaard, B., Breuhaus, P., & Haglind, F. (2014). Modelling, analysis and optimization of energy systems on offshore platforms. DTU Mechanical Engineering.

Process Systems Enterprise. gPROMS Introductory User Guide. London, UK, 2004.

Peng, D.-Y., & Robinson, D. B. (1976). A New Two-Constant Equation of State. Industrial & Engineering Chemistry Fundamentals, 15(1), 59–64. https://doi.org/10.1021/i160057a011

Stephanopoulos, G. (2009). Process Systems Engineering: From Solvay to the 21st Century. A History of Development, Successes and Prospects for the Future. In Computer Aided Chemical Engineering (Vol. 27, pp. 149–155). https://doi.org/10.1016/S1570-7946(09)70246-9

Thomas, P. (1999). Simulation of Industrial Processes for Control Engineers. Elsevier Science.

Voldsund, M., Ertesvåg, I. S., He, W., & Kjelstrup, S. (2013). Exergy analysis of the oil and gas processing on a North Sea oil platform a real production day. Energy, 55, 716–727. https://doi.org/10.1016/j.energy.2013.02.038

Chapter 4

Dynamic Simulation of Offshore Gas Processing Plant for Normal and Abnormal Operations

Muhammad Shalauddin Khaled, Syed Imtiaz*, Salim Ahmed, and Sohrab Zendehboudi

Department of Process Engineering

Faculty of Engineering and Applied Science,

Memorial University of Newfoundland, St.

John's, Newfoundland, Canada.

A version of this chapter has been prepared for submission as a journal article. Muhammad Shalauddin Khaled developed this work under the direction and supervision of Dr. Syed Imtiaz, Dr. Salim Ahmed, and Dr. Sohrab Zendehboudi. They provided continuous technical guidance, checked the results, reviewed the manuscript, and modified the final version of the manuscript. In this chapter, the manuscript is presented with altered figure numbers, table numbers and reference formats in order to match the thesis formatting guidelines set out by Memorial University of Newfoundland.

Abstract

Offshore oil and gas production is contributing to almost 30% of the total global oil and gas production. Since access to the offshore facilities is difficult, there is interest in monitoring the production facilities remotely. Multivariate statistical methods can be effectively used to monitor the offshore gas production plant. In this research work, monitoring of an offshore production plant is described. To demonstrate the monitoring cycle, a benchmark model for the offshore facilities is required. Mathematical modeling and simulations are useful tools for designing and predicting the accurate behavior of a production plant. As the first phase, we simulate an offshore oil and gas production plant using the process modeling tool, Aspen HYSYS. The model is based on the process specifications of a gas processing plant at the North Sea platform reported by Voldsund et al. (2013). Several common faults from different fault categories, such as actuator faults and disturbances, are introduced and simulated in the dynamic system. A total of seven dynamic scenarios are investigated, and their impacts on the overall hydrocarbon production are analyzed. According to the results, the dynamic simulation can accurately generate the system response, including responses during faulty conditions. The simulations files, normal, and abnormal data are made available electronically. The developed model can be used as a benchmark system to test monitoring algorithms for offshore production facilities. In the second phase, we will describe the monitoring scheme for the plant.

Keywords: Aspen HYSYS, Offshore production facilities, Process modeling, Dynamic simulation, Disturbance, Actuator fault

4.1 Introduction

Offshore production and processing facilities are located in remote locations and are exposed to extreme conditions. Recently, due to digitalization initiatives by the offshore industries, interest in real-time optimization and remote monitoring of offshore production and processing facilities has increased. One of the main prerequisites for building optimization and monitoring tools is to have a high fidelity model for the system. Several researchers have worked on developing a model for offshore production facilities, primarily using commercial simulators (e.g., Aspen HYSYS, Aspen Plus, and Pro II). A list of relevant literature is presented in Table 4.1.

Table 4.1: Summary of modelling and simulation of offshore oil and gas production facility.

Researchers	Application case	Objective	Contributions and findings
(Cho et al., 2018)	Conceptual steady-state modeling of an offshore topside process.	Analyze to improve the environmental standards, reduce utility consumption, and maximize profit.	a. The use of recycling streams increases peak oil, gas, and water production rate. b. Higher and lower economic profits are gained during peak oil production and water production, respectively. c. Additional multi-stage separation increases the capital costs, which are the highest during peak gas production and lowest during peak water production.
(Nguyen et al., 2016)	Steady-state analysis of three actual Norwegian platforms in the North Sea and one platform in the Norwegian Sea.	Reduce the electrical or thermal energy used in the plant by modifying the system.	a. They proposed the following strategies for energy savings: re-designing of units, re-dimensioning the compressors, promoting energy and process integration, implementing multiphase expanders, and using waste heat recovery cycles. b. Up to 20% energy savings and reduction in CO_2 emissions are possible where the highest energy can be saved in anti-surge recycling.
(Nguyen et al., 2014a)	A steady-state model for a Norwegian Sea	Exergy analysis to measure energy	a. Most exergy destruction happens for the rejection of high-temperature exhaust

	offshore platform was developed and calibrated, based on measured data and engineering assumptions.	consumption and exergy destruction /losses.	gases, gas turbines, heat exchanges, compression, and anti-surge recycling operations. b. Several steam Rankine and low-temperature power cycle configurations were proposed and evaluated based on their investment costs and thermodynamic performance.
(Nguyen et al., 2014b)	A steady-state model for an offshore plant located at the Norwegian Continental Shelf region, called the Draugen Platform, was evaluated.	Energy and exergy efficiency analysis.	a. The highest exergy destruction happens in gas treatment (51%), recompression (12%), and production manifold (10%). b. Energy is mostly consumed in recompression and compression sections, condensate treatment, and glycol regeneration systems.
(Voldsund et al., 2014)	A steady-state model for four North Sea offshore platforms was analyzed and compared.	Exergy analysis to calculate exergy destruction.	a. The largest exergy destruction occurs in gas treatment and production manifold, which is 27% and 10%, respectively. b. Significant exergy destroys due to flaring in two of the platforms. c. Exergy destruction at fuel gas and seawater injection is less than 3%.
(Kim et al., 2014)	A conceptual stochastic steady-state simulation and optimization of an offshore platform	Find the maximum profit value calculated from the difference between product sales and operating costs for a multistage separation process.	a. Condensation recycling train has the ability to adjust the vapor pressure of crude oil. b. An increase in the separation stage also improves the system performance. c. Condensation recycling increases profits more than increasing the number of separation stages.
(Voldsund, et al., 2013)	Steady state modeling and simulation of a real production day on North Sea platform using measured process data.	Exergy analysis to measure maximum and minimum exergy destruction.	a. Exergy destruction occurs in processes where pressure increases and decreases, such as compression trains, pressure reduction valves, and recycling. b. Most exergy destruction takes place in reinjection trains (10,400 kW), production manifold (4600 kW), and recompression train (4150 kW).
(Nguyen et al., 2013)	Conceptual steady-state modeling of processes on the North Sea oil and gas platforms.	Exergy analysis to calculate and find the most contributing exergy destruction and the corresponding units.	a. Most exergy is destroyed by about 65% in power generation and waste heat recovery and 35% in oil, gas, and water processing system. b. Most exergy losses are due to the rejection of high-temperature exhaust gases from utility and flaring system.

			c. Exergy destruction combustion chambers can be reduced by decreasing the overall air-to-fuel ratio. d. Exergy losses in heat recovery can be partly recovered by using a bottoming cycle such as an organic Rankine cycle. e. Exergy losses in the flaring system can be reduced by limiting continuous flaring and recovering the gases in the processing plant.
(Voldsund et al., 2012)	Steady-state simulation of an oil platform located in the North Sea based on a real production day with available measured process data.	Exergy analysis to calculate the power consumption and its applicability to improve system efficiency.	a. The highest exergy destruction is related to compression of the gas. b. With increasing the adiabatic compressor efficiencies by two percentages, the power consumption is reduced to 3% while exergetic efficiency is increased to 0.33. c. By eliminating the anti-surge recycling of the gas, the specific power consumption reduced to 15% while the exergetic efficiency is increased to 0.38.
(Natarajan & Srinivasan, 2010)	Dynamic simulation of a conceptual offshore oil and gas production platform.	Develop a dynamic model and multi-model based approach for process fault monitoring.	a. Three real case scenarios, such as normal, faulty, and maintenance activities, are simulated using a dynamic model. b. The proposed model can be applied in a distributed manner using the limited available computational resources. c. The proposed model can detect the faults earlier, while monolithic monitoring algorithms are not suited due to the variety of operating states.
(Mourad, et al., 2009)	A real case steady-state thermodynamic model for building a new unit of separation and compression process in Southern Algeria (USC).	Estimate the intermediate stage pressure to minimize cost.	a. Graphical representation, known as minimum compression energy, is efficient to determine the intermediate separation pressure values. b. Intermediate feedstocks in a multi-stage separation affect the shape of the compression energy curve as a function of pressure. c. Although the integration of separation batteries reduces the investment costs, it produces more gas and degrades the oil quality.
(Bahadori, et al., 2008)	Conceptual steady-state simulation of a four-	Optimize the adjusting appropriate separator	a. The quality of the produced oil is increased by around 0.4˚ and 0.5˚ API

	stage oil separation unit using the fluid properties of the Pazanan-Asmari reservoir in Iran.	pressure in a crude oil production unit.	for the summer and winter, respectively. b. The oil production rate is increased by 6 and 5 m^3/day during the summer and winter by optimizing separator pressure using the proposed split C7+ cuts method. c. Gas–oil ratio in the summer is higher than that in the winter, whereas the oil production rate in the winter is higher than that in summer. d. The quality of the produced crude oil in the winter is much better compared to the summer. The average API in the summer is 36.7˚, whereas the API in the winter is 38˚.
(Boyer & O'Connell, 2005)	Real case steady-state analysis based on the survey by Devon Energy Production Company, L.P. (Devon) on its G. A. Ray No. 93 oil and gas production plant.	Minimize the operating pressure of low-pressure separator in order to reduce flashing losses as well as increase the annual profit.	a. The sales price of the produced gas is increased to $6,896 per year after reducing the operating pressure of the low-pressure separators. b. The sale of potential methane gas has been increased to approximately 336,000 SCF/year. c. The recovered flash gas can also lower the emissions of volatile organic compounds and hazardous air pollutants.

Although a few models have been developed for offshore gas processing facilities, the models were primarily developed for design and optimization purposes. Hence, all reported models are steady-state models. To establish a real-time monitoring system, dynamic models are required, which are scarce in the literature for modeling/simulation of offshore production and processing plants. This causes real challenges/difficulties in developing and testing monitoring systems for offshore facilities. The goal of this research work is to develop a dynamic model for an offshore gas processing plant. The model presents appropriate noise and disturbances similar to actual plants. In addition, the model has a good fault description, and it is capable of simulating normal data as well as faulty data for a number of significant faults in the system.

4.2 Methodology for Building Process Model

The steps for making a process model are depicted in Fig. 4.1.

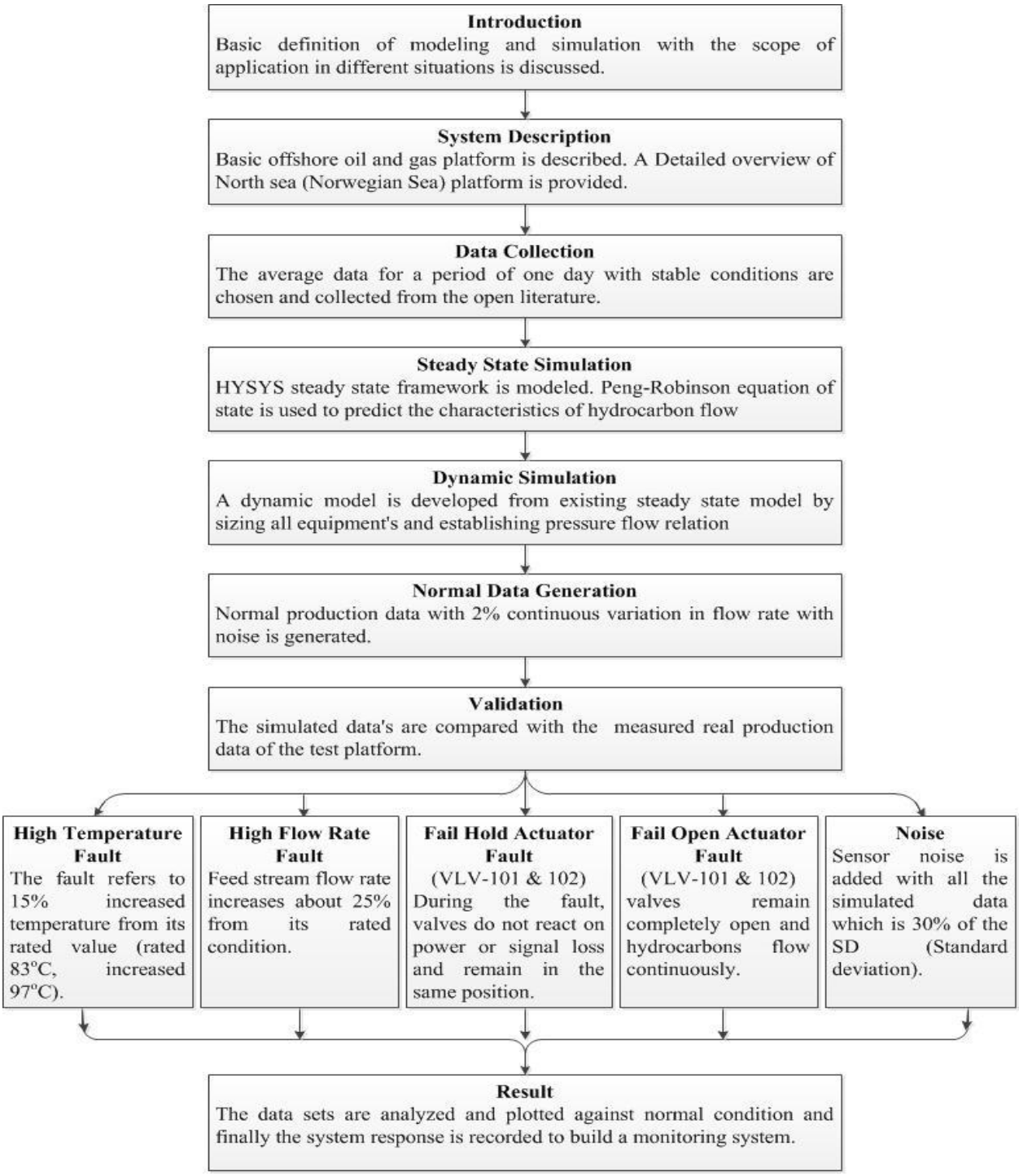

Fig. 4.1: Basic flowchart for modelling and simulation of the offshore production facility.

This section presents a general description of offshore oil and gas platforms and the steps for building the dynamic model, with particular focus on a facility located in the North Sea region. The present work is based on the model reported in (Voldsund et al., 2013). Aspen HYSYS is used to construct a steady-state model to analyze an oil and gas producing platform. In this paper, we extend the steady-state model to a dynamic model for studying the dynamic response of the system. First, a steady-state model is built using Aspen HYSYS. The simulation result is validated through extensive performance evaluation and comparison with real production data available in the literature (Voldsund et al., 2013). Some additional excitations are added with the feed system in the model using customized Aspen HYSYS functional block externally to simulate the normal variation in production data with time. The sensor noise description appropriate for the system is also designed and added with the responses to create more realistic reactions for the system. Finally, several common faults from different fault categories, for example, sensor fault, actuator fault, and disturbance fault are created and simulated in the dynamic system.

4.3 System Description

In this study, an actual oil-producing platform that has been in operation for more than 20 years in the Norwegian Sea is considered (Voldsund et al., 2013). It produces oil, gas, and water where the oil is transported to the nearby platform through the export pipelines, produced gas is recompressed and reinjected for pressure coverage, and water is neutralized and released in the sea. The plant can be categorized as a high gas-to-oil ratio with high feed pressure and temperature. The power requirement of this plant is approximately 25 MW, and the heating requirement is less than 1 MW. All the measurements are recorded for a typical production day.

4.3.1 Process Overview

The overall process is divided into several functional units, such as well section, production manifold, separator unit, export pump unit, recompressor, drainage system, fuel gas treatment, and reinjection unit. Five separate production wells with different fluid flow properties such as flow rate, pressure, and temperature are connected in the production manifold. The operating pressure of the well stream varies from 80 to 170 bar. The overall pressure is reduced to 70 bar before entering the separation process. The process flow diagram of the plant is shown in Fig. 4.2.

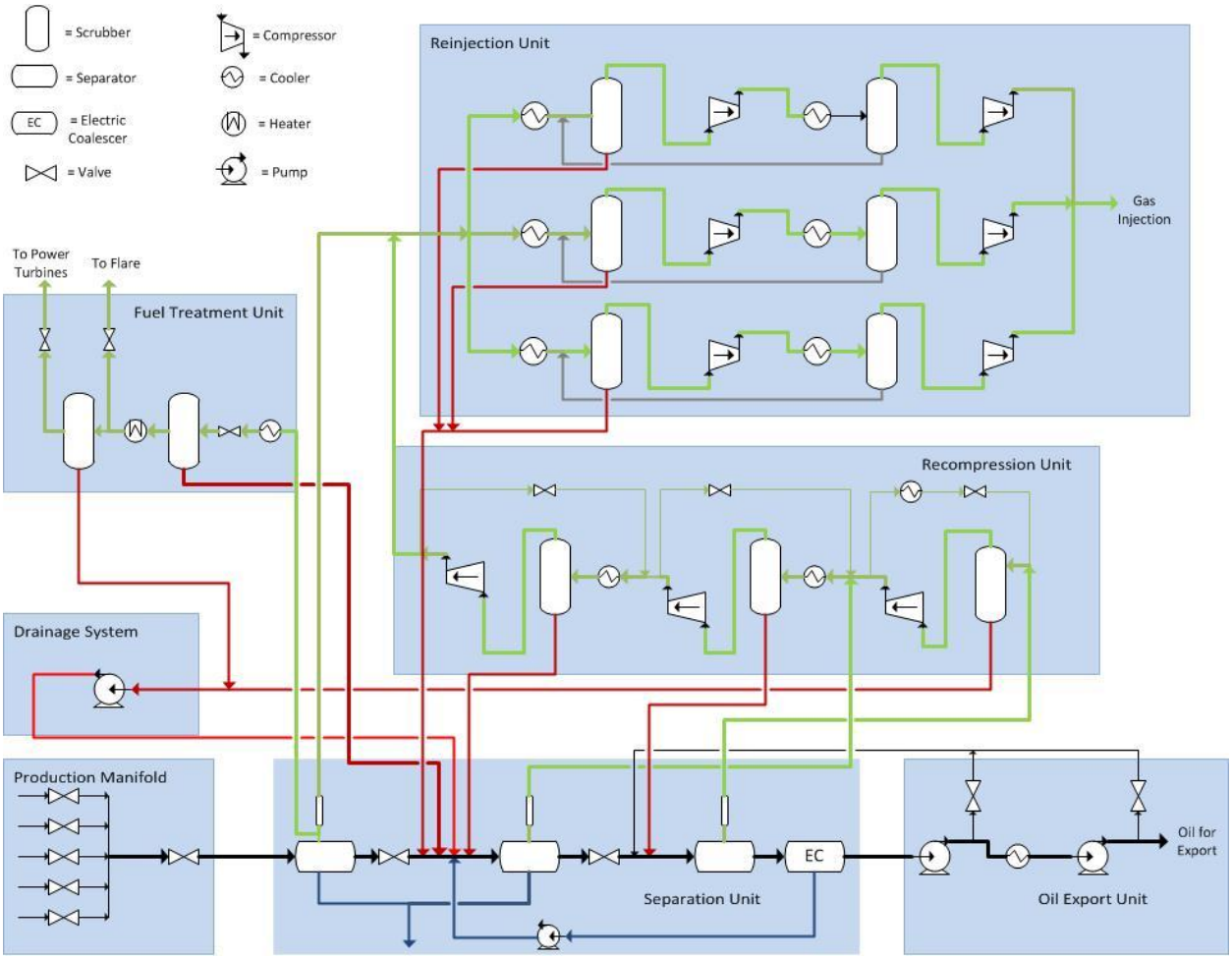

Fig. 4.2: Process flow diagram of the Norwegian Sea oil and gas platform with modifications.

The separation unit, shown in Figure 3, consists of two three-phase separators (V-100 and V-101), one two-phase separator (V-114), and one electrostatic coalescer (V-102). Gas, oil, and water are separated by using the gravitational separation. Before introducing a new separator, the pressure is reduced to optimize the final production. Separated oily water from the first and second stage of the three-phase separators enters the water treatment processing unit. A certain proportion of separated fluid (oil and water) is pumped and recycled back to the entry of the second stage, three-phase separator. Oil pressure of the coalescer output is reduced to 2.8 bar and the oil then goes to the export pump unit.

The export pump unit includes one cooler and two pumping sections where the produced oil is cooled and pressurized up to 32 bar. To make a consistent oil flow through the compressors, a certain amount of oil recycles back to the entry of the third stage, two-phase separator.

The recompression process unit is made of three sub-units, where each of them has one cooler, one scrubber, and one compressor. Scrubbers are used to remove the remaining water from gas, save the compressor from pressure hunting, and increase its efficiency. Gas from the third stage of the two-phase separator, with a pressure of 2.8 bar, enters the first stage recompression scrubber and is fed into the compressor to increase the pressure. A portion of the gas is recirculated and cooled to the same subsystem, known as the anti-surge recycling system, to keep a minimum constant flow through the compressor and prevent surging. 92%, 69%, and 72% of the total gas are recycled to the first, second, and third recompression subsystems, accordingly. The condensed water from the scrubber is sent to the drain system. After leaving the first stage compressor, it enters the second stage recompression where the gas stream from the second stage of the three-phase separator mixes with it. Then the condensed water is sent back to the third stage of the two-phase separator. Similarly, it enters the third stage and finally

leaves the recompression unit at 70 bar. The remaining condensation is sent back to the entry of the second stage, three-phase separator. The gas from the first stage of the three-phase separator mixes with it and goes to the reinjection unit.

The reinjection unit consists of three parallel reinjection trains. Each train has two scrubbers, two coolers, and two compressors. The main objective of this unit is to increase the gas pressure to match the injection pressure of the well so that the gas can be injected into the reservoir. The condensed stream from each unit is sent back to the entry of the second stage of the three-phase separator.

A small portion (3%) of gas from the first stage of the three-phase separator enters the fuel gas treatment unit. This unit includes two scrubbers, one cooler, and one heater. After cooling the gas and reducing its pressure, it is fed to the first scrubber. Condensation output is sent back to the entry of the second stage of the three-phase separator. The gas is then heated to remove moisture and is separated into two flow streams. One flow is fed to the second scrubber, and the other flow stream is taken for the flare system. After leaving the second scrubber, the remaining gas is directed to the power turbines, and the condensation is sent to the drain system. The drain system pumps the condensation and recycles it back to the entry of the second stage of the three-phase separator.

A case study is carried out in this section, focusing on real-time industry data. The feed stream temperature (80 to 87^{o}C) and Gas to Oil Ratio (GOR) (2800) is significantly high in this plant. In addition, it has a pressure range of 88 to165 bar. The measurement data is chosen in a way that can represent the average value of a consistent and stable typical production day. The average oil and injected gas flow rates are 132.5 Sm^3/h and 369 × 103 Sm^3/h, where the maximum deviations are 10 Sm^3/h and 103 Sm^3/h, respectively.

4.4 Steady-State Model Formulation

The steady-state model needs to be built before implementing and simulating the plant wide dynamic behavior; the steady state model provides the initial conditions for the dynamic model. It is also essential to gather equipment information and flowsheet specifications before starting a dynamic simulation such that a set of differential equations can be solved with respect to time. Few assumptions should be made with respect to the actual physical system to facilitate the modeling using Aspen HYSYS, as given below:

4. Aspen HYSYS does not have a coalescer in the equipment library. In this study, one two-phase separator is used instead of the electrostatic coalescer.
5. In the real case, condensate from the coalescer is sent back to the second stage of the three-phase separator. In this work, it enters the third stage of the two-phase separator without using any pump considering two reasons: The pump detects vapor fraction in the condensation; and it is not practical to add the recycle (2.8 bar) in the second stage separator without pumping as it significantly reduces the required inlet pressure of the separator.
6. In real conditions, the recycle flow is directly connected to the system, but in this simulation, the mixer is used to take multiple inputs and provides a single output feed to the system.

Based on the above assumptions, a steady-state model for the system is developed for the entire gas processing plant. In this study, the Peng-Robinson (Peng & Robinson, 1976) equation of state is used to determine characteristics for gas and oil flows. Since the steady-state model is mostly a reproduction of the model given in Voldsund et al. (2013), the details of the steady-state

model are provided in the supplementary materials. It should be noted that a converged and validated steady-state model is a necessary step to build a dynamic model.

4.5 Dynamic State Model Formulation

The dynamic simulation requires the solution of a system of ordinary differential equations (ODE) to capture the transient behavior of the system. It can also be used to assess and enhance the control and monitoring of the production system. If a sudden change in the system is possible during the process operation, and the system has a significant time delay or a slow dynamics, a dynamic simulation is required to study the system behaviors.

4.5.1 Sizing of Equipment

The transition from steady-state to dynamic simulation involves a pressure drop throughout the plant. It is necessary because the flow is determined based on the pressure drop in Aspen HYSYS dynamics. Therefore, it is vital to have a valve in between every pair of holdup volumes. The dynamics of any unit are mostly dependent on its size. Hence, various units used in the simulation need to be sized before the transition to a dynamic state. All unit operations in the simulation should be sized using actual equipment or pre-defined sizing techniques.

4.5.2 Separators

The specifications of the liquid holdup are crucial as the level controller is used based on this information. The holdup value can also be calculated based on the steady-state residence time (volume of fluid/flow rate), where approximately 10 minutes is a suitable value for the liquid streams and 2 minutes for the vapor streams. The real sizing values used in the plant for all separators are unknown. Therefore, it is assumed that the vessel volume for three-phase horizontal flat cylinder separator is 85 m^3, where the diameter and length are 4.163 m and 6.245

m, respectively. This dimension is typically used for the separators in oil and gas industries. Liquid holdup, which represents the level of liquid within the column, is assumed at 50% for three-phase separators and 40% for two-phase separators.

4.5.3 Valves

Aspen HYSYS dynamics automate valve sizing based on the linear valve type (other types are also available), a 50% valve opening, and user specified pressure drop, and current flow rate. It also calculates the flow coefficient, Cv, that will allow the valve to pass 100% of the upstream flow rate through the valve at the designed opening position. The flow coefficient is widely used to determine the size of the valves. It is defined as the flow capacity of a valve (in U.S gal/min) of water at 60°F through a valve with a pressure loss of one pound per square inch at a specific opening position. Cv is valid for both turbulent and laminar flow, as defined below (Smith & Zappe, 2004):

$$C_v = Q\sqrt{\frac{G}{\Delta P}} \qquad (4.1)$$

In Equation (1), G refers to the Specific gravity; ΔP is the differential pressure in psi; and Q represents the volumetric flow in U.S gal/min. The 'Manufacture specific method' is chosen for valve sizing, and the 'universal gas sizing' is selected for valve vapor flow models. Linear option for valve operating characteristics and Cv for sizing conditions are selected. Initiating the 'size valve' option determines the value of Cv when the valve is 50% open with a specific pressure drop. In the dynamic section, 'pressure-flow relation' for dynamic specification and check valve for preventing the backflow are enabled. In the same section, the first-order mode is chosen for actuator parameters. Actuator time constant value is set to 5 seconds; linear actuator rate is $1.0e^{-2}$

and K value for the damp factor is 0.9500. The properties of all valves used in this dynamic simulation are summarized in Table 4.2.

Table 4.2: Valve characteristics in dynamic state.

Valve	Delta P (kPa)	C_1 (Ratio for valve)	K_m (Valve recovery coefficient)	C_v (Liquid sizing coefficient)	C_g (Gas Sizing Coefficient)
VLV-100	2000	33.5	0.9000	3686	1.23e+005
VLV-101	6150	33.5	0.9000	27.34	914.99
VLV-102	570	33.5	0.9000	97.17	3252.1
VLV-112	2940	33.5	0.9000	7.498	250.94
VLV-113	1050	33.5	0.9000	12.58	420.95
VLV-104	290	33.5	0.9000	13.47	450.93
VLV-105	1322	33.5	0.9000	36.49	1221.3
VLV-111	5100	33.5	0.9000	7.697	257.58
VLV-114	2015	33.5	0.9000	33.33	1115.5
VLV-115	2910	33.5	0.9000	1.066	35.669

4.5.4 Heaters/Coolers

'Product temperature specification' is selected for all heaters and coolers in dynamic model details where the values for product temperature and volume are specified based on temperature requirements of the specific unit. K value is obtained by enabling the specification of K.

4.5.5 Pumps and Compressors

For the pumps, only the efficiency [%] and pressure rise [kPa] options are needed. The other dynamic specifications depend on the above data. Similarly, for dynamic compressors, the adiabatic efficiency and duty are required in the dynamic specification section.

4.5.6 Mixers

In the steady-state mode, 'Set outlet to lowest inlet' is selected for parameters in the automatic pressure assignment section in the mixer. Aspen HYSYS set the exit stream pressure of the mixer based on the lowest inlet stream. This is not practical because several streams may enter with different pressures at one time. In a dynamic simulation state, the 'Equalize all' option is selected instead of 'set outlet to lowest inlet' as it gives the same pressure to all attached streams, which is realistic.

4.5.7 Modifications and Additional Assumptions

Separator unit. Vapor output from the third stage of two-phase separator (electric coalescer) goes to the first stage recompression unit. It can be ignored because it does not have any vapor flow. Adding this stream to other separators in the separation unit causes improper pressure merging. For the same reason, no mixer is used in the incoming streams of the second stage separator (MIX-114). Also, one additional mechanical valve, VLV-110, is used in the first stage of the three-phase separator vapor output to control the flow rate of the reinjection unit, which is demonstrated in Fig. 4.3.

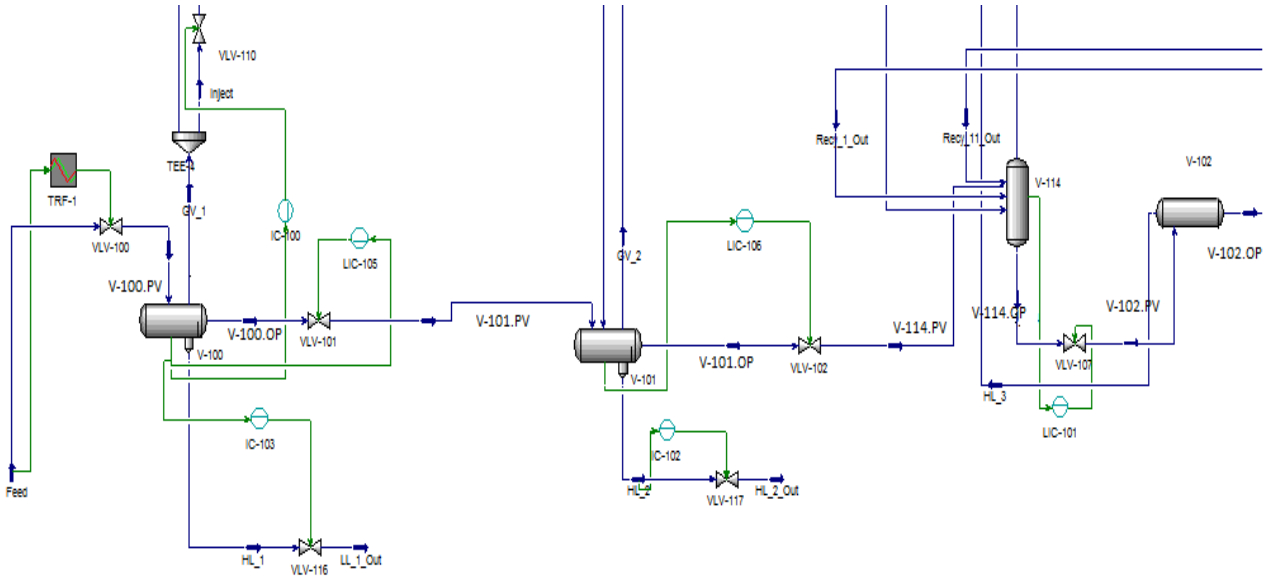

Fig. 4.3: Separator section modification to adapt for modelling.

Recompression unit. In the Aspen HYSYS dynamics, the incoming pressure of different streams in a mixture should be equal. For this reason, the recycles from all three-recompression units enter directly into the scrubber instead of mixing in the mixer due to their reduced pressure. Thus, the mixers (MIX-110 and MIX-111), which were used in a steady-state before, are not included in a dynamic state. For the same reason, the cooler E-101 in the second stage recompression unit is divided into two coolers: a mainstream cooler (C_3) and a recycle cooler (C_6). The other cooler, E-102, in the third stage recompression unit is also divided into two coolers: a mainstream cooler (C_4) and a recycle cooler (C_5). Also, two extra coolers (C_9 and C_10) are used with the condensate output (recycling to the separation unit) of the second and third stage recompressions to reduce the temperature. Otherwise, this high-temperature condensate recycle will destabilize the temperature requirement of the separation unit. A dynamic model of the recompression unit is depicted in Fig. 4.4.

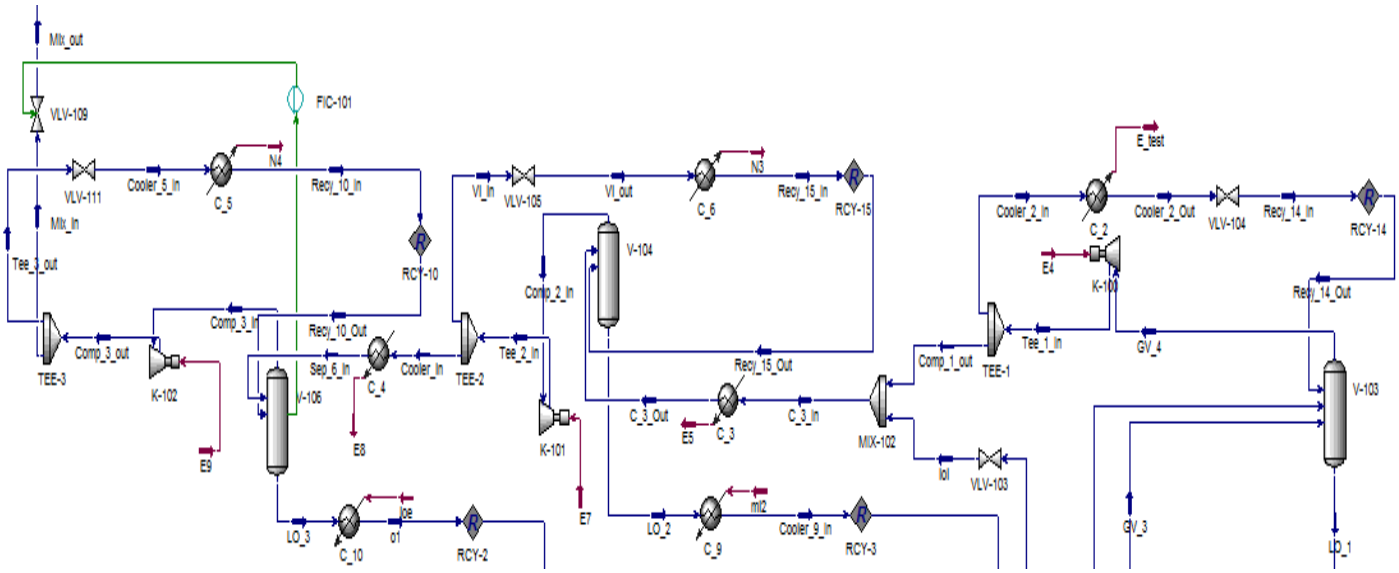

Fig. 4.4: Recompression unit modification to meet process requirements.

Two extra mechanical valves are used in this section. One (VLV-109) is employed in the third stage recompression scrubber output to control the flow rate going towards the reinjection unit. The second valve (VLV-103) is used to reduce the output vapor pressure of the second stage, three-phase separator (which is mixing with the first stage recompression output in a mixer MIX-102) to maintain equal pressure flow of the mixer.

4.5.8 Control Strategies and Equipment

In this study, many control loops are set to regulate the system. Generally, in the three-phase separator, hydrocarbons are separated into three portions: vapor, light liquid, and heavy liquid. This simulation reveals that light liquid (oil) is also produced along with the heavy liquid (water) and leaves the system, which is not desirable in this study. Due to this loss, the amount of light liquid production is significantly affected. Therefore, two flow controllers are used in the first and second stage of the three-phase separator so that the flow rate of the heavy liquid can be

lowered. It also decreases water production, which is acceptable as the main focus is on oil and gas production in our case in this study.

4.5.9 PID Controllers

While most of the proportional–integral–derivative (PID) controllers are utilized in the separation unit, one is used in the fuel treatment unit, and another in the recompression unit. The properties of the PID controllers are given in Table 4.3.

Table 4.3: Controller values for all valves.

Control Name	**Process variable source (PV)**		**Output target (OP)**		**Type**	**Action**	**Gain, K_c**	**Integral time T_i (sec)**
	Object	variable	Object	Variable				
LIC-105	V-100	Liquid percent level	VLV-101	Actuator desired position	PI	Direct	11.0	1.00
LIC-106	V-101	Liquid percent level	VLV-102	Actuator desired position	PI	Direct	12.0	1.00
LIC-101	V-114	Liquid percent level	VLV-107	Actuator desired position	PI	Direct	1.80	67.9
IC-100	V-100	Liquid vol. flow (std.cond.GV-1)	VLV-110	Actuator desired position	PI	Reverse	11.0	1.00
IC-103	V-100	Liquid vol. flow (std.cond.HL-1)	VLV-116	Actuator desired position	PI	Reverse	1.0	0.1
IC-102	V-101	Liquid vol. flow (std. cond.	VLV-117	Actuator desired position	PI	Reverse	1.0	0.1

		Liquid phase)						
FIC-101	V-106	Liquid vol. flow (std. cond. Liquid phase)	VLV-109	Actuator desired position	PI	Revers e	11.0	1.00
IC-104	V-100	Liquid vol. flow (std. cond. Liquid phase)	VLV-106	Actuator desired position	PI	Revers e	13	1.00

4.5.10 Transfer Function Block

A transfer function block is a logical operator that takes a specific input and applies a transfer function on it to give an output. Transfer function blocks are used to add disturbances in the streams. In this study, hydrocarbon feed comes from five different wells. This feed stream is susceptible to several disturbances due to fluctuations in pressure, temperature, and flow rate of the wells with time. A transfer function block is used to add disturbances to the feed and continually vary the flowrate by adding noise. The following general equation relates the input to the output using a transfer function:

$$Y(s) = G(s)\, X(s) \qquad (4.2)$$

where Y(s), G(s), and X(s) represent the system output, transfer function, and system input, respectively. There are several types of transfer functions. A second-order sine wave transfer function is used (to make the flow wavy) as follows:

$$G(s) = \frac{K}{s^2 + \omega^2} \qquad (4.3)$$

In Equation (3), ω = (1/T) is the frequency of oscillation; *T* is the period of oscillation; *K* stands for the amplitude of the sinusoid; and *s* refers to the Laplace transform variable. The inverse Laplace of the sine wave transfer function is expressed below:

$$g(t) = K \sin(\omega t) \quad (4.4)$$

The K (gain) is the amplitude ranging from the minimum and maximum values of process variable (PV) and output target (OP). 2% PV offset (% of PV span) operational parameter is selected for configuration in the parameter section. To add external noise to the feed, 2% standard deviation for PV is chosen. VLV-100 position is chosen as the OP target, and liquid volume flow (feed) is selected as the source variable shown in Figure 5. The amplitude of the sine wave parameter (K value in Equation (3)) is set to 26% with a period (T) of 25 minutes.

After sizing the equipment and setting up the control strategies, the system is ready for simulation in the dynamic mode. Dynamic simulation is essentially a solution of a system of ordinary differential equations. It requires setting up a few parameters related to the solver. The following properties are selected for the solver: automatic control, units in minutes, acceleration 0.40, display interval 1.0, real-time factor 0.2, and integration step size 0.5 second. Static head contributions and an implicit check valve model are enabled for the operation.

4.6 Measurement Noise

Measurement noise is an integral part of many process systems that arises in measured data from different sensors. This noise is also known as a random error, observational noise, or statistical uncertainty. It is combined with measured data but is different from systematic measurement errors (Baton, 1997). The systematic error is seen in measurement data due to some

external factors such as a calibration error, and physical and/or electromechanical defect in the meter (Bevington et al., 1993). With all the outputs of the simulated system, the measurement noise of appropriate variance is added. Measurement noise is sampled from a random normal distribution. The variance of the measurement noise is set to a fraction of the magnitude of the actual value, and a fraction of the normal variation of the variable. In some cases, both factors are taken into account. Fig. 4.5 presents the measured feed flowrate data after addition of measurement noise.

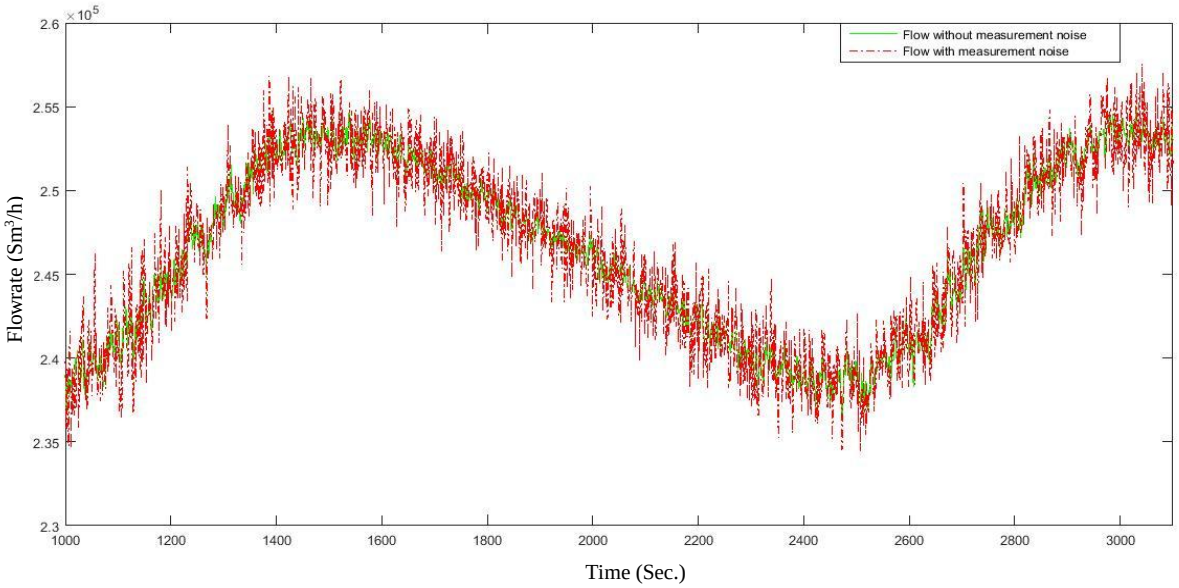

Fig. 4.5: Normal feed flow with measurement noise.

4.7 Generation of Faulty Conditions

In process systems, faults can be classified into three major categories: (i) sensor fault, (ii) disturbance, and (iii) actuator fault. The dynamic model can be used to simulate all these three types of faults. In this study, two scenarios of disturbance faults and four scenarios of actuator faults are simulated. The introduced faults with brief description are provided in Table 4.4.

Table 4.4: Type, location and brief description of corresponding faults.

Fault category	Type of fault	Fault location	Description
Disturbance faults	High flow rate	Feed	The feed flow coming from five consecutive well is increased by about 25% from its rated condition (2.45 × 105 Sm^3/h).
	High temperature	Feed	The feed temperature is increased by 5% from the rated temperature (83 ˚C). It is found that increasing temperature by more than 5% in a faulty state, the simulation becomes unstable due to the pressure-flow merging problem of the plant.
Actuator faults	Fail hold	VLV-101	Fail hold happens typically when the valve does not react on power or signal loss and remains in the same position. This failure can also result from the physical failure of the valve. This type of fault is not desirable for the process where it needs continuous production without stopping.
		VLV-102	
	Fail open	VLV-101	Fail open condition occurs due to the loss of input power or signal in the actuator. In this situation, the valve remains fully open, and hydrocarbons flow continuously at its maximum without any control. Fail open is a safety mechanism for preventing overpressure of a blocked line, e.g., in the cooling system, or during a catastrophic failure.
		VLV-102	

4.8 Results and Discussion

Results from the model validation and the simulation scenarios and corresponding discussions are presented in this section. The steady-state simulation results are compared with the

production data from the existing system to validate the model. Also, the dynamic simulation at normal and different faulty conditions are analyzed.

4.8.1 Model Validation

Steady state model. The model outputs are validated with operational data from an existing well provided by Voldsund et al. (2013). The comparison is made for different parameters such as pressure, temperature, and flow rate. The validation results of the oil volume flow rate and pressure are listed in Tables 4.5 and 4.6.

Table 4.5: Validation result of fluid flow rate against measured data from Voldsund et al. (2013).

Produced fluid	Unit	Measured data	Simulated value	Percentage error
Export oil	Sm^3/h	132.5 ± 0.4	110.2	16.5%
Reinjection gas	$10^3\ Sm^3/h$	369 ± 17	357	1.4%
Produced water	Sm^3/h	67 ± 5	37	40%
To flares	Sm^3/h	335 ± 14	320	0.31%
To power turbines	Sm^3/h	9630 ± 170	9546	0.9%

Table 4.6: Validation result of pressure value against real data from Voldsund et al. (2013).

Produced fluid	Unit	Measure data	Simulated value	Percentage error
Export oil	bar	32.1 ± 0.3	32.2	1.25%
Reinjection gas	bar	236 ± 2	236	0.85%
Produced water	bar	8.77 ± 0.09	70.0	706%
To flares	bar	9.30 ± 0.09	9.30	0.97%
To power turbines	bar	18.25 ± 0.18	18.25	0.99%

The simulated values match well with the measured values for most cases except for produced water. In the real system, a water treatment process exists where the traces of oil are removed. This process is not described in the literature; hence, the conditions assumed in the present work might be different from the real conditions, leading to the discrepancy.

4.8.2 Dynamic Model

The dynamic state of the entire plant is simulated, and the results are presented in this section. For each case, the simulation model is executed for a total of 10800 seconds (3 hours) until it reaches a stable state. A total of 38 crucial parameters are chosen for data simulation, and three variables - flow rate, pressure, and temperature - are considered for each parameter. Therefore, total 114 variables (38 × 3) were simulated and measured from the dynamic system. Due to space/page constraint, only a few essential variables' simulation results such as feed, produced oil, reinjection gas, turbine, and flare are discussed in this section.

Feed. Based on pressure-flow characteristics, the average hydrocarbon flow rate in the feed stream is found to be 2.45×10^5 Sm^3/h, which varies approximately ±5%, and it takes around 30 minutes for one complete cycle. This feed flow also contains a noise level, which is 2% of the average flow rate. The other two variables in the feed stream, pressure and temperature, remains unchanged, as illustrated in Fig. 4.6.

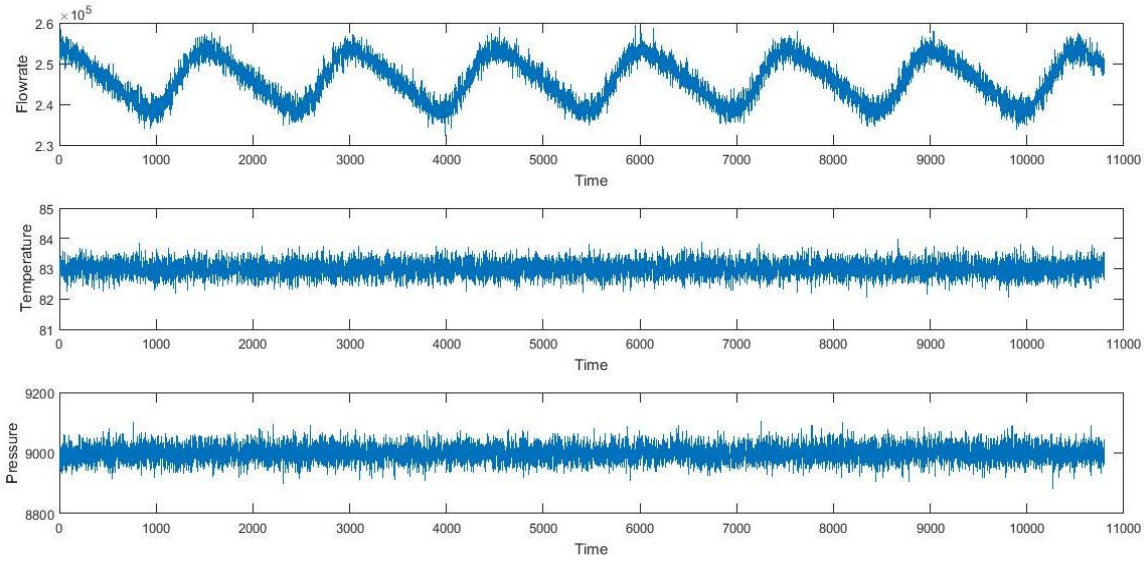

Fig. 4.6: Dynamic response of the feed flowrate, pressure, and temperature.

Produced oil. The maximum flowrate of the produced oil in the dynamic simulation is obtained to be 77.87 Sm^3/h, while in steady-state, this flow rate is 110.2 Sm^3/h. The temperature and pressure are also reduced to 49 ± 0.16˚C and 32 bar, respectively. The flow rate of the produced oil is reduced to approximately 32 Sm^3/h in the dynamic state because the dimensions of the equipment and their properties used in the real plant (three-phase and two-phase separators, scrubber, coalescer, and holdup liquid percent) are not known; also, the flow rate, pressure, and temperature specification of the recycle streams, entering the separation unit, are not known.

The characteristics of the produced oil are presented in Fig. 4.7.

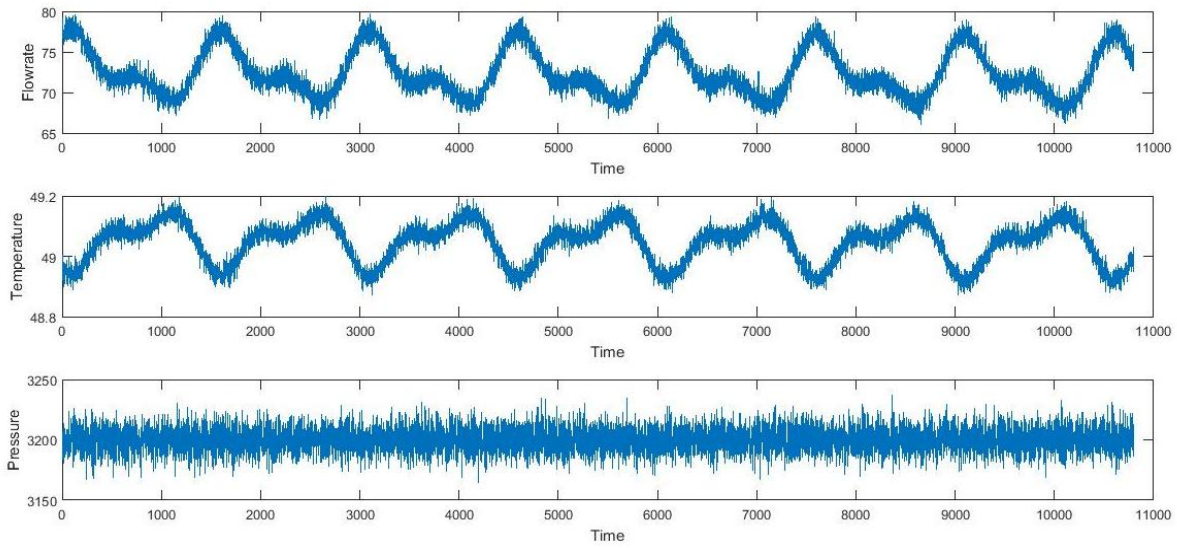

Fig. 4.7: Dynamic response of the produced oil flow rate, pressure, and temperature.

Reinjection. The maximum flowrate of reinjection gas in the dynamic simulation is estimated to be 193910 Sm^3/h while in steady-state, this flow rate is 375×10^3 Sm^3/h. The flowrate is decreased to approximately 1.6×10^3 Sm^3/h in the dynamic state compared to the steady-state simulation (the same reason as described above for this reduction). The temperature and pressure are increased to $127 \pm 0.5^{\circ}C$ and 236 bar, respectively, as presented in Fig. 4.8.

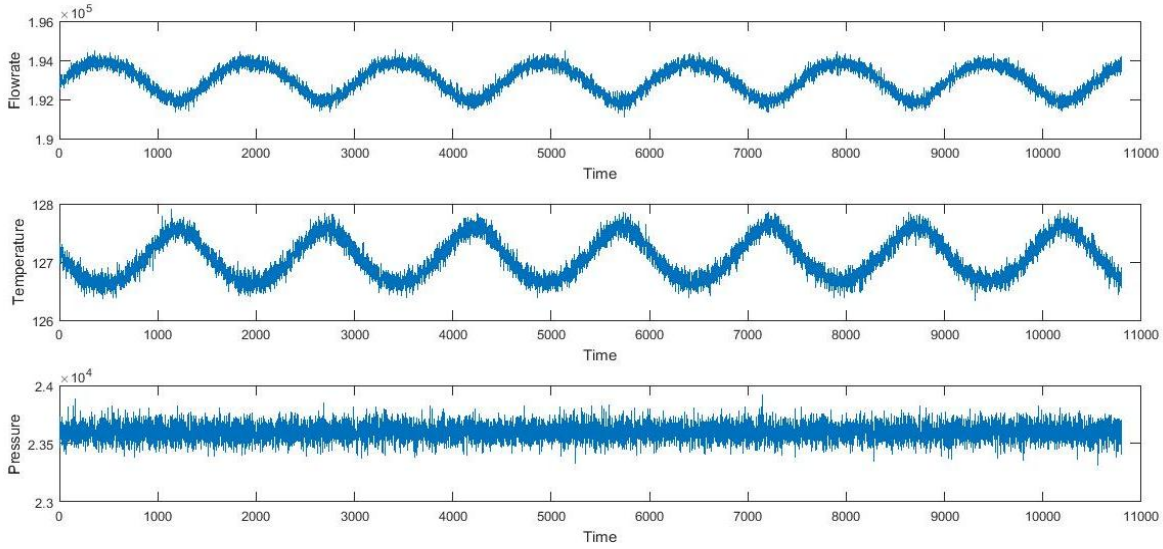

Fig. 4.8: Dynamic response of the reinjection flow rate, pressure, and temperature.

Turbine gas. The average flowrate of the turbine gas in the dynamic state is determined to be 10111 Sm^3/h while in the steady-state, this flow rate is 9546 Sm^3/h; implying the rate is increased to 565 Sm^3/h in the dynamic state. The temperature and pressure remain almost constant (46.24˚C and 18.25 bar) according to Fig. 4.9.

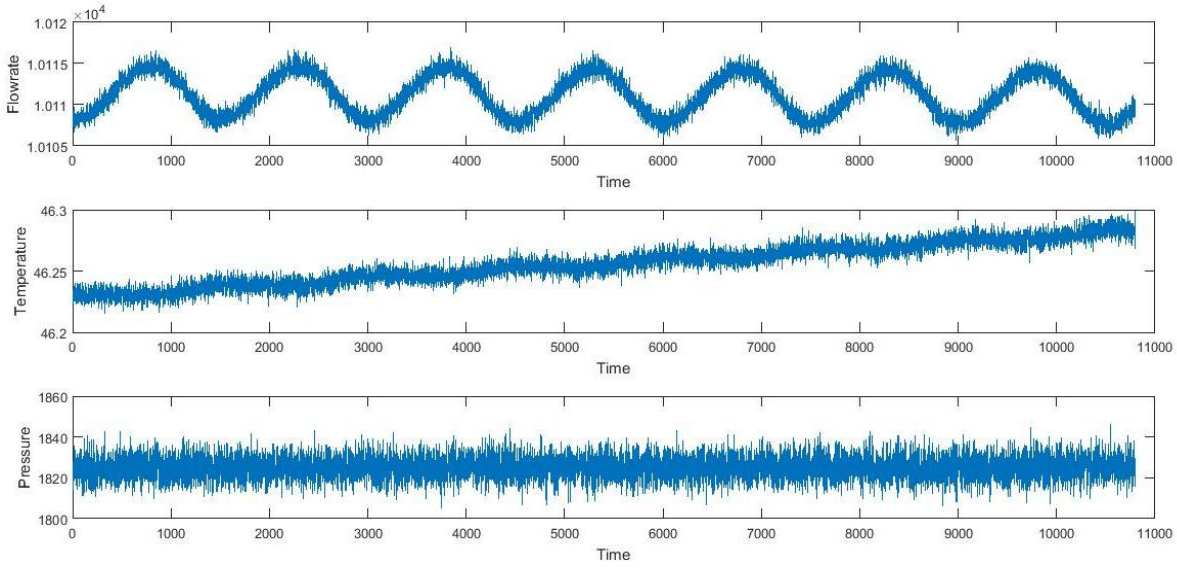

Fig. 4.9: Dynamic response of the turbine gas flow rate, pressure, and temperature.

Flare. The maximum flowrate of flare gas obtained from the dynamic simulation is 333 Sm^3/h. In the steady-state process, this flow rate is 320 Sm^3/h. Thus, it is increased by 13 Sm^3/h, compared to the flowrate of the steady-state simulation. The pressure and temperature remain almost constant, which are 47.85˚C and 9.3 bar, respectively (see Fig. 4.10).

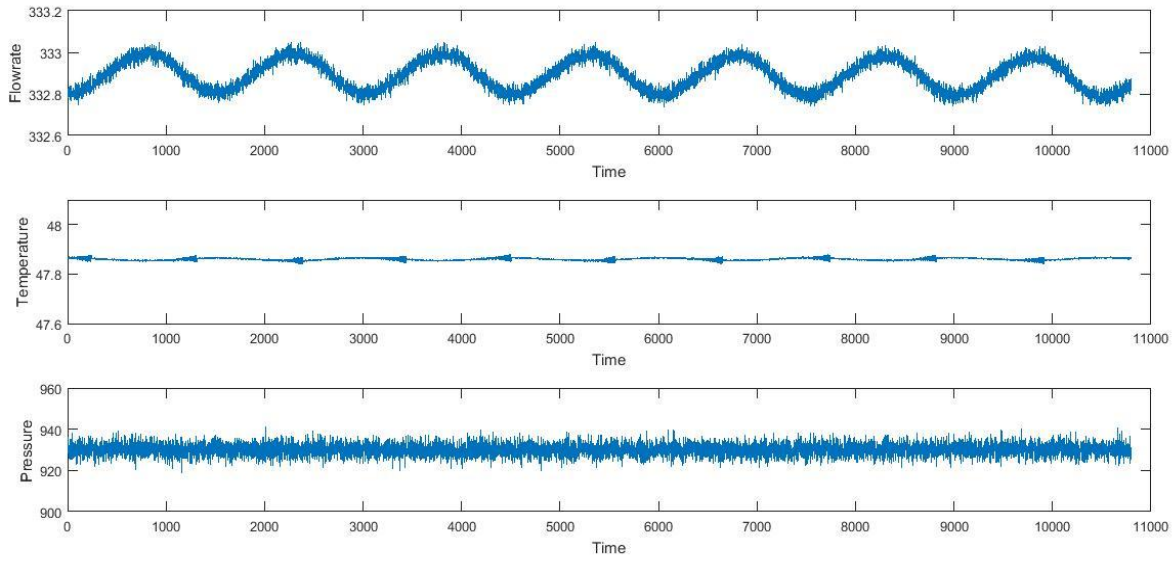

Fig. 4.10: Dynamic response of the flare gas flow rate, pressure, and temperature.

4.8.3 Dynamic Simulation of System Faults

Actuator fault for Valve, VLV-101. This valve is located after the first stage of the three-phase separator. The light liquid leaving this separator goes to the second stage of the three-phase separator through this valve. Although, the actuator fault is simulated for two valves, VLV-101, and VLV-102, the result of only one valve (VLV-101) is presented here due to space constraint.

Fail hold: The simulation is run up to the first 50 minutes in the normal mode. Fail hold fault is then activated that remains active for the next 130 minutes. Only the important variables, which may cause substantial changes upon the failures, are discussed in this section. The flow rate for feed stream to separator 2 (V-101.PV) remains constant at 37.51 Sm^3/h without any variation while the flow rate in the normal condition varies from 37.35 Sm^3/h to 31.11 Sm^3/h. The temperature is slightly decreased from its standard value 81.35˚C to 81.26˚C. On the other hand, the pressure slightly drops to 53.50 bar from its normal value of 53.33 bar.

Produced oil (V-102.OP) flow rate is slightly lowered and varies between 76.7 Sm^3/h to 74.3 Sm^3/h, where the normal flowrate is within the range of 77.9 Sm^3/h and 68.3 Sm^3/h. The temperature is also reduced and varies around 48˚C, wherein normal condition temperature range is 48.9˚C- 49.15˚C. The pressure remains unchanged.

The flowrate into the recompression unit (VLV-109.OP) is increased from its normal value of 9656.69 Sm^3/h to 9665.05 Sm^3/h. The temperature and pressure remain almost the same. Fig. 4.11 depicts all process variations.

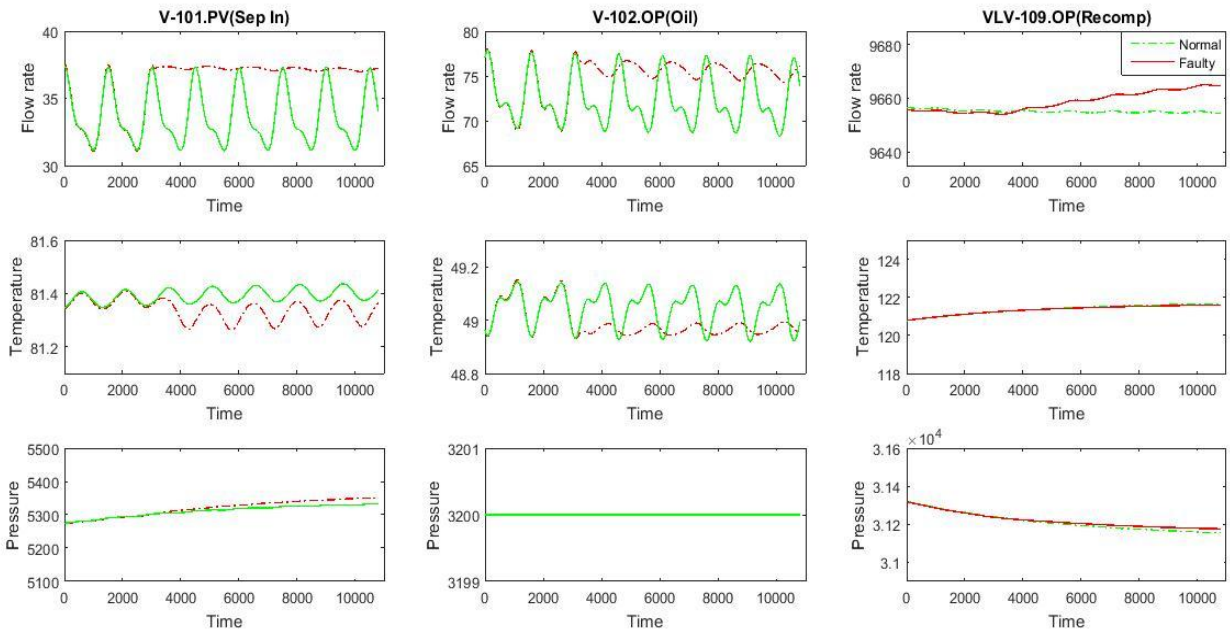

Fig. 4.11: Comparative investigation on normal and fail hold faulty conditions for separator, produced oil, and recompression.

Fail open: Feed to Separator (V-101.PV), Produced oil (V-102.OP), and recompression output (VLV-109.OP) flowrates are increased to 58 Sm^3/h, 80 Sm^3/h, and 10493 Sm^3/h from their

average magnitudes of 33.7 Sm^3/h, 72.5 Sm^3/h, and 9655 Sm^3/h, respectively. The separator and produced oil flowrates show a sudden high pick of 153.8 Sm^3/h and 226.2 Sm^3/h for 10 minutes during 3200 to 3800 seconds time period.

The temperature is decreased in all the cases from 81.2˚C, 49˚C, and 122˚C to 80˚C, 47.2˚C, and 113˚C, respectively, with a sharp depth of 78.42˚C and 47.4˚C in V-101.PV and V-102.OP. The pressure in V-101.PV, and VLV-109.OP is increased to 66.4 bar and 332 bar, respectively while the pressure of V-102.OP remains unchanged. The variations of flow rate, temperature, and pressure are illustrated in Fig. 4.12.

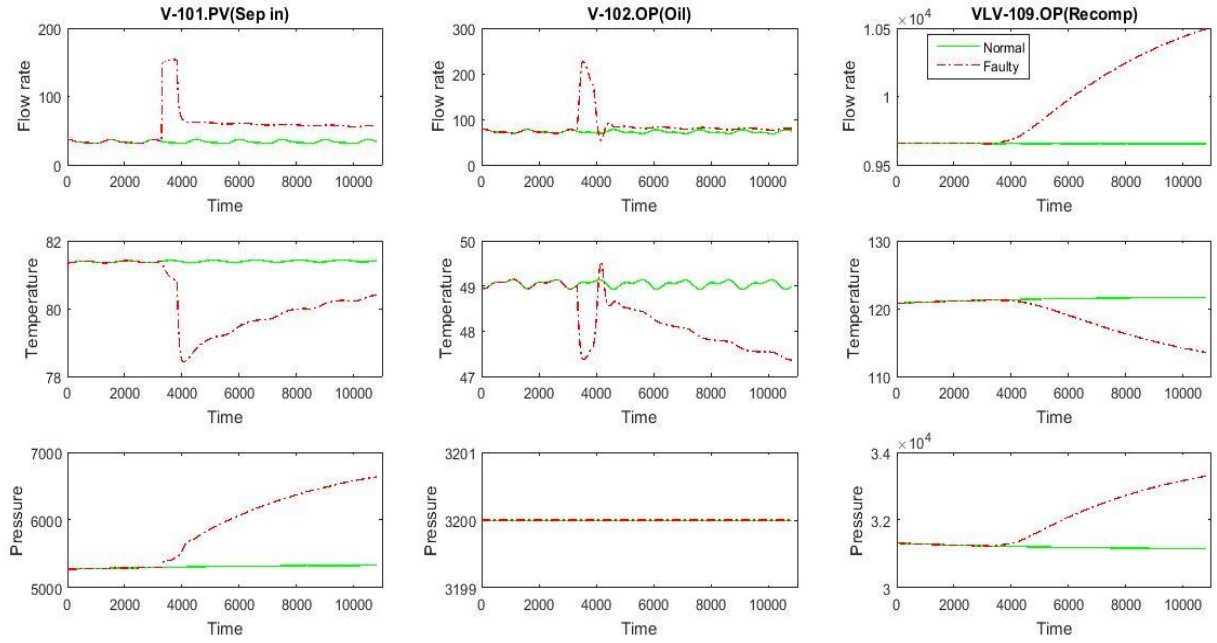

Fig. 4.12: Comparative investigation on normal and fail open faulty condition for separator, produced oil, and recompression.

The flowrate in the reinjection unit remains almost constants while it is reduced in turbine and flare to 10101.7 Sm^3/h and 332.6 Sm^3/h from their average values 10107.6 Sm^3/h and 332.8 Sm^3/h, respectively.

There are no significant changes in temperature and pressure for all three cases due to fail open faults in valve VLV-101, as depicted in Fig. 4.13.

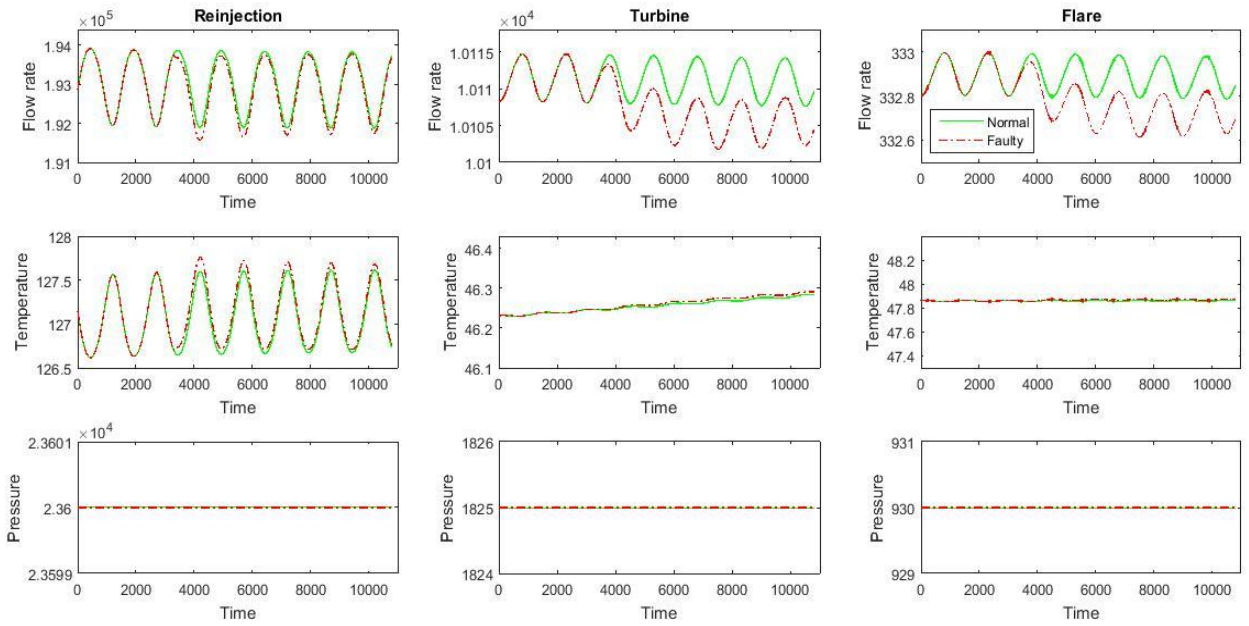

Fig. 4.13: Comparison between normal and fail open faulty conditions for reinjection, turbine, and flare.

High temperature fault. Upon an increase in the feed (TRF-1.PV) temperature from 82˚C to 87˚C, the produced oil and recompression flowrates are reduced to 49.7 Sm^3/h and 9637.5 Sm^3/h from their average values of 68.3 Sm^3/h and 9654.5 Sm^3/h, respectively. On the other hand, the temperature of produced oil (V-102.OP) is slightly increased from 49.1˚C to 49.7˚C while it remains almost the same in recompression unit (VLV-109.OP). The pressures of all these three

sections are not affected by the temperature fault except in the recompression unit where a negligible reduction in the pressure is noticed (see Fig. 4.14).

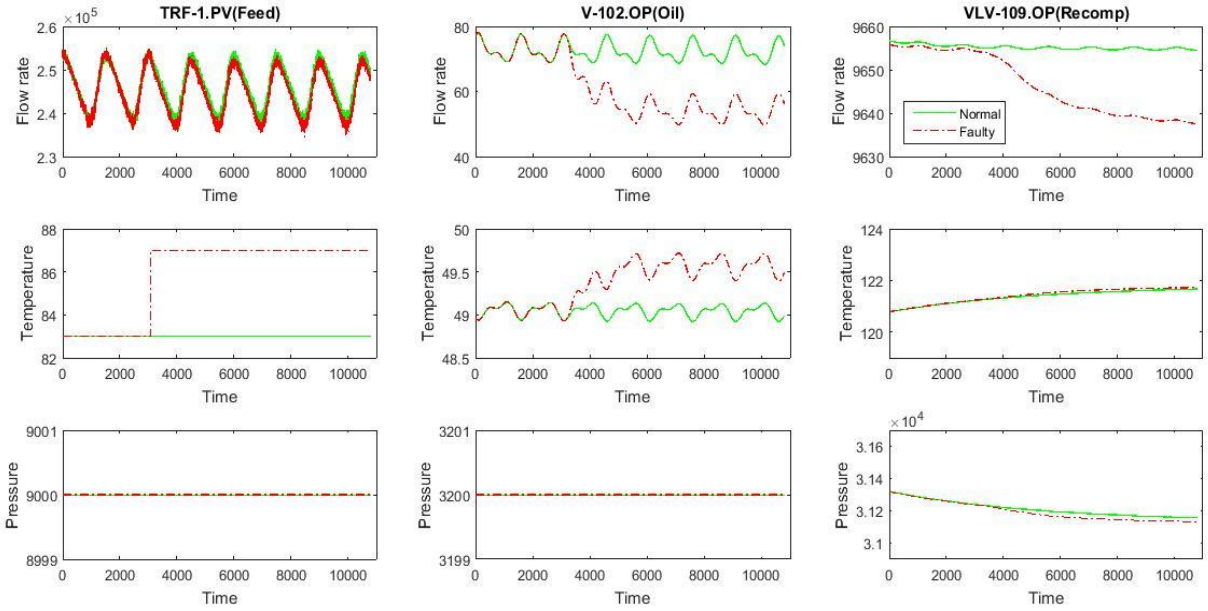

Fig. 4.14: Comparative study on normal and high temperature fault for feed, produced oil, and recompression.

The Flowrates in reinjection, turbine, and flare units are lowered to 191684 Sm^3/h, 9945 Sm^3/h, and 328 Sm^3/h from their average magnitudes of 191872 Sm^3/h, 10108 Sm^3/h, and 333 Sm^3/h, respectively. On the other hand, the temperature of the turbine and flare are slightly increased to 46.47˚C and 48.1˚C from normal 46.2˚C and 47.8˚C where this increase is very minor in recompression unit (e.g., 127.6˚C to 127.7˚C). The pressures of all these three cases remain unchanged, as demonstrated in Fig. 4.15.

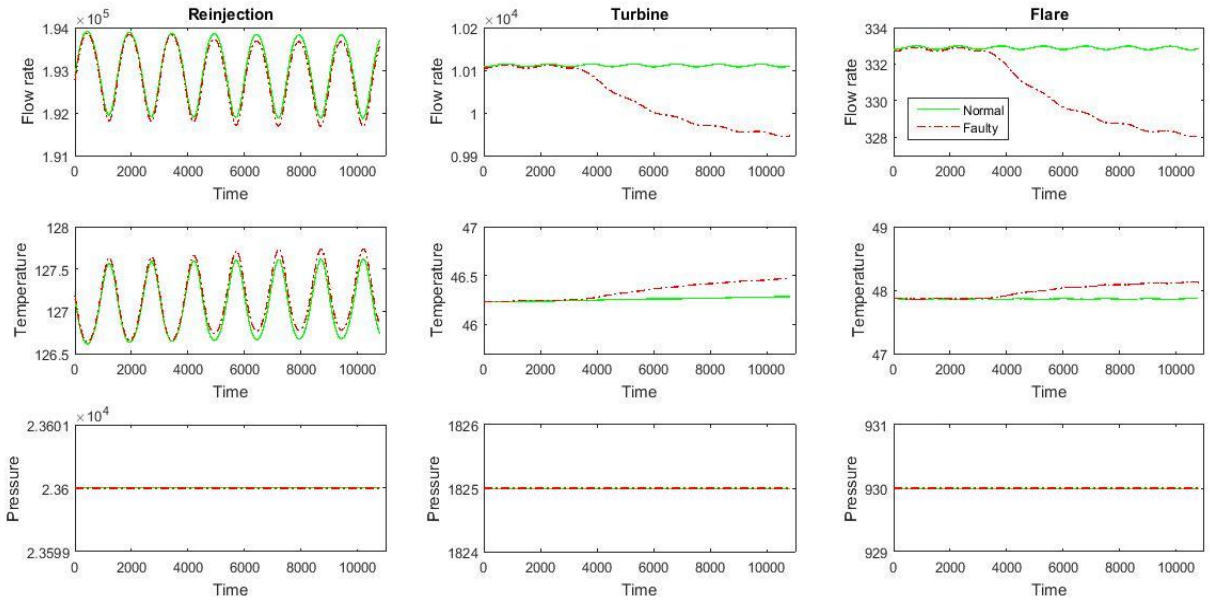

Fig. 4.15: Comparative study on normal and high temperature fault for reinjection, turbine, and flare.

High flowrate fault. Due to the high flow rate of the feed from 246137.8 Sm^3/h to 333823 Sm^3/h, the produced oil and recompression flowrates are increased to 126.7 Sm^3/h and 9855.6 Sm^3/h from their average values of 72.5 Sm^3/h and 9655.2 Sm^3/h, respectively. The temperatures of the produced oil and recompression unit are slightly dropped to 48.2˚C and 119.4˚C from 49˚C and 121.4˚C, respectively, while the temperature of the feed stream is constant. The pressures of the feed and recompression unit increase to 112.5 bar and 318 bar from 90 bar and 312 bar, respectively, where the pressure of the produced oil remains unchanged, as shown in Fig. 4.16.

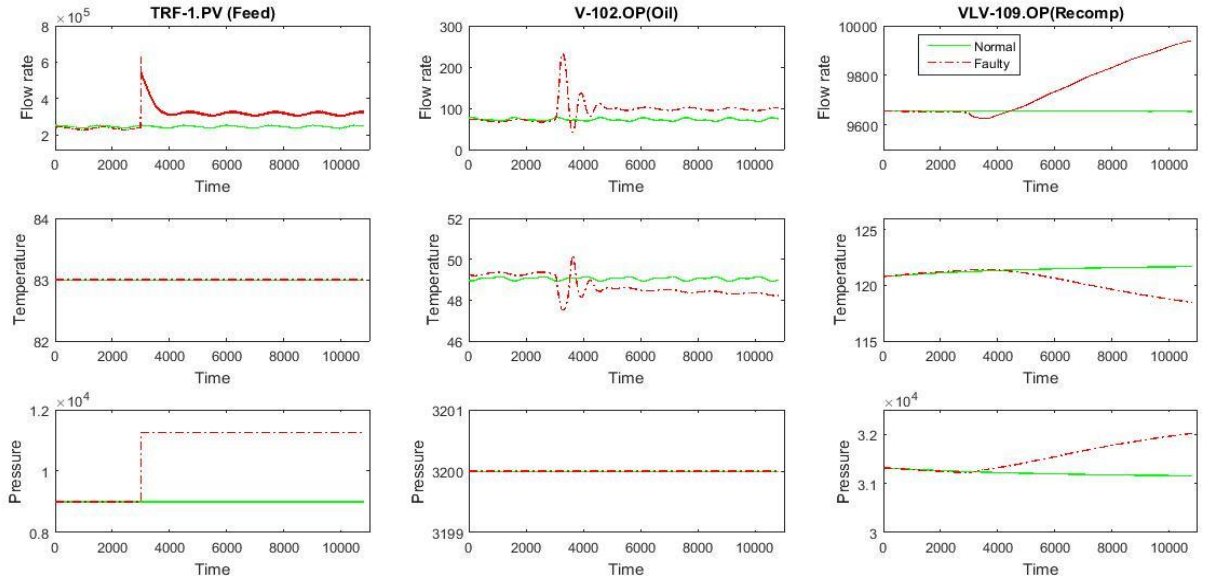

Fig. 4.16: Comparative study on normal and high flowrate disturbance fault for feed, produced oil, and recompression.

The flowrates of the reinjection, turbine, and flare are increased to 248612 Sm^3/h, 12185 Sm^3/h, and 395 Sm^3/h from their average magnitudes of 192994 Sm^3/h, 10111 Sm^3/h, and 333 Sm^3/h, respectively. The temperatures in all three cases are dropped to 105.7˚C, 43.8˚C, and 44.5˚C from 127.1˚C, 46.3˚C, and 47.86˚C, respectively. The pressure in all these three cases remain unchanged, as depicted in Fig. 4.17.

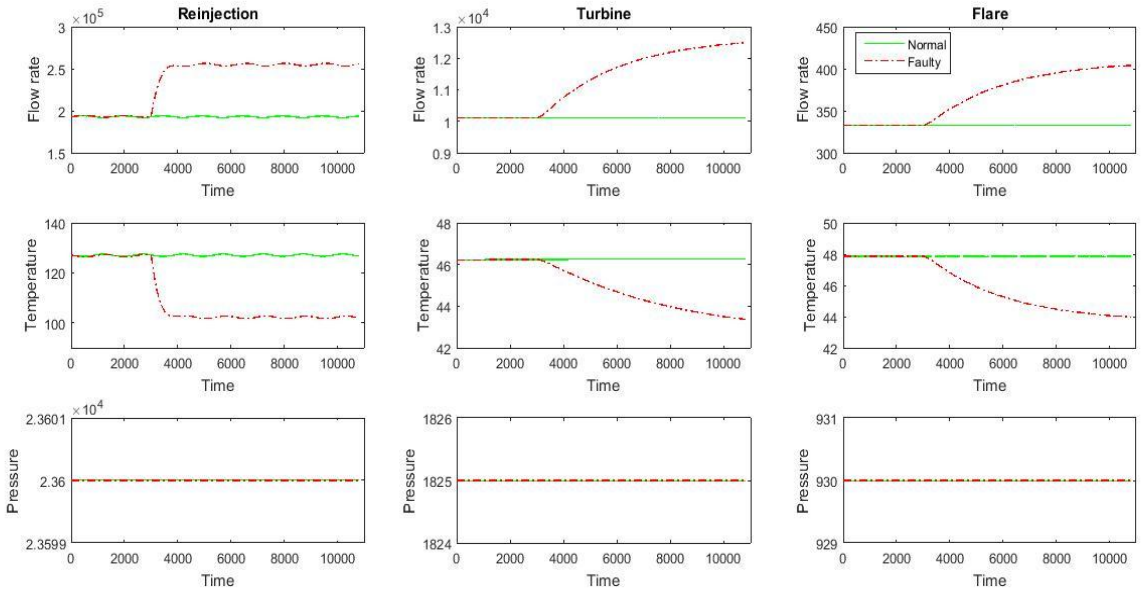

Fig. 4.17: Comparative study on normal and high flowrate disturbance fault for reinjection, turbine, and flare.

4.9 Conclusions

A dynamic model for an offshore production facility in the North Sea is introduced and simulated using the Aspen HYSYS plant simulator. This work represents the possibilities of simulating dynamic responses of oil and gas processing plants during normal and various faulty operating conditions. The model is built through considering five producing wells and several topside units: separation, export pumping, recompression, reinjection, and fuel treatment units. Dynamic responses from each operating unit are recorded and validated with data collected from an oil and gas production plant in the Norwegian part of the North Sea. Based on the research results, the dynamic simulation can successfully describe the dynamic behaviors of the system. There is a good agreement between the model outcomes and the real production data except for the produced water from separation units. Several issues related to dynamic simulations are

explored and resolved including modification of process flow diagram for convergence, implementing and tuning of PID controllers, adding transfer function block in Aspen HYSYS for dynamic simulation, and addition of measurement noise to simulate real life conditions. A total of six faulty scenarios are introduced and simulated. The developed model can be used to simulate similar offshore processing plants with some modifications. It can also be utilized as a benchmark system to test monitoring algorithms.

References

Bahadori, A., Vuthaluru, H. B., & Mokhatab, S., 2008. Optimizing separator pressures in the multistage crude oil production unit. Asia-Pacific Journal of Chemical Engineering, 3(4), 380–386. https://doi.org/10.1002/apj.159

Baton, U. N., 1997. "An introduction to error analysis" by John R. Taylor. Strain, 33(4), 133–134. https://doi.org/10.1111/j.1475-1305.1997.tb01061.x

Bevington, P. R., Robinson, D. K., Blair, J. M., Mallinckrodt, A. J., & McKay, S., 1993. Data Reduction and Error Analysis for the Physical Sciences. Computers in Physics, 7(4), 415. https://doi.org/10.1063/1.4823194

Boyer, B. E., & O'Connell, S., 2005. Optimize Separator Operating Pressures to Reduce Flash Losses. SPE/EPA/DOE Exploration and Production Environmental Conference. Presented at the SPE/EPA/DOE Exploration and Production Environmental Conference, Galveston, Texas. https://doi.org/10.2118/94373-MS

Cho, Y., Kwon, S., & Hwang, S., 2018. A new approach to developing a conceptual topside process design for an offshore platform. Korean Journal of Chemical Engineering, 35(1), 20–33. https://doi.org/10.1007/s11814-017-0258-z

Kim, I. H., Dan, S., Kim, H., Rim, H. R., Lee, J. M., & Yoon, E. S., 2014. Simulation-Based Optimization of Multistage Separation Process in Offshore Oil and Gas Production Facilities. Industrial & Engineering Chemistry Research, 53(21), 8810–8820. https://doi.org/10.1021/ie500403a

Mourad, D., Ghazi, O., & Noureddine, B., 2009. Recovery of flared gas through crude oil stabilization by a multi-staged separation with intermediate feeds: A case study. Korean Journal of Chemical Engineering, 26(6), 1706–1716. https://doi.org/10.1007/s11814-009-0236-1

Natarajan, S., & Srinivasan, R., 2010. Multi-model based process condition monitoring of offshore oil and gas production process. Chemical Engineering Research and Design, 88(5–6), 572–591. https://doi.org/10.1016/j.cherd.2009.10.013

Nguyen, T.-V., Fülöp, T. G., Breuhaus, P., & Elmegaard, B., 2014a. Life performance of oil and gas platforms: Site integration and thermodynamic evaluation. Energy, 73, 282–301. https://doi.org/10.1016/j.energy.2014.06.021

Nguyen, T.-V., Jacyno, T., Breuhaus, P., Voldsund, M., & Elmegaard, B., 2014b. Thermodynamic analysis of an upstream petroleum plant operated on a mature field. Energy, 68, 454–469. https://doi.org/10.1016/j.energy.2014.02.040

Nguyen, T.-V., Pierobon, L., Elmegaard, B., Haglind, F., Breuhaus, P., & Voldsund, M., 2013. Exergetic assessment of energy systems on North Sea oil and gas platforms. Energy, 62, 23–36. https://doi.org/10.1016/j.energy.2013.03.011

Nguyen, T.-V., Voldsund, M., Breuhaus, P., & Elmegaard, B., 2016. Energy efficiency measures for offshore oil and gas platforms. Energy, 117, 325–340. https://doi.org/10.1016/j.energy.2016.03.061

Peng, D.-Y., & Robinson, D. B., 1976. A New Two-Constant Equation of State. Industrial & Engineering Chemistry Fundamentals, 15(1), 59–64. https://doi.org/10.1021/i160057a011

Smith, P., & Zappe, R. W., 2004. Valve selection handbook: engineering fundamentals for selecting the right valve design for every industrial flow application. Elsevier.

Voldsund, M., He, W., Røsjorde, A., Ertesvåg, I. S., & Kjelstrup, S., 2012. Evaluation of the oil and gas processing at a real production day on a north sea oil platform using exergy analysis. Proceedings of ECOS, 153-166.

Voldsund, M., Ertesvåg, I. S., He, W., & Kjelstrup, S., 2013. Exergy analysis of the oil and gas processing on a North Sea oil platform a real production day. Energy, 55, 716–727. https://doi.org/10.1016/j.energy.2013.02.038

Voldsund, M., Nguyen, T.-V., Elmegaard, B., Ertesvåg, I. S., Røsjorde, A., Jøssang, K., & Kjelstrup, S., 2014. Exergy destruction and losses on four North Sea offshore platforms: A comparative study of the oil and gas processing plants. Energy, 74, 45–58. https://doi.org/10.1016/j.energy.2014.02.080

Chapter 5

Fault Detection and Diagnosis of Offshore Production Facility Using Principal Component Analysis and Artificial Neural Network

Muhammad Shalauddin Khaled, Syed Imtiaz*, Salim Ahmed, and Sohrab Zendehboudi

Department of Process Engineering, Memorial University, St. John's, NL, Canada.

A version of this chapter has been prepared for submission as a journal article. Muhammad Shalauddin Khaled developed this work under the direction and supervision of Dr. Syed Imtiaz, Dr. Salim Ahmed, and Dr. Sohrab Zendehboudi. They provided continuous technical guidance, checked the results, reviewed the manuscript, and modified the final version of the manuscript. In this chapter, the manuscript is presented with altered figure numbers, table numbers and reference formats in order to match the thesis formatting guidelines set out by Memorial University of Newfoundland.

Abstract

Artificial neural network (ANN) has been proved to be a useful tool for fault detection and identification. However, application of ANN to process systems is often challenging due to the high number of monitored variables, which leads to considering many neurons to model the system. The problem is even acute when modelling dynamic processes, as the number of variables increases many folds due to inclusion of the lagged variables in the data set. Training of such a large scale network is time-consuming and provides poor performance with a high error rate. In this paper, principal component analysis (PCA) and dynamic PCA (DPCA) are combined with ANN to reduce the dimension of the training data set. PCA or DPCA extracts the main features of the measured variables. Instead of raw data, lower dimensional score vectors are used to train ANN, where ANN performs the classification for anomaly detection. The PCA-ANN and DPCA-ANN approaches are implemented and compared with ANN for processing time, fault detection accuracy, and total error rate. Results show that the use of the scores instead of the raw data reduces the time to train ANN to a fraction and results in a greater accuracy in detection and classification. The proposed approach is successfully validated, considering several real-life like faults associated with an existing offshore process platform.

Keywords: Artificial neural networks; Principle component analysis, Dynamic principle component analysis, Process monitoring, Fault detection.

5.1 Introduction

The monitoring of offshore oil and gas processing plants is important to prevent catastrophic events such as the Ocean Rangers (Dong et al., 2015) and the Deep Water Horizon Blowout (ALNabhani, 2018). Process systems usually have a large number of variables containing process information that needs to be monitored for detecting and diagnosing possible faults. Data-driven approaches, especially the multivariate methods, are suitable to monitor process systems due to the ability to handle a high number of variables and to give an early indication of a fault. Data based methods do not require any process model or expert knowledge and are easier to implement (Qin, 2012; Tidriri et al., 2016). Two types of data-driven Fault Detection and Diagnosis (FDD) methods, multivariate statistical analysis, and machine learning approaches are widely accepted and applied in various industrial processes. Commonly used multivariate statistical analysis methods include principal component analysis (PCA), partial least squares (PLS), independent component analysis (ICA), and Fisher discriminant analysis (FDA), whereas the machine learning approaches include artificial neural networks (ANNs), neuro-fuzzy methods, support vector machine (SVM), Gaussian mixture model (GMM), K-nearest neighbor (KNN), and Bayesian network (BN).

It has been reported that the application of any particular FDD method is not capable of fulfilling all the prerequisites for accurate fault detection and diagnosis (Ding et al., 2009; 2011). A hybrid model is a unique strategy where several techniques complement each other and perform as a collective problem-solving method in one single FDD framework. Many researchers have investigated the application of different FDD methods and found that none of the individual techniques is adequate to meet all the requirements for a highly accurate and efficient diagnostic system (Venkatasubramanian et al., 2003c; Seng Ng & Srinivasan, 2010;

Tidriri et al., 2016). Chiang et al. (2015) proposed a three-step framework combining Modified Distance (DI) and Modified Casual Dependency (CD) to integrate the data-driven and causal connectivity-based techniques with the propagation path-based feature. Jiang et al. (2015a) modeled a canonical variate analysis (CVA) approach based on the feature representation of causal dependency (CD). Jiang et al. (2015b) developed a model integrated canonical variate analysis (CVA) and Fisher discriminant analysis (FDA) scheme called CVA–FDA. Jiang & Huang (2016) proposed a distributed monitoring system integrating multivariate statistical analysis and Bayesian network for large-scale plant-wide processes. Gharahbagheri et al. (2017) introduced a model through integration of diagnostic information from various diagnostic tools such as Kernel Principle Component Analysis (KPCA) and sensor validation module with process knowledge using BN. Deng et al. (2017) designed an enhanced KPCA model called fault discriminant enhanced KPCA (FDKPCA).

These days, the use of machine learning (ML) approaches has become the most alluring and effective way to obtain information from large sets of data. ML tools do not require an explicit model. The extreme computational power enabled ML to become a popular FDD method (Severson et al., 2016). ANN-based fault diagnosis in batch chemical plants has been developed where ANN structure is accompanied by a knowledge-based expert system (KBES) in a block-oriented configuration (Ruiz et al., 2000). ANN-based process monitoring, control, and fault detection have been studied and successfully applied to detect sensor faults in the Tennessee Eastman (TE) plant. It has been proven that the neural network systems have the ability to capture and model the process dynamics, even if the process contains non-linearities (Ahmad and Hamid, 2001). A method combining SVM architecture and a knowledge-based approach has been proposed to detect the faults in Tennessee Eastman process (Kulkarni et al., 2005).

Salahshoor et al. (2010) implemented a model combining multiple classifiers such as support vector machine (SVM) with an adaptive neuro-fuzzy inference system (ANFIS) to improve FDD tasks. A self-adaptive growing neural network (SAGNN) has been introduced to build an automatic structure and parameter tuning process. This algorithm enables the network to add nodes and change the structure corresponding to the supervised learning. Also, SAGNN combined ANN with a Discrete Wavelet Transform (DWT) to obtain significant features in the measured signals (Barakat et al., 2011). An extensive review of ANN architecture and its application in chemical industries such as sensor data analysis, fault detection, process identification, and control has been presented in the literature (Pirdashti et al., 2013). Gao & Hou (2016) proposed a multi-class support vector machine (SVM) based process supervision and fault diagnosis scheme called GS-PCA. In this approach, (i) PCA is used to reduce the feature dimensions, (ii) optimization of the SVM parameters is accomplished with the grid search (GS) method to increase prediction accuracy with reduced computational load, and (iii) genetic algorithm (GA) and particle swarm optimization (PSO) are employed for classification accuracy. Yu (2016) proposed (i) a joint local intrinsic and global/local variance preserving projection algorithm (JLGLPP) to obtain information from process data and, (ii) local/nonlocal manifold regularization-based Gaussian mixture model (LNGMM) to evaluate process data distributions with nonlinear and multimodal characteristics. Zhou et al. (2016) developed a novel approach called variable contribution k-nearest neighbor (VCkNN) to eliminate the limitations of contribution analysis (CA) based kNN in fault isolation applications. A GMM framework combining kernel Fisher discriminant analysis (KFDA) and discrete wavelet transform (DWT) has been proposed to improve the classification performance of the conventional approaches (Md Nor et al., 2017). A distributed Gaussian mixture modeling (GMM) and monitoring mechanism

for large-scale plant-wide processes with multiple operating conditions were developed by Zhu et al. (2018).

The focus of this work is to improve classification capability of ANN for high dimensional data sets. One of the difficulty with applying ANN to high dimensional process systems is that the network size becomes very large; thus, it requires more time to train the network and also there is no generalization, leading to poor prediction ability. The problem becomes even harder for the dynamic systems. In order to model dynamic systems, lagged variables are added to the data matrix which substantially increases the dimension of process data matrix. As a result, the network size of the ANN increases dramatically, and the performance of the ANN deteriorates. In order to minimize the structure of ANN and improve its performance in fault detection and diagnosis, we use PCA to reduce the dimension of the data. PCA is one of the widely used dimensionality reduction techniques that transforms original correlated variables to a set of uncorrelated variables (Jackson, 1991). A new hybrid methodology is proposed through integrating, PCA and DPCA with ANN, referred to as PCA-ANN and DPCA-ANN, respectively. The proposed methodology is tested using data from a plant-wide simulation model of a real offshore oil and gas processing plant in order to monitor the realistic faults associated in production facilities. Cumulative percent variance (CPV) method is used for selecting principal components (PC). Then ANN employs this reduced number of PCs to train the model and to detect and diagnose faults.

This paper is organized as follows: Section 5.2 describes the system. Section 5.3 describes PCA, DPCA, and ANN based fault detection method. Section 5.4 explains the methodology of three different case studies. Section 5.5 discusses the results as well as advantages and

limitations of the proposed techniques. Finally, the results are summarized, and conclusions are made on the suitability of the proposed methodology in section 5.6.

5.2 System description

5.2.1 Process Overview

The data used in this study is generated by performing a dynamic simulation of an offshore production plant. A Norwegian Sea oil and gas platform is chosen for the simulation reported in Voldsund et al. (2013). The overall process is divided into well section, production manifold, separator unit, export pump unit, recompression, fuel gas treatment, and reinjection unit. Hydrocarbons from five wells are fed into the separation unit through a production manifold. The separation unit consists of two three-phase separators, one two-phase separator, and one electrostatic coalescer. The oil, gas, and water are separated in the separation unit. From the separator unit, oil is fed into the export pump unit; gas is entered into the recompression and reinjection unit, and water is sent to the water treatment unit. The produced oil is transported through export pipelines, and the water is released into the sea after neutralization. The recompression unit includes three scrubbers, compressors, and coolers. The gas from the separation unit is compressed to a higher pressure in this section, and the condensate from each scrubber is recycled back into the system. The gas from the recompression unit and the separation unit is combined and fed to the reinjection unit. This unit has six scrubbers, compressors, and coolers where the pressure of the gas is increased to a level that can be injected into the reservoir to enhance the production efficiency. The condensate from the scrubbers is recycled to the system. A portion of the gas from the separation unit is fed to the fuel treatment unit. This unit has two scrubbers, one heater, and one cooler. The gas from the first scrubber

enters the flare system where the produced gas from another scrubber is entered to the turbine unit. The power required for the normal operation of the platform is generated using the turbine. Also, the condensation from each scrubber is recycled to the system. The detail information about the system is given in Khaled et al. (2019). The process flow diagram of the plant is demonstrated in Fig. 5.1.

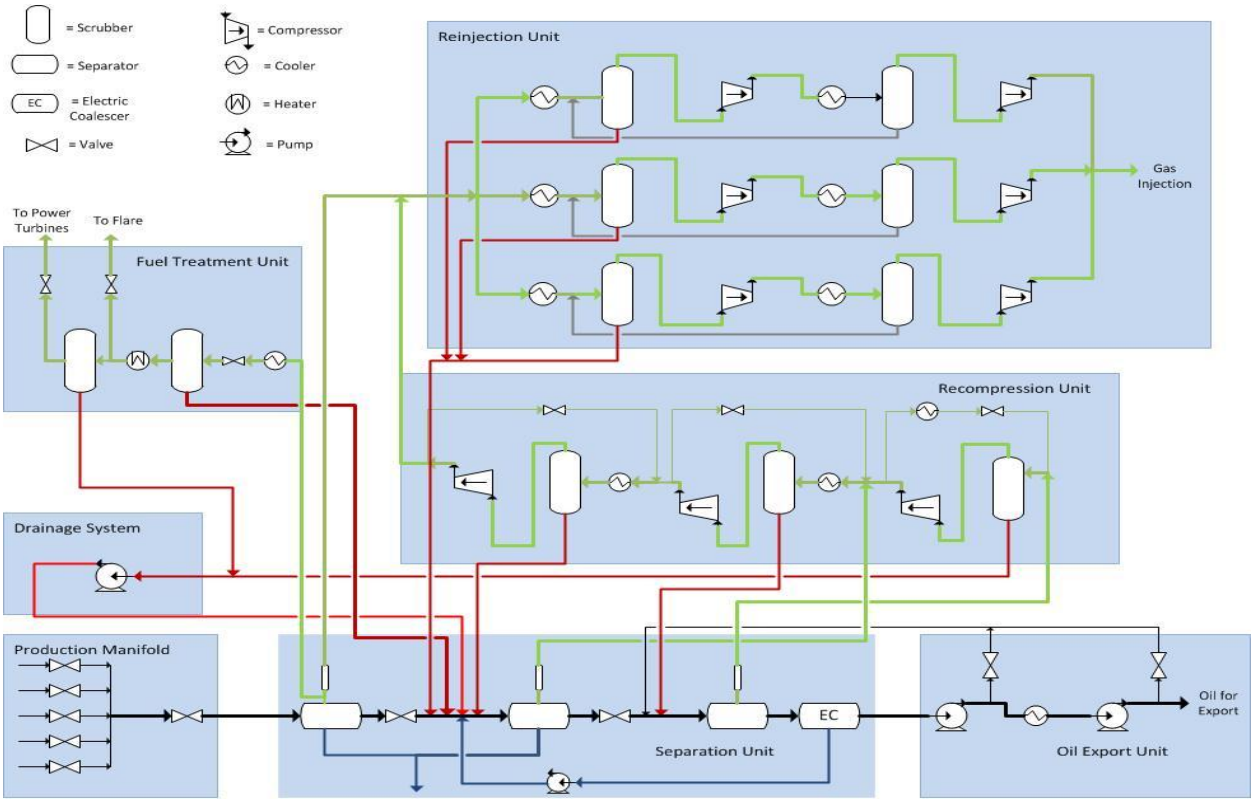

Fig. 5.1: Process flow diagram of the Norwegian Sea oil and gas platform with modifications from Khaled et al. (2019).

5.2.2 Process Fault Description

A total of six faulty scenarios, four actuator faults, and two disturbance faults are simulated. Fail open and fail hold faults are considered as actuator faults, while high temperature and high flowrate are taken into account as disturbance faults.

i. High Flowrate Fault: A step type disturbance is introduced into the feed stream**.** The flow rate of the feed stream is increased by 25% from its rated condition (2.45×105 Sm^3/h) and the simulation data for three hours is recorded.

ii. High Temperature Fault: The temperature of the feed stream is increased by 5% (from 83˚C to 87.5˚C). It should be noted that the simulation becomes unstable for a bigger disturbance after running a few minutes due to the pressure-flow merging problem of the system.

iii. Actuator Fault: Generally, the actuator fail occurs when the power supply or the activation signal in the actuator fails. Usually, there are three basic actuator faults (i) fail open, (ii) fail close, and (iii) fail hold. Fail open and fail hold fault are considered for simulation in this study. A fail open type actuator fault is considered for the two valves used in the separation unit (once at a time), as shown in Figure 1. The valve is operating at 50% in normal condition. When the fault hits the system, it goes from 50% to fully open (e.g., 100%) and remains open. Following the fail open fault, a fail hold type actuator fault is also considered for the same two valves separately in the separation unit. The valve is operating at 50% in normal condition. When the fault hits the system, it is fixed at 50% position without changing its flow direction.

5.3 Methods

In this section, a fault detection and diagnosis method is designed by combining principle component analysis (PCA) and artificial neural network (ANN). PCA is utilized to reduce the dimensions of the data matrix. PCA projects the data to a lower dimensional space called principal components (PCs). Instead of using raw data, the scores of the PCs are used to train the

ANN. This allows a compact structure for the ANN. The different components of the monitoring scheme are described in the following subsections.

5.3.1 Preliminaries

Principle component analysis*:* PCA is the most extensively used linear dimension reduction technique in process industries (McGregor, 1997). This technique conserves the maximum variations while discarding very little information (Mallick & Imtiaz, 2013). It delivers new set of uncorrelated variables from a pool of correlated variables using linear transformation. For a given data set $X \in |R^{n \times m}$, containing *n* measurements and *m* samples, the linear projection can be established by applying singular value decomposition (SVD), as given below:

$$S = U \sum V^T \quad (5.1)$$

In Equation (1), $U \in |R^{n \times n}$ and $V \in |R^{m \times m}$ are the orthogonal matrices and $\sum \in |R^{n \times m}$ represents a pseudo diagonal matrix. The loading vectors ($\mathbf{P} \in |R^{n \times a}$) are characterized by the column of U that corresponds to the largest "*a*" singular values. Principle components, also known as scores, can be defined as follows:

$$T = P^T X \quad (5.2)$$

Dynamic principle component analysis: Static PCA does not capture the time correlation of a process system as it assumes no time dependency in the existing data points. This features makes the PCA suitable only for steady state or time averaged behavior of a system. In order to detect the faults in a reasonable time frame, higher frequency data is required, and the model should include system dynamics. Dynamic PCA is similar to the static PCA in its approach; however, the data matrix also includes time-shifted vectors. DPCA considers the serial correlations by

correlating each observation vector to the previous observations. The process dynamics and time dependent relationships among variables can be represented together as follows:

$$X_D(t) = \begin{bmatrix} X(t)^T & X(t-1)^T & \cdots & X(t-l)^T \\ X(t-1)^T & X(t-1)^T & \cdots & X(t-l-1)^T \\ \vdots & \vdots & \ddots & \vdots \\ X(t+l-k)^T & X(t+l-k-1)^T & \cdots & X(t-k)^T \end{bmatrix} \quad (5.3)$$

in which, l refers to the number of lagged variables added in the augmented dynamic matrix and $X(t)^T$ introduces the m-dimensional observation vector at any time instant *t*. Applying traditional PCA on the above augmented matrix in order to have dynamic characteristics results in the following expression:

$$Y = U^T X_D \quad (5.4)$$

In Equation (4), U represents the transformation matrix consisting of eigenvectors where Y is the projection of extended data matrix X_D with a new set of U. Clearly, DPCA can run into dimensionality problem especially for large *l*.

Artificial neural network: There are two types of ANN: feedforward NN and recurrent NN (Jain et al., 1996). In this work, the feedforward NN is used for execution as it does not have stability problem like recurrent NN. Most of the researchers have used neural network applications for fault detection and classification through implementing the multilayer feed forward (Kezunovic & Rikalo, 1996). The classification performed by a neural network is basically a feed forward multilayer perception model with different types of transfer functions used in the layers.

i. Input layer: ANN takes *n* number of inputs (X_1, $X_2 \ldots X_i$), which are represented by the following equation:

$$Z_i^n\ (\mathrm{k}) = \mathrm{X_i}\,(\mathrm{k}) \qquad (5.5)$$

ii. Hidden layer: The hidden layer contains a number of neurons (representing the inputs) and associated with weights W_{ij}. The sum of all inputs and their weights can be written as follows:

$$HL_j^h\ (k) = \sum_{i=1}^{mn} z_i^n\ (k).\ W_{ij} \qquad (5.6)$$

The weights W_{ij} are primarily specified as a random value between +1 and -1 in order to tune according to the input value.

iii. Transfer function: The outputs from the hidden layer are allocated to the transfer function for further processing. Sigmoid transfer function is widely used as the activation function in NN classifier. The function will return 1 if the feed value is larger or identical and will return 0 if it is smaller than the threshold value. The transfer function is given below:

$$\sigma_j^h\ (\mathrm{k}) = \frac{1}{1+\exp(-HL_j^h\ (\mathrm{k}))} \qquad (5.7)$$

iv. Output layer: The output function can be represented as:

$$OP_q^r\ (\mathrm{k}) = \sum_j^{nh} \sigma_j^h(k)\ .\ \mathrm{w_{jq}} \qquad (5.8)$$

Finally, the output layer can be represented as follows:

$$\mathrm{Y} = \frac{1}{1+\exp(-OP_q^r\ (\mathrm{k})\ )} \qquad (5.9)$$

5.3.2 Proposed PCA/DPCA-ANN

In the ANN method, the number of neurons depends on the size of data. The neurons increase proportionally in number with an increase in the number of input variables. It is previously discussed that the PCA/DPCA tool is used to reduce the dimension of the large data set.

Therefore, it is possible to reduce the processing time of ANN by reducing the number of input variables to the ANN. Fig. 5.2 illustrates the procedures of the PCA/DPCA-ANN approach.

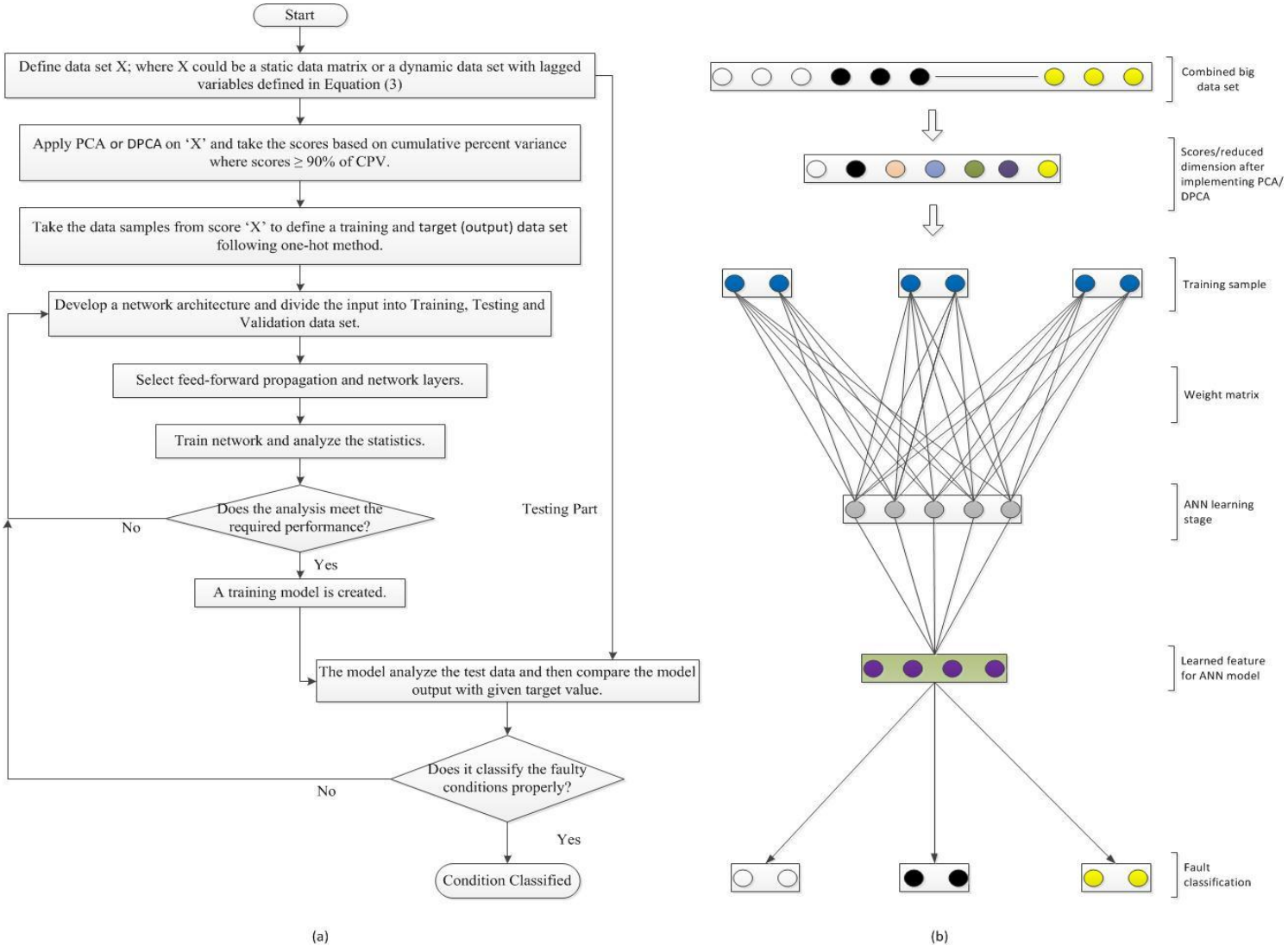

Fig. 5.2: (a) Flow diagram (b) Illustration of PCA/DPCA-ANN based fault detection and diagnosis method.

In fig. 5.2 (a), a data set 'X' including normal and different faulty conditions is collected from the historical process data. In the case of dynamic data, 'X' will comprise of time-shifted vectors to represent a dynamic time-varying data matrix. Then, PCA is applied to the data matrix 'X' and

the scores are obtained. The number of scores is selected based on equal or greater than 90% of CPV explained by the scores. Hence, the data matrix is significantly reduced without losing any vital information. The 40% score data from each normal and abnormal condition are taken to make training and target data set for the ANN by following one-hot method. Later, the target data is split into the testing and validation groups in order to develop an ANN architecture and estimate the parameters. A model is created after selecting the appropriate algorithm and network layer. This model analyzes the entire data set 'X' to identify the faults. If it does not predict the conditions accurately, the model needs to be reconstructed. It can be performed by changing the percentage of total data assigned to training, testing, and validation phases, and the number of the network layers. This process will be continued until the model identifies the faults accurately. Fig. 5.2 (b) is a graphical representation of the methodology described in fig. 5.2 (a).

5.4 Case study

5.4.1 Data Selection

The simulation data, including normal condition and six different faulty conditions, is generated based on the model developed by Khaled et al. (2019) and described in the previous section. The processing unit has a large number of variables measured throughout the plant. A total of 105 key variables are selected for monitoring purpose. Variables are organized in columns, and measurements are in rows. Data are collected for 3 hours with a sampling intervals of 10 seconds; this results in a data matrix of dimension 1,081 × 105. From the data set, 400 data samples (which is approximately 40% of the original data) are taken as training samples. Therefore, the combined data set considering all scenarios (1 normal and six abnormal) becomes (2800 × 105). The data set is divided into two subsets where 70% training data (1960 data

samples) are presented to the network during training and the network is adjusted according to its error. 15% validation data (420 data samples) are used to measure the network generalization, and to halt training when generalization stops improving. This set is used to validate the multi-layer perception by comparing the actual data with the estimated outputs. 15% testing data (420 data samples), which have no effect on training, provide an independent measure of network performance during and after training.

The target data is a set of data which is used to classify the input data set in different segments based on their nature of pattern. 'One-hot' method is followed for specifying the target value. The target data set denoted by Y = [Y_1 Y_2 Y_3 Y_4 Y_5 Y_7] consists of binary indicators, "0" and "1". The indicator matrix will have the same dimension as the input data set. In this case, the target matrix will have a dimension 2800 × 7, where each block of 400 data samples will indicate one specific condition, indicated by one output status of Y. A typical representation of the output indicator matrix is shown in Table 5.1, where $I \in R^{400\times1}$ is a vector with elements "1", and $O \in R^{400\times1}$ is a vector with elements "0".

Table 5.1: Target output and the corresponding status.

Y_1	Y_2	Y_3	Y_4	Y_5	Y_6	Y_7	**(Output Status)**
I	0	0	0	0	0	0	Normal or Fault Free Condition (Y1)
0	I	0	0	0	0	0	High Temperature Fault (Y2)
0	0	I	0	0	0	0	High Flowrate Fault (Y3)
0	0	0	I	0	0	0	V-101 Fail Hold Actuator Fault (Y4)
0	0	0	0	I	0	0	V-101 Fail Open Actuator Fault (Y5)
0	0	0	0	0	I	0	V-102 Fail Hold Actuator Fault (Y6)
0	0	0	0	0	0	I	V-102 Fail Open Actuator Fault (Y7)

5.4.2 Case 1: ANN without Data Compression

This section provides the detailed properties of NN model and the steps to design a network model for fault detection and classification.

The following main steps need to be taken for building a neural network structure: (1) A training data set representing all the cases (normal and all fault conditions) that neural network takes as the inputs; (2) Choosing a training algorithm; (3) Train the NN to create a model; (4) Test the NN model with an untrained data set including the normal and faulty data. In this work, the proposed fault detection and diagnosis approach is based on multi-layer feedforward network with sigmoid hidden neurons and linear output neurons (fit net). It can fit multi-dimensional mapping problems arbitrarily well, given consistent data and enough neurons in its hidden layer. Levenberg-Marquardt backpropagation algorithm is used to train the model by minimizing root mean square (RMS) error.

i. Training data set: We use the data set 'X' which is a 2800 × 105 matrix (as described at the beginning of this section) to train the model. Normally the number of hidden layers (and the number of neurons) are determined by the trial and error to attain the best fit. In this study, 20 hidden layers are chosen to train the network. Table 5.2 shows the comparison between 2, 10, 20, and 30 hidden layers based on MSE, accuracy rate and processing time.

Table 5.2: Comparison between 2, 10, and 20 hidden layers based on SME, accuracy and processing time.

Hidden Layer	Mean Square Error (MSE)	Accuracy	Processing Time
2	0.0812	57.00%	1 minutes 26 seconds
10	4.06E-06	81.00%	5 minutes 52 seconds
20	1.10E-05	82.00%	7 minutes 39 seconds
30	9.67E-05	84.00%	26 minutes 50 seconds

It is clear from the above table that the use of 2 hidden layers gives maximum error and lower accuracy rate. The accuracy of 20 hidden layers is more prominent than 10 hidden layers, where SME for both layers is almost the same. For 30 hidden layers, the processing time is significantly high compared to the hidden layers 10 and 20. Though the accuracy rate is increased a little, it is not practical to consider such higher processing time. After comparing all those factors, 20 hidden layers have been chosen in this study. Fig. 5.3 shows the validation performance for 20 hidden layers.

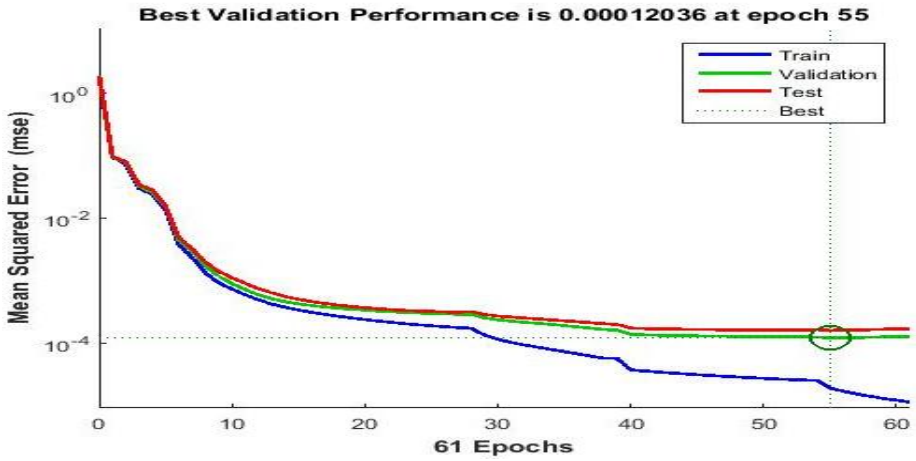

Fig. 5.3: Validation performance plot for 20 hidden layers.

ii. Classification of fault using ANN model: To conduct fault classification, a model is generated after training the network. Each cluster formed in the clustering progression is allocated a level based on different types of patterns. The goal of the network model is to classify new patterns based on the evidence learned during the training period. The classification is mainly conducted on the basis of the Euclidean distance between new pattern and the cluster center. If the distance of a new pattern becomes smaller compared to the radius of any closest cluster, it will be considered a new member of this existing cluster. On the other hand, if this distance becomes greater, compared to the radius of the nearer cluster, the new pattern will be assigned a label based on the class membership on the three adjacent clusters.

5.4.3 Case 2: Combining PCA with ANN

This section describes the proposed ANN model linked with PCA for fault detection and classification. Since the number of variables is large, the nodes of input layer for the ANN structure are also very high. PCA is employed to reduce the dimension of the data set with a goal to obtain a more parsimonious structure for the ANN. The complete procedure is described in Section 3.2 and Figure 2. Here, we briefly describe the PCA used in each data set of (1081 × 105) to reduce the dimensions. CPV is checked for all principle components or scores and continued until it reaches a certain percentage. It is observed that 20 principal components (PCs) explain 91% CPV. Therefore, the first 20 PCs are retained, and the dimension of original data set is reduced from (1081 × 105) to (1081 × 20) data matrix. The graphical representation of PCs with respect to variances (e.g., scree plot) is depicted in Fig. 5.4.

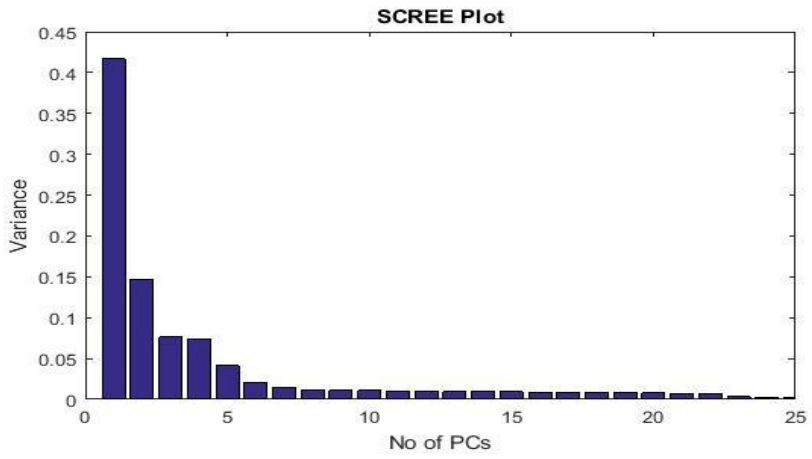

Fig. 5.4: Scree plot for the variance contribution of 25 principle components.

Following the data reduction, the same neural network algorithm described in Section 3.2 is trained using newly constructed scores ($T^{2800 \times 20}$) obtained through projection of the original data set ($X^{2800 \times 105}$). The validation and testing data are also similar to Case 1 where 70% of the data for training, 15% of the data for validation and 15% of the data for testing are used. The target data set with corresponding output status and the number of hidden layers are also the same as Case 1 except the number of input nodes to the neural network is reduced to 20 compared to 105 for Case 1. Subsequently, the trained model is used for detection and classification of faults.

5.4.4 Case 3: Combining DPCA with ANN

The procedure for training the model is similar to that described in Section 3.2 with the goal to obtain a parsimonious structure of the ANN. The only difference between this case and PCA-ANN is the construction of data matrix X. In order to capture the dynamic relationship among the variables, an augmented data set is created including the lagged variables. In this study, we take into account 4 time shifted variables, X(t), X(t-1), X(t-2), and X(t-3). The original data set has the dimension of (1078 × 105) and with additional 3 time shifted variables; the data matrix

has the size of (1078 × 420), which exhibits a significant increase in the data size and justifies some measures for dimension reduction. Similar to Case 2, PCA is applied on the augmented data matrix (1078 × 420). It is found that 90% CPV are captured by 25 scores. Therefore, only the first 25 PCs are retained for training, implying that the dimension of the original data set is significantly reduced. The graphical representation of PCs with variances is shown in Fig. 5.5.

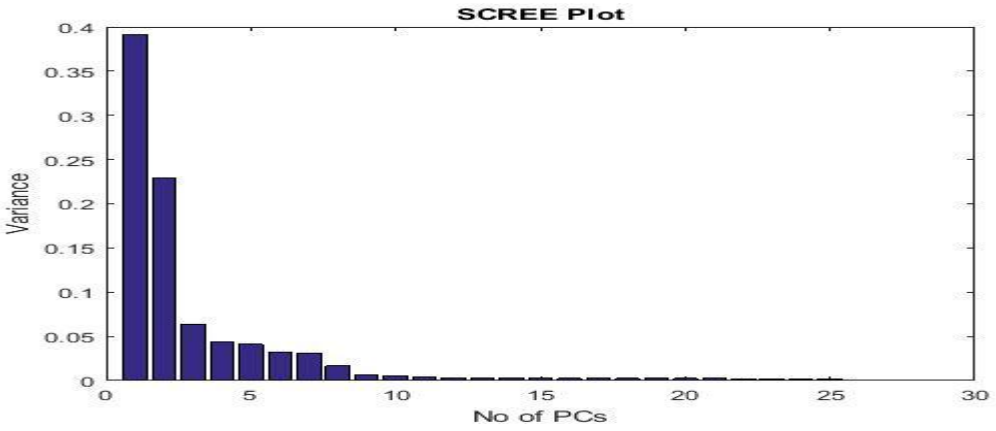

Fig. 5.5: Change in cumulative percent variance with the number of PC's

5.5 Results and Discussion

The main goal for the study is to solve the dimensionality problem in applying ANN to large scale systems. The simulation is performed in MATLAB and the system configuration of the computer is given in Table 2. The processing time varies, depending on the system configuration. We compare the neural network structure, processing time, and the FDD performance of the three methods: ANN, PCA-ANN, and DPCA-ANN. Among these three methods, DPCA-ANN deals with a large number of variables due to addition of the lagged variables in the data matrix.

5.5.1 Processing Time

The rating and specifications of the PC used for simulation are listed in Table 5.3.

Table 5.3: System configuration of the PC.

Rating	Specification
Processor	Intel(R) Core(TM) i3-2370M CPU @ 2.40GHz 2.40 GHz.
Installed memory (RAM)	4.00 GB (3.38 GB usable)
System type	32-bit Operating System

Training the ANN without any data compression takes 7 minutes and 39 seconds, PCA-ANN takes 1 minutes 35 seconds, and DPCA-ANN takes 1 minutes 36 seconds for classifying the faults , as presented in Fig. 5.6.

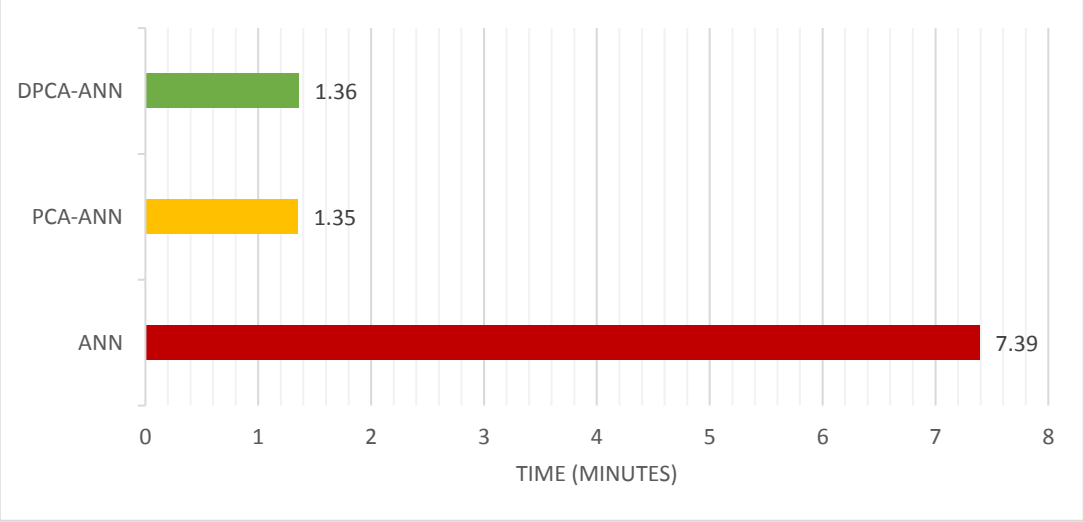

Fig. 5.6: Processing time for ANN, PCA-ANN, and DPCA-ANN based FDD methods.

5.5.2 Fault Detection and Diagnosis Performance

The three diagnosis methods are tested for six different types of faults. Confusion matrices for ANN, PCA-ANN, and DPCA-ANN systems are presented in Tables 5.4 to 5.6.

The confusion matrix for ANN based fault detection and its characteristics is shown in Table 5.4.

Table 5.4: Confusion matrix for ANN without data compression.

Predicted / Actual	Normal Condition	Fault 1 (HF)	Fault 2 (HT)	Fault 3 (FH-V101)	Fault 4 (FO-V101)	Fault 5 (FH-V102)	Fault 6 (FO-V102)
Normal	443	0	0	0	0	638	0
Fault 1 (HP)	0	719	0	0	0	362	0
Fault 2 (HT)	0	0	1081	0	0	0	0
Fault 3 (FH-V101)	0	0	0	1081	0	0	0
Fault 4 (FO-V101)	0	0	0	0	765	316	0
Fault 5 (FH-V102)	0	0	0	0	0	1081	0
Fault 6 (FO-V102)	0	0	0	0	0	0	1081

It is found that ANN detects high temperature fault (HT), fail hold fault (FH-V101), fail hold fault (FH-V102), and fail open fault (FO-V102) accurately. However, it falsely identifies normal condition as high flowrate fault (HF) and fail open fault (FO-V101). The performances of these three cases are 40%, 66%, and 70%, respectively. The Overall accuracy which can be defined as $\frac{\mathrm{TP}}{TP+TN+FP+FN}$ (TP, TN, FP, and FN represent true positive, true negative, false positive and false negative, respectively.) is obtained to be 82%.

Table 5.5 summarizes the vital information on the confusion matrix for ANN and PCA based fault detection.

Table 5.5: Data based on confusion matrix while using the PCA based ANN model.

Predicted / Actual	Normal Condition	Fault 1 (HF)	Fault 2 (HT)	Fault 3 (FH-V101)	Fault 4 (FO-V101)	Fault 5 (FH-V102)	Fault 6 (FO-V102)
Normal	932	0	0	0	0	149	0
Fault 1 (HP)	0	1081	0	0	0	0	0
Fault 2 (HT)	0	0	1081	0	0	0	0
Fault 3 (FH-V101)	0	0	0	1081	0	0	0
Fault 4 (FO-V101)	0	0	0	3	1078	0	0
Fault 5 (FH-V102)	35	0	0	0	0	1046	0
Fault 6 (FO-V102)	0	0	0	0	0	5	1076

The confusion matrix (see Table 4) shows that PCA based ANN detects high flowrate fault (HF), high temperature fault (HT), and fail hold fault (FH-V101) accurately. On the other hand, it detects other four conditions with small false alarm rate. The detection rate of these 4 cases are above 95% except the first case (86%) as the false alarm is comparatively higher (149) than the other 3 conditions (3, 35, and 5). The overall accuracy is found 97% for this application.

The confusion matrix for the ANN and DPCA based fault detection is presented in Table 5.6.

Table 5.6: Performance evaluation of DPCA based ANN model based on confusion matrix.

Predicted / Actual	Normal Condition	Fault 1 (HF)	Fault 2 (HT)	Fault 3 (FH-V101)	Fault 4 (FO-V101)	Fault 5 (FH-V102)	Fault 6 (FO-V102)
Normal	1012	1	0	0	0	68	0
Fault 1 (HP)	0	1075	6	0	0	0	0
Fault 2 (HT)	0	0	1072	9	0	0	0
Fault 3 (FH-V101)	0	0	0	1069	12	0	0
Fault 4 (FO-V101)	0	0	0	0	1066	15	0
Fault 5 (FH-V102)	4	0	0	0	0	1059	18
Fault 6 (FO-V102)	0	0	0	0	0	0	1081

It is concluded from the confusion matrix that the DPCA based ANN technique is able to identify all the normal and faulty conditions almost accurately with a negligible false alarm rate. The detection rates for all conditions are above 94%, implying a very satisfactory performance. Also, the overall precision is 98%.

5.6 Conclusions

In this paper, an effective strategy obtained through integrating PCA/DPCA and NN is proposed for improving the performance of conventional NN for large-scale systems. Noisy measurement data in regular operation and different faulty conditions are collected for testing purposes from the simulation/modeling of an offshore oil and gas processing plant. Single ANN, static PCA-ANN, and DPCA-ANN models are implemented to detect and classify the faults, accordingly. It is clear from the results that applying ANN without data compression takes not

only long processing time, also leads to poor accuracy. PCA-ANN technique takes less processing time with a better accuracy level except it detects the normal condition 86 percent. The DPCA-ANN approach takes marginally more processing time, compared to PCA-ANN depending on the number of lagged variables. DPCA-ANN delivers slightly higher accuracy, compared to the PCA-ANN. The lowest accuracy for any individual case for the DPCA-ANN system is above 94 percent, which is comparatively much better than the other two approaches.

References

Ahmad, A., Hamid, M. K. A., & Mohammed, K. (2001). Neural networks for process monitoring, control and fault detection: application to Tennessee Eastman Plant. In Malaysian Science and Technology Congress.

ALNabhani, K. (2018). Safety During Offshore Drilling Operation. In Methods in Chemical Process Safety (Vol. 2, pp. 207-268). Elsevier.

Barakat, M., Druaux, F., Lefebvre, D., Khalil, M., & Mustapha, O. (2011). Self adaptive growing neural network classifier for faults detection and diagnosis. Neurocomputing, 74(18), 3865–3876. https://doi.org/10.1016/j.neucom.2011.08.001

Chiang, L. H., & Braatz, R. D. (2003). Process monitoring using causal map and multivariate statistics: Fault detection and identification. Chemometrics and Intelligent Laboratory Systems, 65(2), 159–178. https://doi.org/10.1016/S0169-7439(02)00140-5

Chiang, L. H., Jiang, B., Zhu, X., Huang, D., & Braatz, R. D. (2015). Diagnosis of multiple and unknown faults using the causal map and multivariate statistics. Journal of Process Control, 28, 27–39. https://doi.org/10.1016/j.jprocont.2015.02.004

Deng, X., Tian, X., Chen, S., & Harris, C. J. (2017). Fault discriminant enhanced kernel principal component analysis incorporating prior fault information for monitoring nonlinear processes. Chemometrics and Intelligent Laboratory Systems, 162, 21–34. https://doi.org/10.1016/j.chemolab.2017.01.001

Ding, S. X., Zhang, P., Naik, A., Ding, E. L., & Huang, B. (2009). Subspace method aided data-driven design of fault detection and isolation systems. Journal of Process Control, 19(9), 1496–1510. https://doi.org/10.1016/j.jprocont.2009.07.005

Ding, S. X., Zhang, P., Jeinsch, T., Ding, E. L., Engel, P., & Gui, W. (2011). A survey of the application of basic data-driven and model-based methods in process monitoring and fault diagnosis. IFAC Proceedings Volumes, 44(1), 12380–12388. https://doi.org/10.3182/20110828-6-IT-1002.02842

Dong, J., Zhang, K., Huang, Y., Li, G., & Peng, K. (2015). Adaptive total PLS based quality-relevant process monitoring with application to the Tennessee Eastman process. Neurocomputing, 154, 77–85. https://doi.org/10.1016/j.neucom.2014.12.017

Gao, X., & Hou, J. (2016). An improved SVM integrated GS-PCA fault diagnosis approach of Tennessee Eastman process. Neurocomputing, 174, 906–911. https://doi.org/10.1016/j.neucom.2015.10.018

Ge, Z., Zhang, M., & Song, Z. (2010). Nonlinear process monitoring based on linear subspace and Bayesian inference. Journal of Process Control, 20(5), 676–688. https://doi.org/10.1016/j.jprocont.2010.03.003

Gharahbagheri, H., Imtiaz, S. A., & Khan, F. (2017). Root Cause Diagnosis of Process Fault Using KPCA and Bayesian Network. Industrial & Engineering Chemistry Research, 56(8), 2054–2070. https://doi.org/10.1021/acs.iecr.6b01916

Jackson, J. (1991). A user's guide to principal components (Wiley series in probability and mathematical statistics. Applied probability and statistics). New York ; Toronto: Wiley.

Jain, A. K., Jianchang Mao, & Mohiuddin, K. M. (1996). Artificial neural networks: A tutorial. Computer, 29(3), 31–44. https://doi.org/10.1109/2.485891

Jiang, B., Zhu, X., Huang, D., & Braatz, R. D. (2015a). Canonical variate analysis-based monitoring of process correlation structure using causal feature representation. Journal of Process Control, 32, 109–116. https://doi.org/10.1016/j.jprocont.2015.05.004

Jiang, B., Zhu, X., Huang, D., Paulson, J. A., & Braatz, R. D. (2015b). A combined canonical variate analysis and Fisher discriminant analysis (CVA–FDA) approach for fault diagnosis. Computers & Chemical Engineering, 77, 1–9. https://doi.org/10.1016/j.compchemeng.2015.03.001

Jiang, Q., & Huang, B. (2016). Distributed monitoring for large-scale processes based on multivariate statistical analysis and Bayesian method. Journal of Process Control, 46, 75–83. https://doi.org/10.1016/j.jprocont.2016.08.006

Karimi, P., & Jazayeri-Rad, H. (2014). Comparing the fault diagnosis performances of single neural networks and two ensemble neural networks based on the boosting methods. Journal of Automation and Control, 2(1), 21-32.

Khaled, M.S., Imtiaz, S. A., Ahmed, S., & Zendehboudi, S. (2019). Dynamic simulation of offshore gas processing plant for normal and abnormal operations. unpublished thesis.

Kezunovic, M., & Rikalo, I. (1996). Detect and classify faults using neural nets. IEEE Computer Applications in Power, 9(4), 42–47. https://doi.org/10.1109/67.539846

Kulkarni, A., Jayaraman, V. K., & Kulkarni, B. D. (2005). Knowledge incorporated support vector machines to detect faults in Tennessee Eastman Process. Computers & Chemical Engineering, 29(10), 2128–2133. https://doi.org/10.1016/j.compchemeng.2005.06.006

Mallick, M. R., & Imtiaz, S. A. (2013). A Hybrid Method for Process Fault Detection and Diagnosis. IFAC Proceedings Volumes, 46(32), 827–832. https://doi.org/10.3182/20131218-3-IN-2045.00099

Maurya, M. R., Paritosh, P. K., Rengaswamy, R., & Venkatasubramanian, V. (2010). A framework for on-line trend extraction and fault diagnosis. Engineering Applications of Artificial Intelligence, 23(6), 950–960. https://doi.org/10.1016/j.engappai.2010.01.027

MacGregor, J. F. (1997). Using On-Line Process Data to Improve Quality: Challenges for Statisticians. International Statistical Review, 65(3), 309–323. https://doi.org/10.1111/j.1751-5823.1997.tb00311.x

Md Nor, N., Hussain, M. A., & Che Hassan, C. R. (2017). FAULT DIAGNOSIS BASED ON MULTI-SCALE CLASSIFICATION USING KERNEL FISHER DISCRIMINANT ANALYSIS AND GAUSSIAN MIXTURE MODEL AND K-NEAREST NEIGHBOR METHOD. Jurnal Teknologi, 79(5–3). https://doi.org/10.11113/jt.v79.11332

Natarajan, S., & Srinivasan, R. (2014). Implementation of multi agents based system for process supervision in large-scale chemical plants. Computers & Chemical Engineering, 60, 182–196. https://doi.org/10.1016/j.compchemeng.2013.08.012

Pirdashti, M., Curteanu, S., Kamangar, M. H., Hassim, M. H., & Khatami, M. A. (2013). Artificial neural networks: Applications in chemical engineering. Reviews in Chemical Engineering, 29(4). https://doi.org/10.1515/revce-2013-0013

Qin, S. J. (2012). Survey on data-driven industrial process monitoring and diagnosis. Annual Reviews in Control, 36(2), 220–234. https://doi.org/10.1016/j.arcontrol.2012.09.004

Rato, T. J., & Reis, M. S. (2013). Fault detection in the Tennessee Eastman benchmark process using dynamic principal components analysis based on decorrelated residuals (DPCA-DR). Chemometrics and Intelligent Laboratory Systems, 125, 101–108. https://doi.org/10.1016/j.chemolab.2013.04.002

Ruiz, D., Nougués, J., Calderón, Z., Espuña, A., & Puigjaner, L. (2000). Neural network based framework for fault diagnosis in batch chemical plants. Computers & Chemical Engineering, 24(2–7), 777–784. https://doi.org/10.1016/S0098-1354(00)00371-9

Salahshoor, K., Kordestani, M., & Khoshro, M. S. (2010). Fault detection and diagnosis of an industrial steam turbine using fusion of SVM (support vector machine) and ANFIS (adaptive neuro-fuzzy inference system) classifiers. Energy, 35(12), 5472–5482. https://doi.org/10.1016/j.energy.2010.06.001

Severson, K., Chaiwatanodom, P., & Braatz, R. D. (2016). Perspectives on process monitoring of industrial systems. Annual Reviews in Control, 42, 190–200. https://doi.org/10.1016/j.arcontrol.2016.09.001

Tidriri, K., Chatti, N., Verron, S., & Tiplica, T. (2016). Bridging data-driven and model-based approaches for process fault diagnosis and health monitoring: A review of researches and future challenges. Annual Reviews in Control, 42, 63–81. https://doi.org/10.1016/j.arcontrol.2016.09.008

Voldsund, M., Ertesvåg, I. S., He, W., & Kjelstrup, S., 2013. Exergy analysis of the oil and gas processing on a North Sea oil platform a real production day. Energy, 55, 716–727. https://doi.org/10.1016/j.energy.2013.02.038

Yu, J. (2016). Process monitoring through manifold regularization-based GMM with global/local information. Journal of Process Control, 45, 84–99. https://doi.org/10.1016/j.jprocont.2016.07.006

Zhang, F., & Ge, Z. (2015). Decision fusion systems for fault detection and identification in industrial processes. Journal of Process Control, 31, 45–54. https://doi.org/10.1016/j.jprocont.2015.04.004

Zhang, Y., & Zhang, Y. (2009). Complex process monitoring using modified partial least squares method of independent component regression. Chemometrics and Intelligent Laboratory Systems, 98(2), 143–148. https://doi.org/10.1016/j.chemolab.2009.06.001

Zhou, Z., Wen, C., & Yang, C. (2016). Fault Isolation Based On k-Nearest Neighbor Rule For Industrial Processes. IEEE Transactions on Industrial Electronics, 1–1. https://doi.org/10.1109/TIE.2016.2520898

Zhu, J., Ge, Z., & Song, Z. (2018). Distributed Gaussian mixture model for monitoring plant-wide processes with multiple operating modes. IFAC Journal of Systems and Control, 6, 1–15. https://doi.org/10.1016/j.ifacsc.2018.09.002

Chapter 6

Conclusion

Offshore oil and gas platforms are complicated and remarkably unified systems that continuously face substantial changes in the field properties and functioning strategies over time. In this study, a dynamic model for an offshore production plant in the North Sea is simulated. The model contains several producing wells and topside units. Dynamic responses from each section are verified and validated with the collected, measured data. Besides, several issues associated with dynamic simulation, such as implementing controllers, transfer function block, and measurement noise are introduced to simulate real-life conditions. It is shown that the HYSYS simulation can successfully predict the dynamic behaviors during normal and various faulty operating conditions of the plant.

Implementation of ANN is time-consuming and provides poor performance in large scale data. A hybrid approach integrating PCA/DPCA and ANN is proposed to mitigate the limitations. PCA/DPCA extracts the main features of the measured variables, whereas the ANN uses these lower-dimensional score vectors to train the network instead of the whole data set. The proposed PCA-ANN and DPCA-ANN approaches are implemented and compared with conventional ANN. Results show that the proposed model has higher accuracy and less time-consuming in detecting and classifying the faults.

6.1 Summary

In chapter 1, the introduction and basic ideas of system modeling, simulation, and monitoring techniques are explained. Research background and the historical development of different simulation software are briefly discussed. Different commercial simulation software, their implementation, and configurations are also introduced.

In chapter 2, Recent literature is reviewed to gain comprehensive knowledge about various monitoring and simulation methods. The review of existing methods is essential before making further efforts to develop a new approach. Moreover, detail state-of-the-art techniques for both monitoring and simulation are reviewed.

In chapter 3, a steady-state framework of an existing North Sea oil and gas platform is carried out. The model is designed based on the measurement data of a real production day. The models have been formulated considering several producing wells and different surface facilities. The result of each processing unit of the steady-state model is compared and validated. Finally, the result concludes that this steady-state model successfully met all the requirements similar to the real processing platform.

In chapter 4, the steady-state model is transformed into a dynamic state, and the requirements for the transition, such as sizing, dimensioning, etc. are performed. Few necessary modifications in the separation unit, recompression unit, recycle streams, and the mixers are done in order to maintain the pressure-flow relation. Many PID controllers, such as level controller (LC), flow controller (FC), etc. are implemented to keep a consistent flow. Measurement noise is added to the feed, and two types of fault: (i) Actuator fault and (ii) Disturbance fault are investigated. A

total of six faulty scenarios (two fail open, two fail holds, high temperature, and high flowrate) are examined.

In chapter 5, performance evaluation of different FDD methods: ANN, PCA-ANN, and DPCA-ANN are carried out. A generic procedure to evaluate efficiency is proposed in this chapter. Each method is implemented separately to detect and identify the six faults generated in section 4. the processing time, accuracy, and error rate in each case are recorded. The ANN method takes 7 minutes, and 39 seconds with 82% accuracy, PCA-ANN takes 1 minute 35 seconds with 97% accuracy, and DPCA-ANN method takes 1 minute and 36 seconds with 98% accuracy. The proposed PCA/DPCA-ANN technique in this thesis shows the best efficiency performance considering the time and accuracy, which can serve as a suitable FDD technique in a large scale system.

6.2 Future Works

The recommended future research directions include:

1. The real dimension and liquid holdup of the equipment (separators, electrostatic coalescer, scrubbers, heaters and coolers) can be studied in future for more accurate dynamic results.
2. Practical investigation about the water treatment process and recycles (such as how they are adding in different units without disrupting the pressure requirement and maintaining proper pressure-flow relation within the system) can be carried out.
3. In this work, in build ANN MATLAB tool is used for pattern recognition. Programable ANN can be used to optimize the output by modifying the weight factors and the number of neurons in hidden layers.

4. Different dimension reduction techniques such as PLS, FDA etc. can be conducted in the future to validate its performance.
5. More faults associated in offshore plant (such as sensor faults) can be incorporated.